

Observations of alongshore variability in intertidal beach development and wave conditions



Utrecht University

Ivo Naus (3947203)

MSc Thesis

First supervisor: Timothy Price

Second supervisor: Gerben Ruessink

Utrecht University, Department of Physical
Geography

MSc Program: Earth, Surface and Water

Date: 30 June 2017

Abstract

As a large part of the world population lives near sandy coasts it is vital to ensure safety from flooding and coastal erosion, which makes the understanding of coastal dynamical processes important. In the past, much research has been done on the behaviour of sandy coasts, although the processes behind alongshore variations in the bar-beach-dune system are not well understood. The bar-beach-dune coupling is a key factor to fully comprehend when considering future coastal protection. Alongshore variations in wave energy dissipation over subtidal bars can generate alongshore differences in the development and accretion of the (intertidal) beach under low-energetic wave conditions, which can lead to areas with less sediment accretion resulting in possible weaknesses in the coastal area. Therefore, possible alongshore variations in intertidal beach development during mild weather conditions need to be investigated to understand beach recovery and alongshore variation therein. To unravel the alongshore variation in morphological development of the intertidal beach in relation to the incident wave conditions, after crossing the subtidal bars during low-energetic wave conditions, a 3-week fieldwork campaign at Vejers Beach, Denmark, was set out. The changes in bathymetry/topography of the intertidal beach were observed under mild weather conditions. Incident wave conditions were measured along the low tide water level; the seaward border of the intertidal beach. The behaviour of the intertidal beach was alongshore variable during mild weather conditions in an inconsistent manner, with alongshore differences in bar migration, bar elevation change and bar height change (between two days), up to 5, 0.15 and 0.25 meter, respectively. And the maximum alongshore difference in the cross-shore position of $z=0$ increased from ± 9 m to ± 15 m during 8 days of low-energetic wave conditions. Furthermore, there were significant correlations between alongshore variations in bar developments and alongshore variations in wave conditions, during a period of low-energetic wave conditions. However, it is uncertain how the alongshore variations in wave conditions originate, how they changed over time and which processes were responsible for the alongshore variations in bar development. Therefore, future research, with a more enhanced instrument setting, is needed to improve the knowledge concerning possible alongshore variabilities in intertidal hydrodynamics and beach recovery.

Table of contents

1. Introduction	5
2. Literature background.....	6
2.1 Hydrodynamics.....	6
2.1.1 Waves.....	6
2.1.2 Currents	10
2.2 Subtidal bars	12
2.3 Intertidal bars	15
2.3.1 Types	15
2.3.2 Formation.....	16
2.3.3 Morphodynamics	16
2.4 Morphological coupling.....	20
2.4.1 Bar-beach-dune coupling.....	20
2.4.2 Alongshore differences in swash	24
3. Research aims.....	24
4. Methods.....	26
4.1 Study site.....	26
4.2 Data	26
4.2.1 Morphological data	26
4.2.2 Wave data	27
4.3 Data analysis.....	29
4.3.1 Morphological data	29
4.3.2 Alongshore comparison of hydrodynamic data	30
4.3.3 Morphological vs. hydrodynamical data	31
5. Results.....	32
5.1 Offshore conditions	32
5.2 Morphology.....	33
5.2.1 Bathymetric/topographic maps	34
5.2.2 Cross-sections.....	35
5.2.3 Bar characteristics.....	39
5.2.4 Slope, Volume and z=0 contour line position.....	42
5.2.5 Location subtidal bars	45
5.3 Hydrodynamics.....	46
5.3.1 Wave height.....	47
5.3.2 Spectral energy.....	49
5.4 Morphological changes vs. hydrodynamics	50
5.4.1 T-test results.....	50
5.4.2 Significant correlations	53

6. Discussion.....	56
6.1 Large scale variation.....	56
6.2 The (intertidal) swash bar.....	57
6.2.1 General development of the bar.....	57
6.2.2 Alongshore variations in bar behaviour.....	58
6.3 Volume, slope and contour line.....	61
6.4 Uncertainties and possible improvements.....	61
7. Conclusion.....	63

1. Introduction

Understanding coastal hydrodynamic processes is important for the coastal defence strategy against natural water from the oceans and seas. As a large part of the world population lives near the coast, it is vital to ensure safety from flooding and coastal erosion. Models are used to predict the consequences of sea level rise for the coastal system, and to find possible weaknesses in coastal areas. It has been predicted that global mean sea level will rise between 0.26-0.55 m, the most favourable scenario, and 0.45-0.82 m, the most extreme scenario, at the end of the century (IPCC, 2014). Moreover, the relative sea level rise (RSLR) is expected to be even larger. This is different for coasts around the world, e.g. at the coast of New York a 0.44 m minimum to 1.58 m maximum RSLR is projected (Carson et al., 2016).

The coastal system consists of three main zones, the subtidal, intertidal and supratidal zones (Figure 1). To optimize the current models, new researches should be done to study the dynamics of certain parts of the coastal system in detail. The whole coastal system, from the subtidal zone to the dunes, interacts with each other. Subtidal bars can spatially alter wave conditions further landward, affecting beach morphology and, in turn, the growth and erosion of dunes. This bar-beach-dune coupling is a key factor to fully understand when considering future coastal protection.

This thesis focusses on alongshore variations in the development of the intertidal zone, along with the alongshore wave conditions arriving at the seaward border of the intertidal zone. And, as subtidal bars can influence the behaviour of the intertidal beach, they are an important factor for this research to take into account. First, the sub- and intertidal processes, morphology and coupling mechanisms will be discussed based on the literature (*Chapter 2*). In *Chapter 3* the research aims will be stated. To accomplish the aims, this research also consists of a fieldwork campaign of which the data was analysed (*Chapter 4*). Furthermore, the results of this fieldwork are described (*Chapter 5*) and discussed (*Chapter 6*). After which the main conclusions of this thesis are drawn (*Chapter 7*).

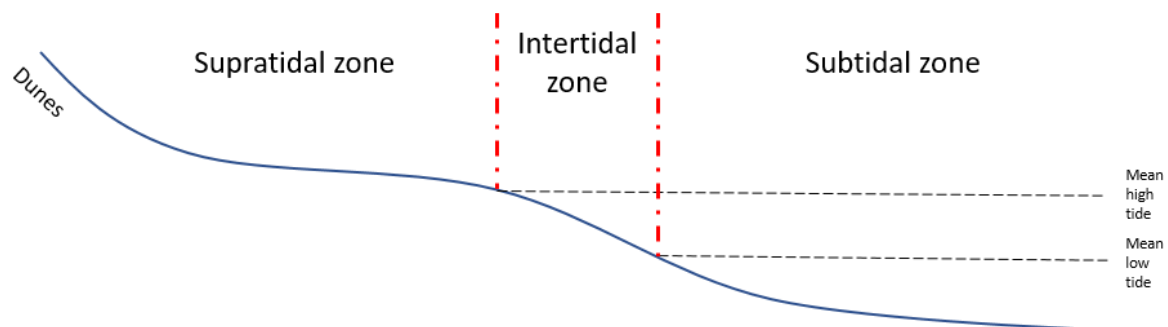


Figure 1: A schematic overview of the nearshore coastal system.

2. Literature background

This literature-study chapter will focus on the processes and morphology of the intertidal beach in relation to the more seaward processes and morphology. First the waves and currents will be treated, as changes/alongshore variations in waves and currents result in changes/alongshore variations in sediment transport and, therefore, morphology (Figure 2). Secondly, the morphology of subtidal bars will be discussed, followed by the morphodynamics of the intertidal beach (bars and shoreline). Finally, the alongshore variabilities in processes and morphology, i.e. coupling mechanisms, will be discussed. In chapter 3, based on the gaps in the current knowledge, the aims of this research will be stated.

2.1 Hydrodynamics

2.1.1 Waves

When sea and swell waves propagate onshore, going into shallower water, they transform due to interaction with the bottom. A usual sequence of transformations towards the shore is, for example: Symmetric sinusoidal waves → symmetric shoaling waves → asymmetric shoaling waves → wave breaking → bores → swash. The occurrence of each wave type can be linked to the ratio of the significant wave height, H_s , over the water depth, h : H_s/h (Masselink et al., 2006). Therefore, each type can occur at a certain cross-shore position. Furthermore, these positions can change due to an alteration in wave climate or due to water depth variations forced by tides (Price & Ruessink, 2008).

Shoaling waves are generally present in intermediate water depths ($H_s/h < 0.3$), the shoaling zone (seaward of the surf zone), and are also known as skewed waves. They have a short, high crest and a broad, flat trough resulting in a characteristic large onshore orbital velocity and a smaller offshore orbital velocity, i.e. velocity skewness (Figure 3a). Because of this velocity skewness the net cross-shore sediment transport is commonly onshore directed, with an increase in transport rate closer towards the breaking point (Masselink et al., 2006; Osborne & Greenwood, 1992).

Asymmetric waves often occur at locations after breaking, generally referred to as the surf zone, where there is a relative large wave height ($H_s/h = 0.5-1$) and are characterised by a saw-tooth shape (Masselink et al., 2006). This includes that it takes a longer time to go from peak crest to peak trough than from peak trough to peak crest, leading to velocity asymmetry (Figure 3b). This shape originates

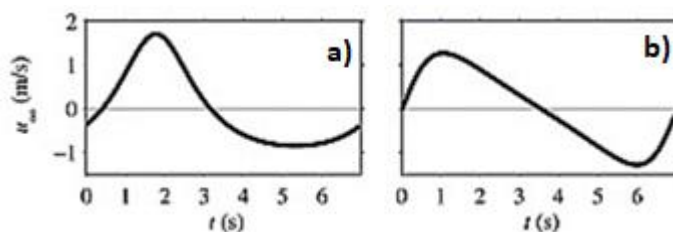


Figure 3: Wave shapes expressed in the free stream velocities. a) Velocity skewness, shoaling wave shape. b) Velocity asymmetry, asymmetric wave shape. Modified figure from Ruessink et al. (2009)

from the breaking waves which convert into turbulent bores. Sediment transport direction can be both on- and offshore directed under asymmetric wave conditions and this mostly depends on the energy of the incident waves. So, on the strength of the undertow (see section 2.1.2).

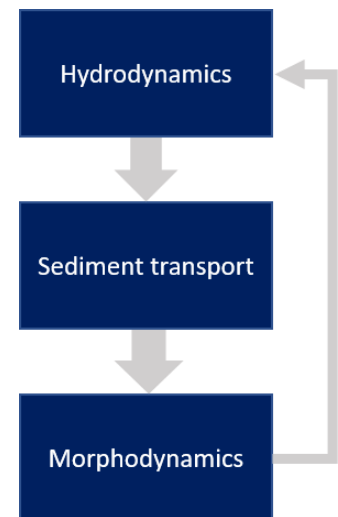


Figure 2: Simplified coastal morphodynamic feedback system.

There are four different breaker types; spilling, plunging, surging and collapsing. What breaker type occurs on a certain beach is dependent on the slope of the bed, the wave height and length. A breaker type can be determined numerically by calculating the Iribarren number at the location (Aagaard & Jensen, 2013):

$$\xi = \frac{\tan\beta}{\sqrt{H_s/L_0}}$$

Where β is the cross-shore bed slope, H_s is the significant wave height and L_0 is the deep-water wave length. At breakpoint, a value of $\xi=0.4$ is commonly used to distinguish between spilling ($\xi>0.4$) and plunging ($0.2<\xi<0.4$) wave breaking. And a value of $\xi=2.0$ is used to separate plunging with surging or collapsing ($\xi<0.2$) (Battjes, 1974).

The swash zone is a result of the 'collapse' of waves on the beach ($H_s/h > 1$). Swash motions generally produce net onshore sediment transport in non-storm conditions (Masselink et al., 2006). This location is variable over the beach due to tides and morphological developments. Swash is the oscillation of the waterline on the beach and is a key process in sediment exchange between ocean and beach (Guedes et al., 2012).

Infragravity waves are waves with lower frequencies than the incident wind and swell waves. These waves originate directly or indirectly from incoming waves and their energy is, therefore, proportional to the energy from these incident waves (Masselink et al., 2014). The wave and current spectra indicate the presence of energy at these low frequencies, where the boundary between incident and infragravity waves is usually set at 0.05 Hz (Figure 8). The infragravity wave energy increases significantly at the inner surf zone compared to the outer surf zone (Figure 5). This is because wave energy dissipation by wave breaking causes energy transfer from the wind/swell wave frequencies to the infragravity waves throughout the surf zone (Aagaard et al., 2013). And, as infragravity waves do not break, they might be of significant importance onshore of the surf zone (i.e. in the swash zone).

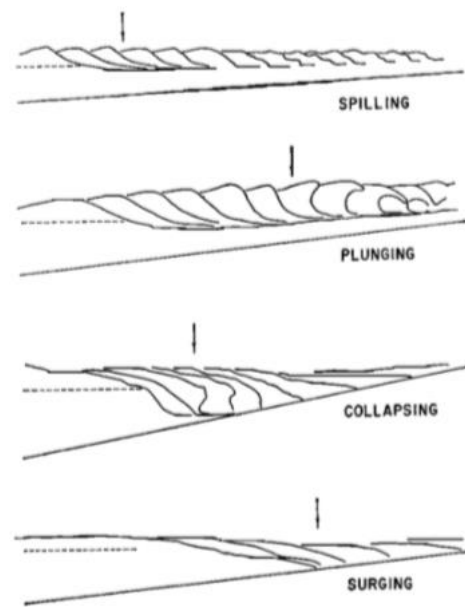


Figure 4: Schematic overview of the four different breaker types, the arrows locate the defined breaking point (Galvin, 1968).

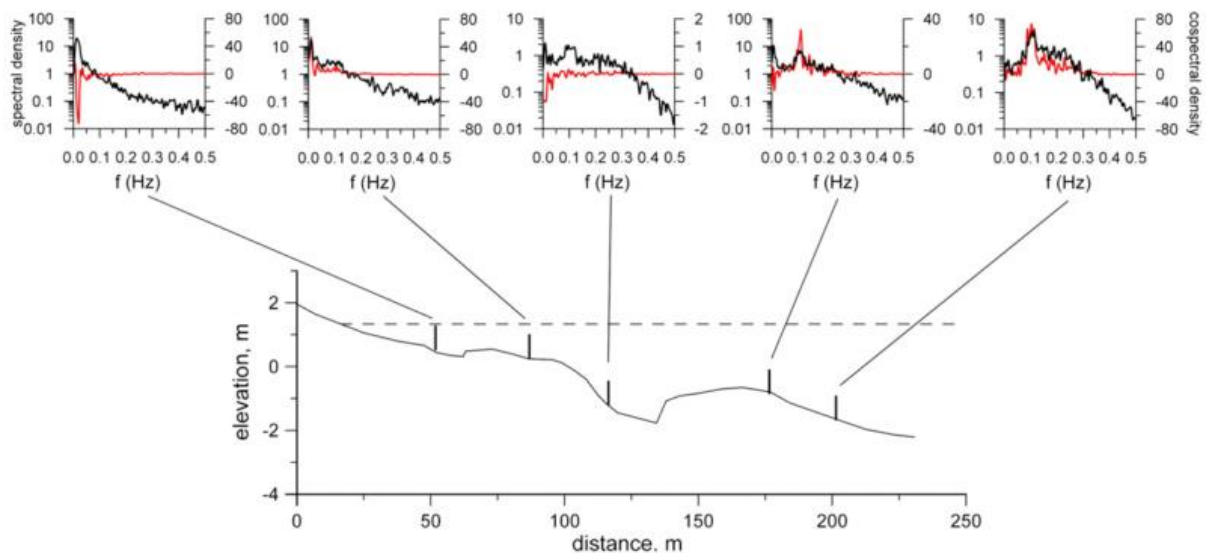


Figure 5: Autospectra of cross-shore velocity (black) and cospectra of net cross-shore oscillatory suspended sediment transport (red) (positive values indicate an onshore net transport) across the inner surf zone. The dashed line in the beach profile marks the mean water level. Figure from Aagaard et al. (2013).

Tidal influences

Tides have a major influence on the position of the different wave zones. Also, the variable water depth determines which processes are active at a given time around and on top of an intertidal bar. During one tidal cycle, different hydrodynamic process zones can shift along the cross-section of an intertidal beach (Figure 6). During high-water, it is most likely (depending on the position of the intertidal bar) that waves will break on top of the bar. And when the water is low, the bar might be affected by swash processes. Therefore, there can be several types of sediment transport, and thus migration, processes at the bar within one tidal cycle. As also pointed out by Masselink et al. (2006) (Figure 7). For instance, during high tide there can be wave breaking on top of the bar with a strong undertow, resulting in an offshore transport on top of the bar, while during low tide swash processes can act on the bar, resulting in an onshore transport.

An influence of tides to intertidal bar migration was recorded by Kroon & Masselink (2002). They investigated the behaviour of multiple intertidal bars under low-energy wave conditions during a spring-to-spring tidal cycle. They found that the amount of bar migration was coupled to the residence times of the swash and surf processes over the bars (Figures 6 and 7). During spring tide the water level goes up and down relatively fast which limits the residence time of the processes, whereas during neap tide the residence times are longer, increasing the amount of sediment transport at a certain location by a certain process (Kroon & Masselink, 2002). So, the residence times are (partly) dependent on the tidal range.

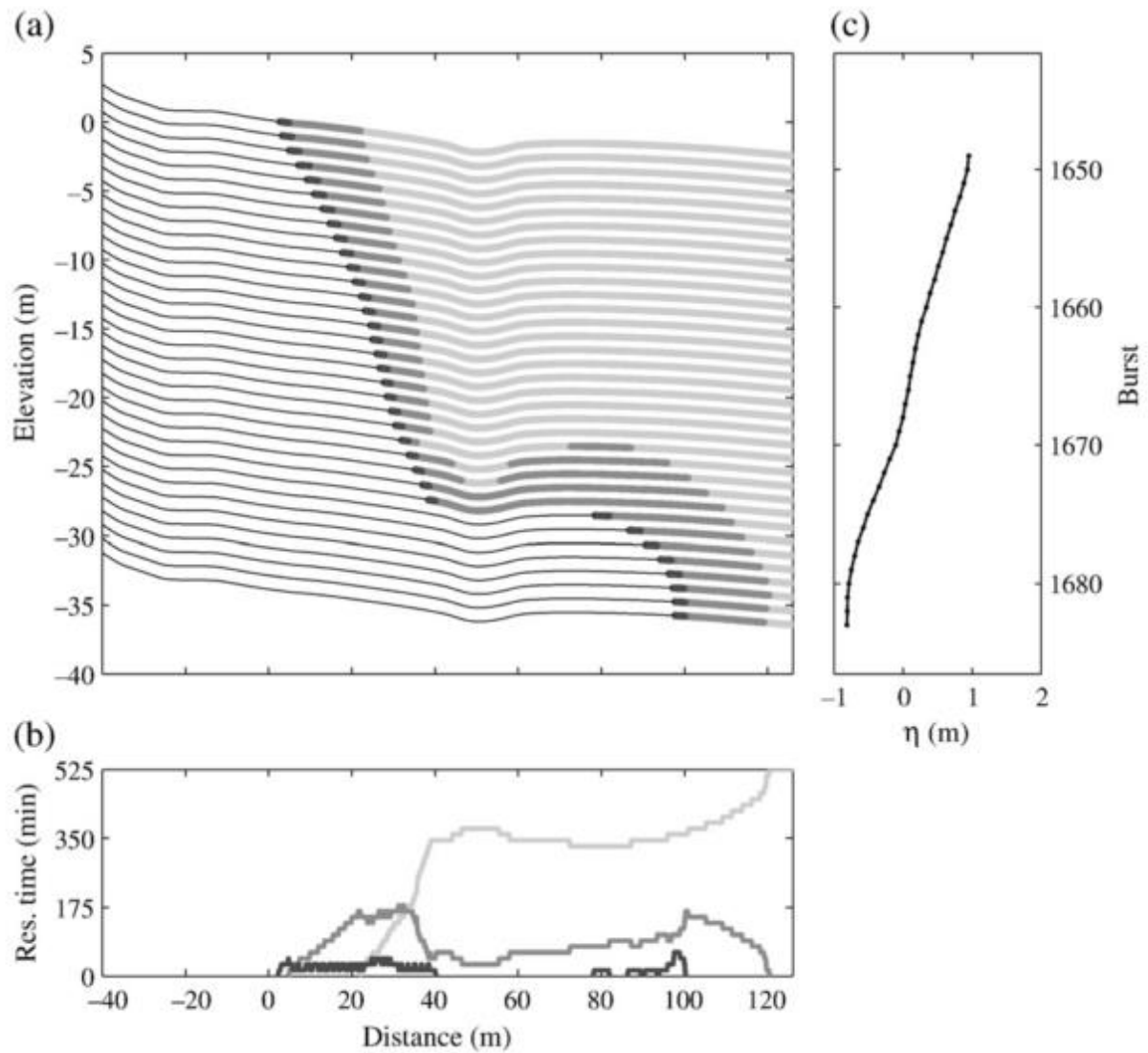


Figure 6: (a) The distribution of the different zones on the intertidal beach during half a tidal cycle, where each subsequent profile is offset by -1m. (b) residence time (in minutes) versus cross-shore distance over half a tidal cycle. (a-b) Swash zone (dark grey), surf zone (medium grey), shoaling zone (light grey) and the thin lines in (a) are the subaerial parts of the beach. (c) shows the offshore water level η (during half a tidal cycle), where one burst is 15 minutes. Figure from Price & Ruessink (2008).

The duration of certain processes at a certain location are also dependent on the incident wave height. Generally, larger wave heights are coupled to wider swash and surf zones, and thus increasing their residence times. The residence time of hydrodynamic processes is governed by the relative tidal range RTR (ratio of the tidal range to the wave height) (Masselink, 1993). Kroon & Masselink (2002) suggest, using the results from their field experiment, that significant morphological change might require conditions characterised by a RTR lower than 30.

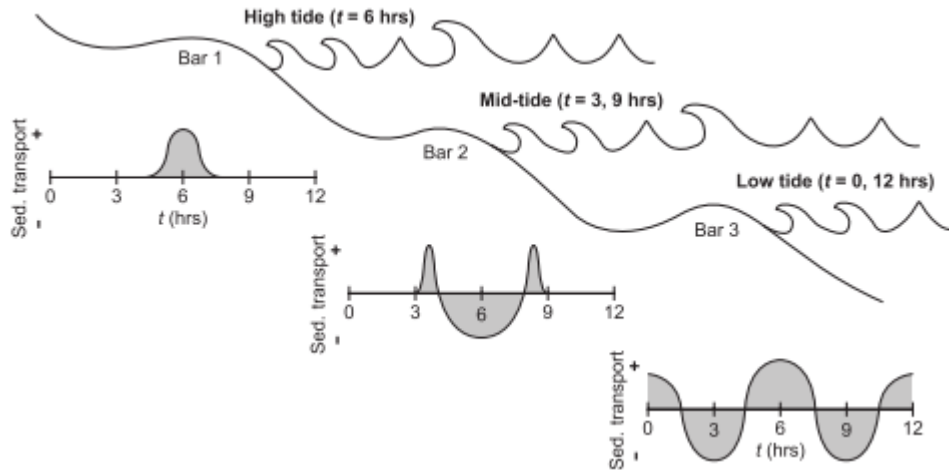


Figure 7: Schematised overview of different sediment transport rates over a single tidal cycle for three intertidal bars on one intertidal beach (Masselink et al., 2006).

Guedes et al. (2011) investigated swash dynamics on an intermediate beach under almost constant, mild, offshore wave conditions. Whether the waves broke before reaching the shoreline was dependent on the tidally controlled water depth above a sandbar. Resulting in a change of wave energy dissipation between low and high tide, which was visible in changes in the swash. Up-swash was found to be a factor of 2 larger during high tide, with little energy dissipation throughout the surf zone, compared to low tide, with much energy dissipation in the surf zone (Guedes et al., 2011). The more energy dissipation in the surf zone, the more energy was found at the infragravity frequencies in the swash distribution (Figure 8). Furthermore, for steeply sloping beaches most of the energy comes from the incident waves, whereas for gently sloping beaches (more dissipative) the energy is highest in the infragravity frequencies. This might suggest that the amount of wave breaking before the swash zone determines the relative importance of infragravity waves (Figure 8). Although, it is still unclear how this is alongshore variable, as predicting wave runup elevations remains extremely complicated and even the most recently developed formulations do not explain the variabilities in up-swash (Senechal, 2017).

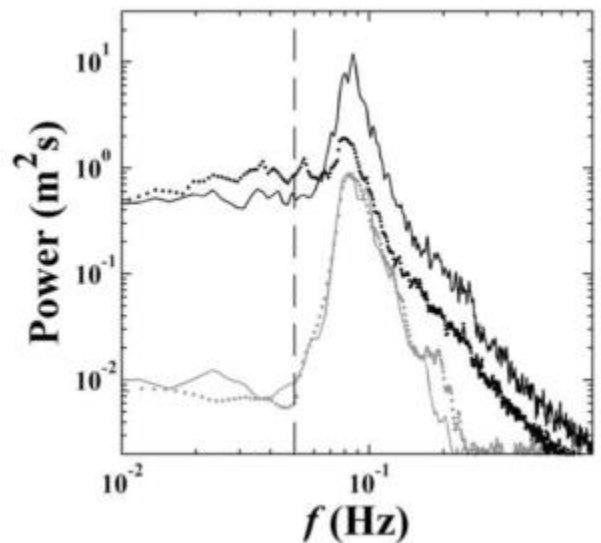
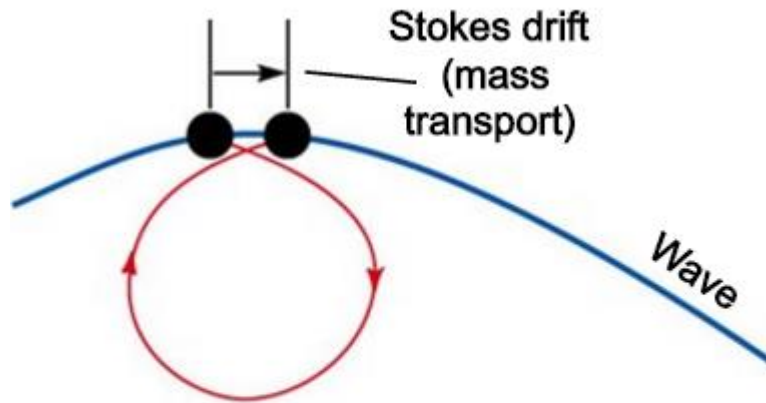


Figure 8: Average of obtained spectra during low tide (dotted line) and during high tide (solid line), plotted on a log-log scale. Runup spectra are shown in black, and offshore spectra are shown in grey. Vertical dashed line highlights 0.05 Hz. Figure from (Guedes et al. (2011)

2.1.2 Currents

There are three cross-shore current components. The high (wind/swell) and low (infragravity) frequency wave oscillations and the mean current (the undertow). As breaking waves pass by they transport a water mass towards the coast. This happens because the orbital motion does not connect to its 'starting point', like a circle, but the end of the motion is shifted a little towards the coast (Figure 9), hence a transport of water mass. This process of mass transport is referred to as Stokes drift. To compensate for this water mass transport there is an offshore directed mean current at the bottom, which is the undertow or bed return flow (Figure 10b).



Open orbit after one period

Figure 9: A schematic example of the mass transport of water by waves; the Stokes drift (figure from: <http://slideplayer.com>)

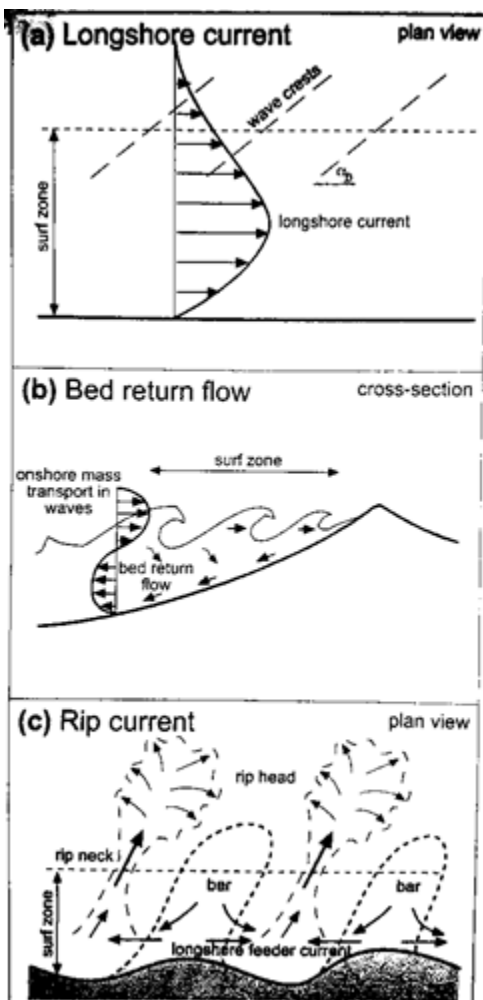


Figure 10: Quasi-steady currents in the surf zone: a) longshore currents due to obliquely-incident waves, b) undertow or bed return flow and c) nearshore cell circulation with rip currents. Figure from Masselink et al. (2014).

Over a cross-section with a subtidal bar the relative importance of the wave components on top of the bar can shift. During fair weather conditions, when the waves do not/barely break on top of the bar, the high frequency waves become shoaling waves (Figure 3a) with a larger onshore than offshore current. The low frequency waves remain symmetric and a (strong) undertow does not develop, resulting in an average net onshore current over the bar. However, under extremer wave conditions the undertow will become stronger as more waves break (Masselink et al., 2014). Under these conditions the undertow will dominate over the other components, resulting in a net offshore current over the bar.

Longshore currents (Figure 10a) are driven by the breaking of obliquely incident waves. The strength of the longshore current depends on the wave energy and the magnitude of the angle of the incident waves, where the longshore current will be strongest if waves arrive with an angle of 45° relative to the shore normal. And the direction of the current is dependent on the incident angle (Masselink et al., 2006).

A three-dimensional nearshore morphology can generate a cell circulation system (Figure 10c). Alongshore differences in bed level elevation can generate alongshore differences in the amount of wave breaking, where more wave breaking will occur at locations with a higher bed elevation. This results in an onshore transport of water and a higher set-up of the water level than at a position with less wave breaking. Naturally, the water will flow from positions with a higher water level to positions with a lower water level. These are

the longshore feeder currents and they carry water to a rip current. Rip currents are strong, narrow, offshore directed currents through the surf zone and start at the confluence of two opposing feeder currents. At the end of the rip current, the rip head, the velocity decreases, the flow expands and the water can flow onshore again between rip currents (Masselink et al., 2014). Under obliquely incident waves the cell-circulation can also become obliquely.

Under mild wave conditions and with an existing intertidal bar a longshore current might also be driven by the morphology of such a bar trough. As the bores and swashes supply water into the intertidal bar trough, and the water cannot easily flow back, the water will flow towards the nearest rip channel/outflow channel out of the trough (Masselink et al., 2006).

2.2 Subtidal bars

Subtidal bars are sandbars located under the low tide water level (Figures 1 and 14) and important to take into account when studying coastal dynamics. Subtidal bars can spatially alter wave conditions further landward, affecting beach morphology and, in turn, the growth and erosion of dunes. As subtidal bars can influence the behaviour of intertidal bars/beach, they are an important factor for this research to take into account. Although this research will not include observations about the dynamics of subtidal bars, it is important to know subtidal bar behaviour and to realise how this can influence onshore wave characteristics and, therefore, morphological evolution of the intertidal beach. The coupling mechanisms will be treated in section 2.4.

Bars usually migrate offshore during storm conditions and onshore during mild wave conditions. During the offshore migration the bar becomes more straight and longshore homogenous. But during the onshore migration a bar usually becomes longshore variable and forms three-dimensional structures, for example, crescentic shapes and rip channels (Aagaard et al., 2008). If the low energetic waves prolong the bar may weld to the shoreline, filling in the trough landward of the bar. Based on the morphology a beach can be classified as being in a certain state.

The standard classification for beach states is the one invented by Wright & Short (1984). They based their classification on observations of inner bar and beach morphology. There are six distinct beach states, ranging from the, most 'up-state', longshore uniform two-dimensional dissipative beach state, through the increasingly three-dimensional states, to the, most 'down-state', two-dimensional reflective beach state (Figure 11). With a typically decrease in wave energy conditions from the high energy wave conditions in the 'up-state' to the prolonged low energy wave conditions in the 'down-state' (Wright & Short, 1984).

The intermediate states are divided based on the separation between sandbar and shoreline and the degree of coupling between bar and beach. A beach in a certain state can change to another beach state and the 'direction' (up-or down-state transition) of the change depends on the incident wave energy. During storms the sandbar moves offshore and the morphology changes to a more longshore continuous trough (separation between bar and beach), so an 'ups-state' transition, whereas a 'down-state' transition, with onshore movement of the bar, usually occurs under lower incident wave energy conditions. The 'up-state' transition is relatively quick while the 'down-state' transition is rather slow (Van de Lageweg et al., 2013).

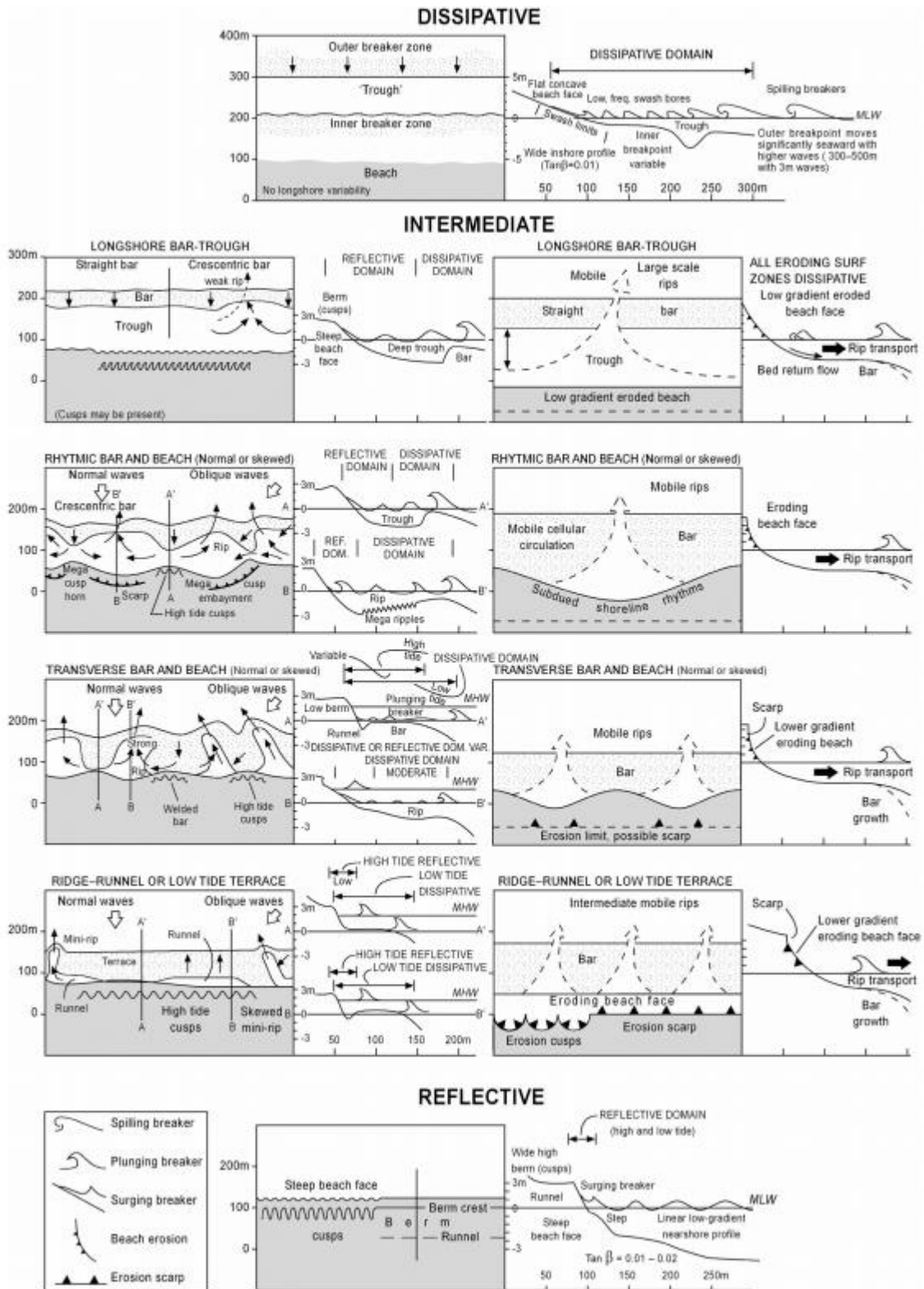


Figure 11: Wave-dominated beach types (states) (from Short, 2006).

The study from Price & Ruessink (2011) suggest an expansion of the classification of beach states. Next to the already recognised beach states; dissipative (D), longshore bar and trough (LBT), rhythmic bar and beach (RBB), transverse bar and rip (TBR), low tide terrace (LTT) and reflective (R), where the first and the last states are end members, they identified two extra intermediate bar states; the erosive transverse bar and rip (eTBR) and the rhythmic low tide terrace (rLTT) (Figure 12). In the case of transition towards an eTBR state the bar is going through an erosional sequence where the barline straightens fast and the trough becomes more continuous as erosional (and oblique) rip channels start to develop (Price & Ruessink, 2011; Short, 2006). The inner bar was often in a rLTT state which is an LTT state with a quasi-rhythmic barline, where the alongshore variability was related to that of the outer bar, indicating some sort of morphological coupling (Price & Ruessink, 2011).

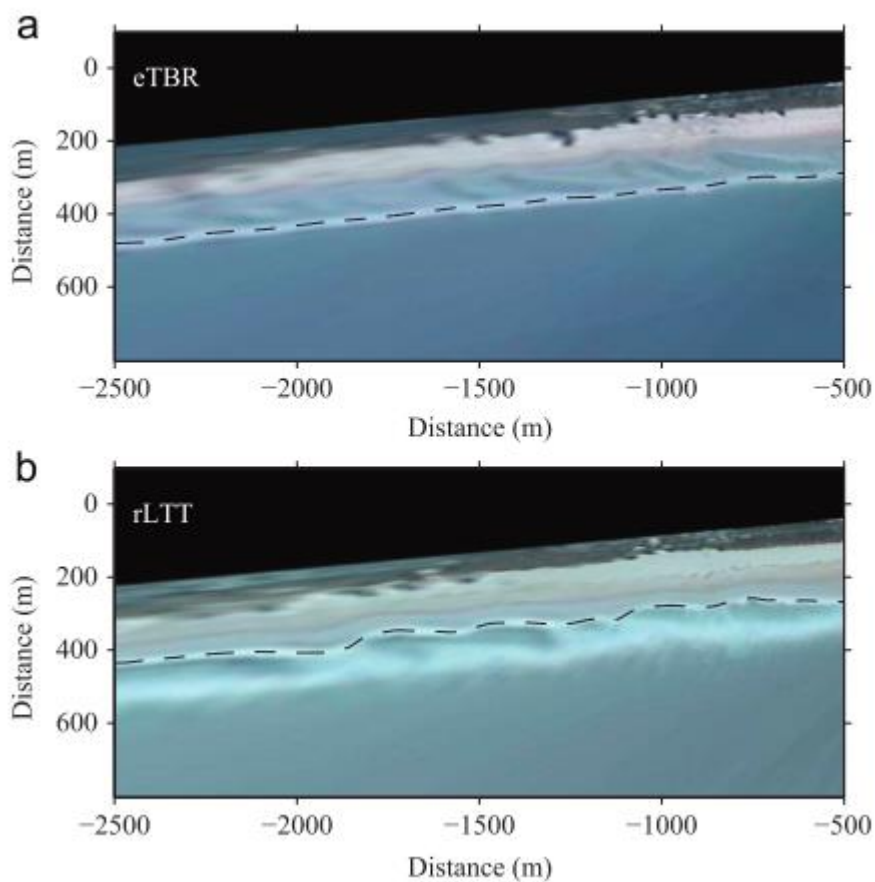


Figure 12: (a) The outer bar in the eTBR state. (b) The inner bar in the rLTT state. The dashed line indicates bar crest. Figure from Price & Ruessink (2011).

Contradicting to what Van de Lageweg et al. (2013) suggested, Price & Ruessink (2011) found that high energy wave events led to abrupt state transitions but did not necessarily corresponded to up-state transitions. Furthermore, they found evidence for a forcing of up- and down-state transitions by the angle of wave incidence. Where up-state transitions coincided with incident wave angles larger than 30° and down-state transitions with angles smaller than 30° . The alongshore currents play a large role in bar straightening (up-state transition) and the observed TBR-eTBR-LBT sequence indicates this (Price & Ruessink, 2011). Not only high-energy wave conditions will straighten the barline, but also sufficient strong alongshore currents might cause this. High-energy wave conditions with shore-normal incidence waves caused a down-state transition, indicating that the occurrence of horizontal cell circulation (which only occurs during shore-normally incidence wave conditions) might

control the state transitions under high-energy wave conditions (Aagaard et al., 2006; Aagaard et al., 1998; Price & Ruessink, 2011).

2.3 Intertidal bars

2.3.1 Types

Intertidal bars are situated in the intertidal zone; the area between the mean low and high-water levels (Figure 1 and 14). The whole intertidal bar system is the bar and its landward trough (Masselink et al., 2006). The bars are significantly important in the exchange of sediment between the beach and the shoreface (Aagaard et al., 2008), as they can migrate in both the on- and offshore direction. They are highly dynamic morphological forms responding rapidly to changes in incoming wave conditions. In general, intertidal bars are roughly parallel to the shore and occasionally forming rip channels and crescentic forms. The amount of intertidal bars on one beach varies from 1 to more than 10 and their dimensions are about 0.5 m in height, 20 m in cross-shore length and 100 m in longshore length (Masselink et al., 2006).

Masselink et al. (2006) distinguished between three types of bars (Figure 13): The slip-face bars, the low-amplitude bars and the sand waves, with increasingly more bars in the cross-shore from left to right. Swash bars are a form of slip-face bars which are formed just above the high-water level (Figure 14) due to the accretion of sediment by swash motions (e.g. Bar 1 Figure 7). General accretion and onshore migration of swash bars are caused by onshore mass transport at gravity wave frequencies along with a water circulation system on the intertidal beach, which includes a water drainage system where the water is channelled alongshore in a runnel to an offshore discharge channel through the swash bar (Houser & Greenwood, 2007).

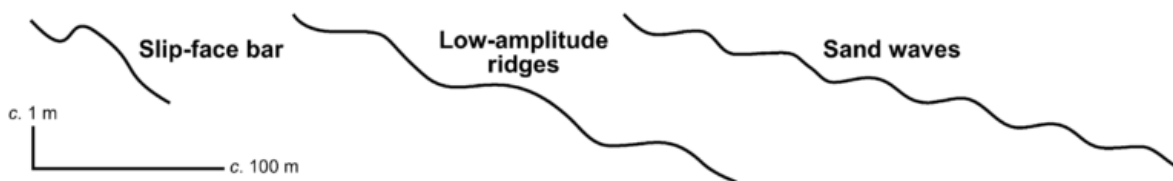


Figure 13: Illustration of the three intertidal bar types (Masselink et al., 2006).

Aagaard et al. (2006) discussed whether there is a fundamental difference between the mobile slip-face ridge and the low-amplitude ridge-and-runnel intertidal bars. Their measurements suggest that an inner surf/swash zone setting is needed to generate large sediment transport (and thus mobile bars). And they argue that at locations with a large tidal range and/or low waves such conditions will last too brief each tidal cycle to generate large migration speeds. i.e. the quasi-static ridge-and-runnel bars. This reasoning might suggest that it is possible for intertidal bars to oscillate between the two types of bars under changing conditions. The condition changes can be seasonally driven with temporal variations in larger and smaller waves, or through spring-neap tidal cycles with large and small tidal ranges (Aagaard et al., 2006). Aagaard et al. (2006) therefore suggest that it would be more reasonable to use the term intertidal bar for both bar types.

After prolonged calm wave conditions an intertidal bar can gradually develop into a berm, located landward of the wave action (Figure 14) (Masselink et al., 2006; Masselink et al., 2014). A berm is formed due to accretion of sediment caused by the welding of an intertidal bar to the supratidal part of the beach (Figure 1). Berms erode under storm conditions.

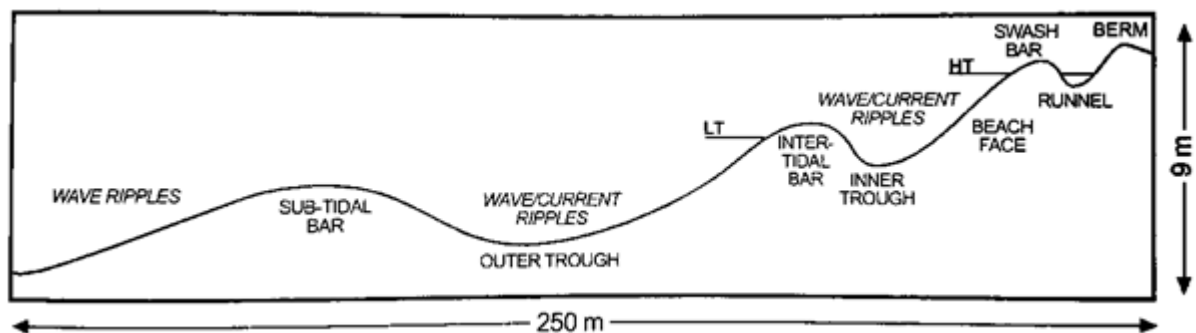


Figure 14: Schematic cross-section showing a typical beach profile. It is unlikely that all these features are present at the same time on the same beach. Figure from Masselink et al. (2014).

2.3.2 Formation

Aagaard et al. (2008) observed the formation of a nearshore bar at the beach of Vejers, Denmark. The development of the bar was linked to the generation of a trough landward of the bar. The trough is a result of a divergence in the sediment flux at that location. A little offshore of the trough location the undertow current was large, while at the trough location there was little undertow and later even an onshore current. The difference in the strength of the undertow is related to the (initially) gentler slope at this location. This caused a sediment transport divergence which excavated the trough. A sediment convergence was also measured just offshore of the trough, where the undertow was initially strong (breaking waves). But onshore sediment transport, just offshore of that location, was generated by skewed waves (before wave breaking). Resulting in a convergence of sediment and thus the formation of the bar crest (Aagaard et al., 2008).

2.3.3 Morphodynamics

Intertidal bars

Onshore intertidal bar migration may be caused by the exposure of the bar to shoaling waves (as discussed before; net onshore current under shoaling waves), so when the bar is located just seaward of the surf zone. Also in the surf zone an intertidal bar is commonly associated to be able to migrate onshore if the waves arriving at the bar are low to medium energetic (weak undertow) (Aagaard et al., 2008). But the most likely mechanism of onshore bar migration is due to swash processes (Masselink et al., 2006). When waves break on the seaward slope of the bar and the swash washes over the bar crest during the up-swash, sediment is brought over to the other side. As water cannot flow back easily in the form of the down-swash, due to the trough, the sediment is deposited on the landward side of the bar. The swash processes will be most effective in causing an onshore bar migration when the bar crest is elevated just above the high tide level, guaranteeing that many swashes will overtop the bar crest (Masselink et al., 2006). The observations from the study from Kroon & Masselink (2002), however, suggest that swash action is not the dominant process in causing onshore migration of intertidal ridges (multiple bars) in macrotidal settings. Moreover, the results show that surf processes were the most responsible for the onshore migration in this setting.

Offshore bar migration generally happens under high energetic wave conditions (Aagaard et al., 2008) when the significant breaker height at the bar exceeds 0.4 m according to Masselink et al. (2006). Under these conditions the undertow is strong enough to cause a net offshore sediment transport, and thus an offshore bar migration. Although, when there is a three-dimensional intertidal bar morphology, the return flow will go through the rip channels instead of over the bar and a horizontal cell circulation pattern might form. Consequently, an onshore migration of the bar may still prevail (Aagaard et al., 1998). Such an onshore migration of an intertidal bar along with a

horizontal cell circulation pattern (including rip channels) has also been studied by Aagaard et al. (2006). They estimated sediment fluxes across an onshore migrating intertidal bar by combining cross-shore and longshore current velocities and sediment concentration measurements. During the onshore migration of the bar, the landward runnel was filled in, changing the morphology and, due to feedback (Figure 2), the hydrodynamics. The study provided evidence for a change in sediment flux. At the beginning of the measurements the sediment was transported shoreward by the swash processes and by the oscillatory flows of both short and long waves under surf-zone conditions, to be deposited on the beach face of the bar (Aagaard et al., 2006). Due to the presence of the runnel the water was channelled alongshore in the runnel, reducing the offshore component. Figure 15 shows the mean onshore current measured at the top of the bar (measuring point 4) measured by Aagaard et al. (2006). This transport asymmetry led to a fast migration of the intertidal bar and, once the runnel was completely filled in, a welding of the bar to the beach. With the disappearance of the runnel the mean cross-shore current and sediment flux turned around and became offshore directed as the water was no longer channelled alongshore (Figure 15). To summarise, with the presence of the runnel and rip channels there was a horizontal circulation pattern, with an onshore sediment flux above the bar. After the runnel had been filled in an offshore directed undertow developed, leading to a vertical circulation pattern (Aagaard et al., 2006).

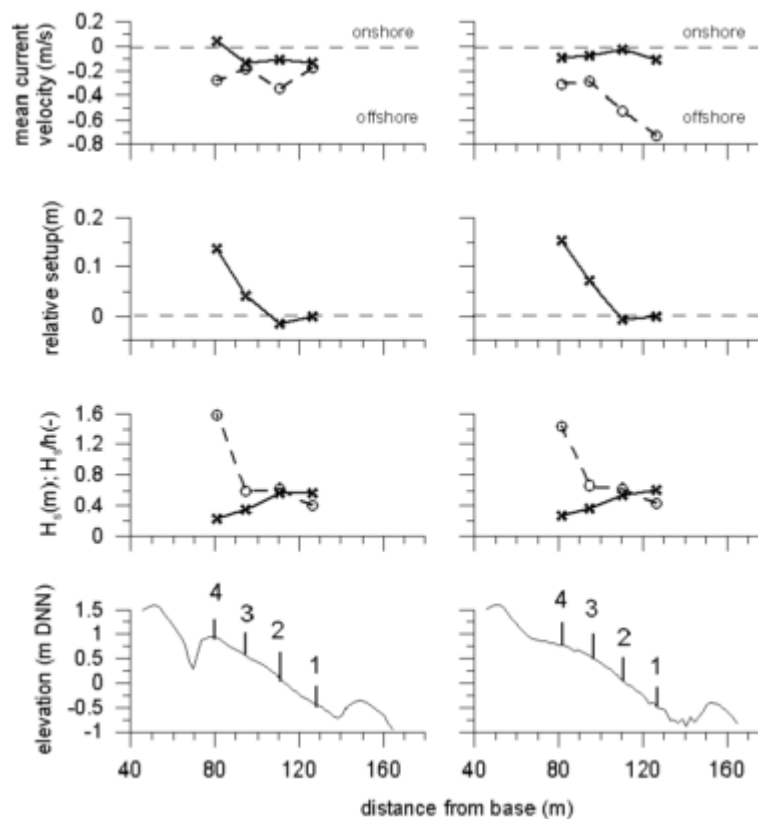


Figure 15: Hydrodynamics recorded during two high tides. The left tide is before the infilling of the runnel, the right tide is after the infilling of the runnel. From the top down, the panels illustrate; cross-shore (solid lines) and longshore (dashed lines) mean currents, relative mean water level setup, and significant wave heights (solid lines) and relative significant wave height (dashed lines). The beach profiles are shown in the bottom panels for reference. Figure from Aagaard et al. (2006).

Houser & Greenwood (2007) have monitored a reversal in intertidal swash bar migration direction during little change in offshore wave height from one tidal cycle to the next one. The conditions are normally associated with offshore bar migration. During the first tidal cycle, they witnessed that the water level was too high for wave breaking to occur on the seaward slope of the bar. Instead, the

waves broke at the bar crest, or landward of it, forcing an offshore sediment transport by the undertow. During the second tidal cycle, water levels were lower and waves breaking occurred on the seaward slope of the bar, leading to an onshore migration of the swash bar. Houser & Greenwood (2007) also found that during the second tidal cycle the re-suspension of sediment was mainly limited to the onshore phase of infragravity oscillations. Individual gravity waves passed as surf bores which re-suspended the sediment. The wave heights, oscillatory velocities and skewed accelerations were larger during the onshore phase of the infragravity waves. Due to the larger water depths during the onshore phase of the infragravity waves, the gravity waves heights were able to increase (Abdelrahman & Thornton, 1987). The larger skewed accelerations compared to those during the offshore phase of the infragravity waves were able to bring more sediment in suspension and therefore it is logical that there was more onshore sediment transport by the infragravity waves (Houser & Greenwood, 2007).

To sum up, the study from Houser & Greenwood (2007) point out the strong tidal influence on the hydrodynamics and bar evolution. Where the direction of migration and the point of wave breaking are dependent on the water depth. Their results suggested a divergent bar migration response with respect to position of wave breaking (Houser & Greenwood, 2007). Larger re-suspension by gravity waves due to their larger skewed accelerations during the crest of infragravity waves led to an onshore sediment transport.

The dependence on the position of wave breaking relative to the bar crest has been recognised before by Sunamura & Takeda (1984). They stated that when a bar migrates onshore, wave breaking must occur on the seaward slope of the bar. They also stated that the bores (formed after the breaking of waves) which advance over the bar, transport the sediment onshore. This process is a slightly different than the one proposed by Houser & Greenwood (2007), who stated that the onshore sediment transport is mainly due the larger amount of suspended sediment (re-suspended by the bores) during the onshore phase of the infragravity waves, which than transport the sediment onshore.

Intertidal bars, like subtidal bars, show a cyclic behaviour throughout their existence. Intertidal bars often are formed around the low tide coastline and migrate onshore under mild wave conditions until they eventually weld to the high-water line. During their existence, they can also migrate offshore, this 'setback' is generally caused due to storm conditions.

Quartel et al. (2007) monitored the behaviour of an intertidal bar for 15 months. The alongshore averaged boundary positions showed a sort of cyclic behaviour where they first gradually migrated onshore after which they experienced a sudden seaward shift (Figure 16). This 'sawtooth' motion had a period between 1 and 4 months (Quartel et al., 2007). The sudden seaward shifts were caused by storm events which lasted longer than 30 hours, had a $H_{rms} \geq 2$ m, an offshore surge level ≥ 0.5 m and a bar trough of less than 20 meters wide in the pre-storm morphology. The onshore migration occurred during low to intermediate energetic conditions.

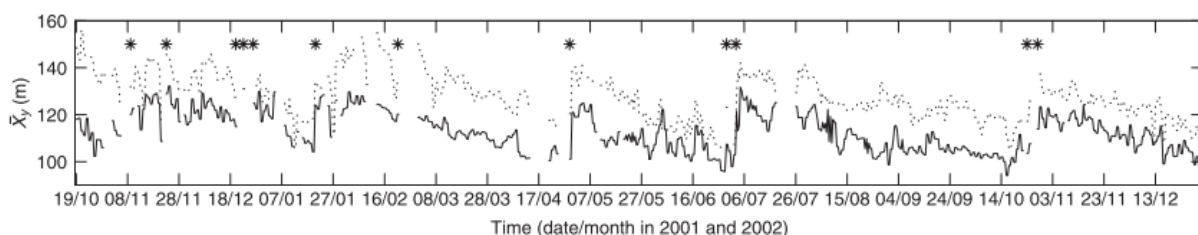


Figure 16: Time series of cross-shore positions of the landward boundary of the intertidal trough (solid line) and bar (dashed line). The stars mark storm events. Figure from Quartel et al. (2007).

Welding of the bar to the high water line was not observed by the study from Quartel et al. (2007). They hypothesised that the agger, a period within the tides with no sea level change, initiates a long residence time for vertical bar growth processes on bars which had already experienced some onshore migration. This might have resulted in relatively longer periods of bar growth processes than bar migration processes during one tidal cycle. And when this is the case the cross-shore bar position is more stable.

Finally, when studying the behaviour of intertidal bar-trough systems, the dynamics of the bar and trough need to be examined separately (Quartel et al., 2007). This is because the bar and trough might behave differently, where the landward boundary of the bar is likely to be more dynamic than that of the trough.

Intertidal beach

The shoreline generally behaves the opposite to the (subtidal) sandbars in terms of migration direction. Onshore shoreline movement (erosion) is associated with a period of higher waves which erode the beach, and offshore movement (accretion) is associated with a period of lower waves which deposit sediment on the beach (Van de Lageweg et al., 2013; Yates et al., 2009) or cause welding of a bar to the beach. Van de Lageweg et al. (2013) set the shoreline position at +0.5 m tidal level. Off- or onshore shoreline movement (accretion or erosion of the beach) is not only dependent on the wave energy, but also on the position of the shoreline. Because, if the shoreline is already further onshore (in its eroded shape), waves have to be higher in order to erode the shoreline and vice versa (Van de Lageweg et al., 2013). This behaviour is related to the fact that shorelines that already suffered from erosion have run out of easy available sand on the beach face to be eroded, slowing the erosion rate, whereas beaches which accreted already have depleted the amount of offshore available sand, slowing the accretion rate (Yates et al., 2009). The magnitude of the incident waves over a certain period is essential in determining the shoreline (and sandbar) response. Since, there is a non-linear relation between shoreline (and sandbar) variation and wave height (Southgate, 1995), suggested by the dependence on absolute shoreline position (Van de Lageweg et al., 2013). Wave height conditions which cause no erosion and no deposition are called 'equilibrium wave height' (Yates et al., 2009).

Quartel et al. (2008) investigated seasonal variability in cross-shore positions of the high-, mean- and low- tide contours. They also looked at the beach width and volume and studied the dependency on the offshore wave conditions. At the end of winter the beach was wide with a small volume due to the more intense and frequent storm events, while during summer the beach became narrower with a large volume (Quartel et al., 2008). At the beginning of winter the three contour lines straightened, simultaneously the dunefoot shifted landwards and the mean low water line shifted seawards. Consequently, the beach profile became flatter during winter. The steepening in summer is caused by the gradual landward migration of the mean low water line, due to a lack of wave breaking resulting in more influence by shoaling waves relative to the undertow (section 2.1). Along with a small influence of the seaward migration of the dunefoot. Concluding, the seasonal pattern is mainly caused by sediment exchange in the cross-shore between the supratidal and lower-intertidal part of the beach (Quartel et al., 2008).

These findings contradict with those from Van de Lageweg et al. (2013) (discussed above) who suggested that the shoreline would migrate onshore, making the beach narrower, under high-energetic wave conditions and vice versa. Also Quartel et al. (2008) found only a weak relation between beach width and volume, indicating that erosion/accretion are not the equivalent to

onshore/offshore shoreline migration. Processes responsible for these contradicting results are still to be found.

Quartel et al. (2008) also witnessed the welding of an intertidal bar to the supratidal beach at the beginning of summer, recorded as an abrupt seaward migration of the mean high-water line and a succeeding decrease in the intertidal beach width.

Aagaard et al. (2005) found that at their study site, under longshore uniform offshore storm wave conditions, there was not a longshore uniform response of the beach. At locations where the beach slope was steeper there was a significant amount of erosion found. Whereas, on a more gently sloping part of the beach, there was a net offshore sediment transport found under surf zone conditions at high tide, which was compensated by onshore sediment transport under swash zone conditions at low tide. Hence, no significant beach change on the gentle sloping parts of the beach. When the steeper parts erode, the beach slope will become more gentle, consequently the amount of erosion becomes less on the gentler beach slope. This suggests a negative feedback between initial beach slope and net sediment transport patterns (Aagaard et al., 2005). Aagaard et al. (2005) suggest two reasons for these differences in sediment balance. Firstly, under surf zone conditions, during high tide, the offshore sediment transport is larger at the steeper slope, which is expected as the undertow is dependent on the wave height and beach slope. Secondly, the breaker type might have an influence in the sediment transport balance. Plunging breakers at the steeper beach generate higher suspended sediment concentrations and therefore larger offshore sediment transport by the undertow. This indicates that the shoreline can respond differently alongshore to certain wave conditions due to the adjacent occurrence of different beach slopes, as dissipative beach states are generally quite stable, whereas steeper slopes are often prone to erosion (Aagaard et al., 2005).

Furthermore, a longshore irregular intertidal bar and two subtidal bars were situated at the study site from Aagaard et al. (2005). These bars might have altered the incoming wave conditions in such a way that the incident waves when arriving at the beach were not longshore uniform and therefore resulted in different erosion/accretion balances. This 'coupling' between bars and beach will be discussed in the next section (section 2.4).

2.4 Morphological coupling

2.4.1 Bar-beach-dune coupling

Daily to weekly spatially and temporally variable beach response is not caused necessarily by day - to week-averages of offshore wave conditions, though by different beach morphology prior to a storm event as well as alongshore variables in beach morphology (Quartel et al., 2008). Furthermore, an alongshore variable beach response can be caused by self-organizing (Coco & Murray, 2007) and template mechanisms, caused by positive/negative feedback processes (self-organizing) and differences in the morphology of further offshore positioned bars (template) (Castelle et al., 2010a). The latter is further elaborated in this section.

This coupling between a sandbar and the shoreline can be expressed in a certain degree of coupling. Where a 180° , out-of-phase, coupling is defined when the beach embayments coexist with the crescentic bar bays (which extend towards the sea), and a 0° , in-phase, coupling is defined where the beach embayments coexist with the horns of the crescentic bars (extend towards the coast) (Sonu, 1973).

Possible, and suggested, processes affecting coupling between sandbar and shoreline are; water depth variability along the crescentic sandbar, the angle of wave incidence and the cross-shore

distance between sandbar and shoreline (Van de Lageweg et al., 2013). The water depth at the (crescentic) sandbar is an important steering factor as it is alongshore variable. Therefore, the wave height will be alongshore variable and, as a result, water circulation patterns (e.g. rip channels) come to existence. The phase of the coupling is mainly affected by the angle of wave incidence, as circulation patterns can result in meandering currents along the shoreline if the incident waves arrive at an sufficient angle relative to the shore normal (Price & Ruessink, 2013). If the angle of wave incidence becomes too large the sandbar variability is wiped out (i.e. no coupling any more) by strong longshore currents. And finally the distance between sandbar and shoreline influences the degree to which sandbar patterns govern the shoreline patterns (Wright & Short, 1984). The role and development of these coupling patterns in determining the evolution of beach states remains a difficult problem as it depends on wave transformation, wave breaking, wave driven currents and the morphology of sandbar and shoreline (Van de Lageweg et al., 2013). Van de Lageweg et al. (2013) state that quantitative observations regarding sandbar-shoreline coupling and the temporal variation in that are needed to advance the theoretical modelling.

The coupling mechanism of double bar systems is studied by Castelle et al. (2010a, 2010b), who introduced a 'novel mechanism that blurs the distinction between self-organization and template mechanisms' (Castelle et al., 2010a). They found that the initial development of coupling patterns is driven by wave refraction and depth-induced wave breaking over the outer-bar. These influence the shoreward variations in wave energy, and thus, longshore variations in set-up which force horizontal circulation patterns over the inner-bar. So the initial erosion and accretion at the inner bar are linked to the geometry of the outer bar (Castelle et al., 2010a). The main conclusion of their research was that the inner-bar morphological patterns are controlled by the relative importance of wave focusing by refraction versus wave breaking over the outer-bar. When wave refraction is the dominant process, there is wave energy focusing shoreward of the outer-bar horns (landward perturbation of the bar). This results in a higher set-up at these locations and thus the development of a circulation pattern with rip channels formed at the location of the outer-bar crescent, which is an in-phase coupling (Figure 17). For a large outer-bar wave length, λ , the onshore flows at the inner-bar are separated sufficiently to form two rip channels in one outer-bar crescent.

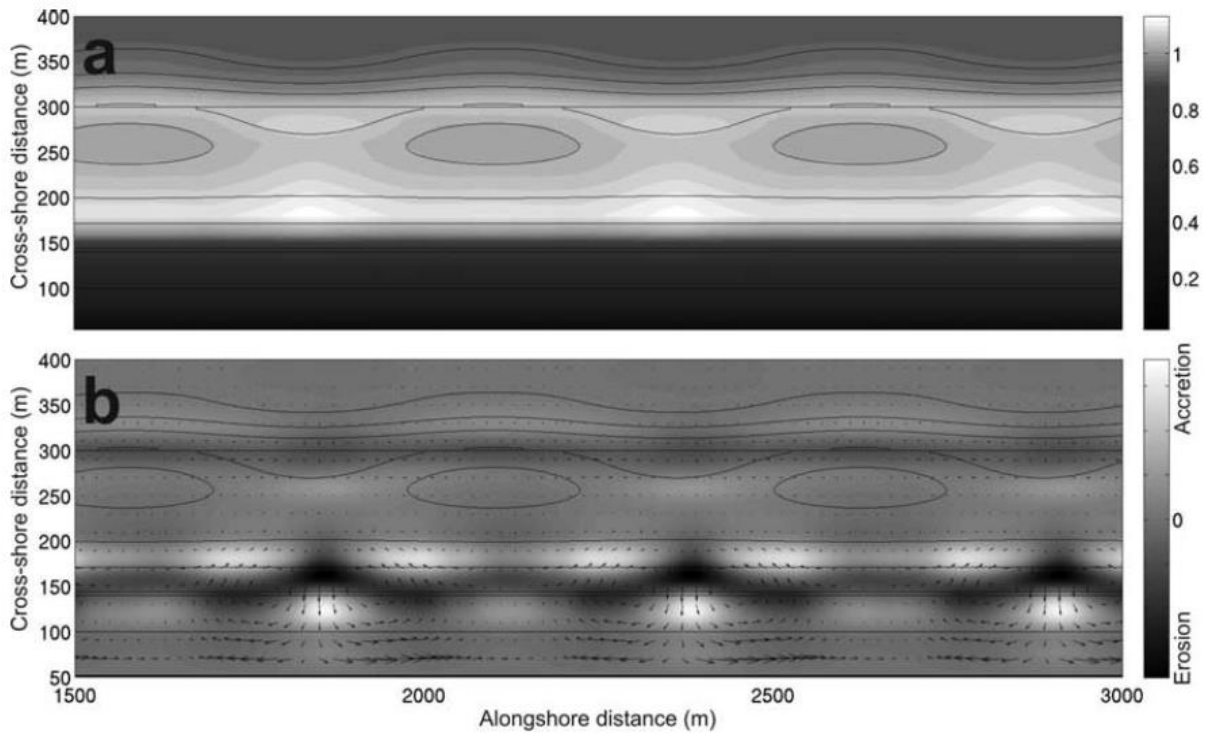


Figure 17: (a) Significant wave height. (b) Resulting wave induced current and erosion/accretion patterns, showing an in-phase coupling and two rip channels at each outer-bar crescent (from Castelle et al., 2010a).

On the other hand, if wave breaking is the dominant process, then the wave energy shoreward of the horns is lower, and thus there will be less set-up at these locations. This results in the development of a rip channel over the inner bar at the location of the outer-bar horn, which is a 180° out-of-phase coupling (Figure 18). Finally, the larger the outer-bar wavelength the harder it is for wave focusing to dominate over wave breaking (Castelle et al., 2010a, 2010b).

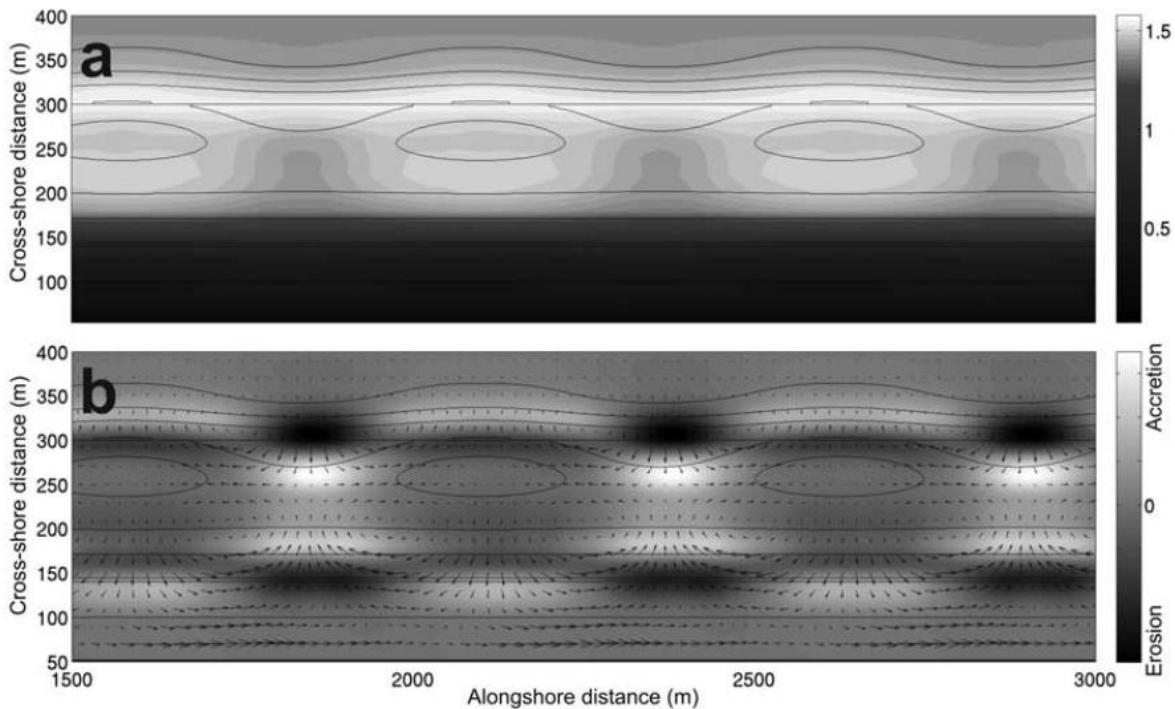


Figure 18: (a) Significant wave height. (b) Resulting wave induced current and erosion/accretion patterns (from Castelle et al., 2010a).

The alongshore variability in inner-bar rip channel is a mixture of self-organising and morphological coupling, and therefore morphological coupling is more important to understand, than previously thought, to predict the evolution of rip channels (Castelle et al., 2010b). The presented concept from Castelle et al. (2010a, 2010b) has never been measured in the field due to a lack of hydrodynamical data. This includes that their hypothesis is still to be tested with real field data.

The role of tides on the coupling effects may be significant as the variation of mean water level above the outer-bar can result in a change in the relative importance of wave breaking and wave refraction. Consequently, a change in horizontal circulation patterns, hence a change in rip channel development, can occur at the inner-bar. This means that the coupling patterns in meso- to macro-tidal environments are more complicated than the idealized scenario from Castelle et al. (2010a, 2010b). This can lead to an alongshore variability in the rip channels. Moreover, further investigation is needed to determine the effects of tidal range on the rip channel development and alongshore variability. As well as the influence of it on the self-organization and coupling mechanisms (Castelle et al., 2010b).

Price & Ruessink (2011) reflect that to sufficiently study inner bar dynamics (or the intertidal beach dynamics), the outer bar geometry, offshore wave conditions and the fraction of wave energy dissipation over the outer bar (i.e. the resulted wave conditions after alteration by the outer bar) should be taken into account. They suggest that future research should involve the classification of coupling between outer and inner bar and further investigation of coupling processes using numerical modelling. Furthermore, they state that studying inner bar dynamics should involve the measuring of wave breaking over the outer bar.

Spatial dune variability

Spatial variability in dunes is a phenomenon which is important to understand because places where dunes are less developed are more prone to be damaged by storm events. Spatial variability can be related to local morphology variations of the; inner-shelf geology, sandbars, beach morphology and beach width (Keijsers et al., 2014). Keijsers et al. (2014) found that beach width mainly controls the amount of dune erosion, namely dunes at narrow beaches erode more frequently than dunes at wide beaches. Moreover, they found that erosion is the main factor in alongshore variability of dune-volume changes. So, the beach width is correlated to the dune-volume changes, with weaker dune development on narrower beaches. This is also recognised by Castelle et al. (2015), who found that the locations of maximum dune erosion were coupled to the locations with the narrowest beach, the embayments of megacusps (Figure 19). Castelle et al. (2015) further state that the morphological forcing template coupling is important to understand for predicting erosional hot-spots in the future. Hence, it is important to study the bar-beach-dune coupling in detail to predict the development of the dune and to anticipate on possible 'weak spots'.

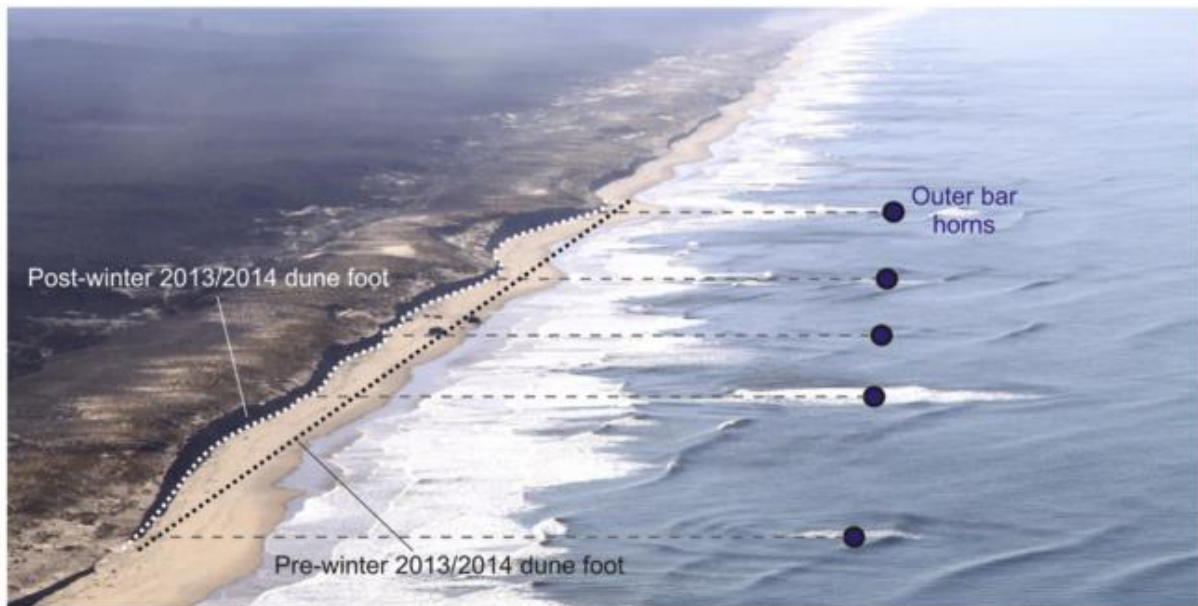


Figure 19: Aerial photograph indicating alongshore variability in dune erosion, where the megacusp horns are coexistent with the outer-bar horns (Castelle et al., 2015).

2.4.2 Alongshore differences in swash

Due to changes in the beach slope at the mean swash location and alongshore patterns in wave breaking over sandbars (energy dissipation), there can be an alongshore variability in swash motions. Observations by Guedes et al. (2012) indicate that the variations are mainly driven by variations in the beach slope. However, when tidal water level variations were also accounted for, the wave breaking on the bar became dominant in controlling the swash height. Guedes et al. (2012) observed an alongshore variation of up to 78% in significant run-up height and was primarily driven at incident wave frequencies. Even though the alongshore changes in beach slope and variability in wave breaking over the bar were distinctively related, Guedes et al. (2012) needed both variations to provide the best fit of alongshore changes in significant run-up height. The infragravity frequencies played a minor role in the alongshore variability of the swash. At these frequencies there was no real correlation between alongshore variations and beach slope or wave breaking patterns. But swash variability might have been caused by edge waves.

More research and data gathering about alongshore variability in swash motions and the accompanying beach development must be done in order to provide better process understanding and future beach changes (using models).

3. Research aims

Aagaard et al. (2005) already touched upon the unanswered question of how and when the sediment is restored on a beach with a quasi-equilibrium slope, after this has been eroded by storms. In other words: which processes are involved in the sediment transported onto the beach in mild weather conditions, and where/when do these processes take place on the intertidal beach? Furthermore, it is a major issue to model sediment transport on intra-wave time scales, while a significant fraction of the cross-shore transport may be due to waves (Aagaard & Jensen, 2013). These time-dependent sediment concentrations might be significantly different for different wave types.

Van de Lageweg et al. (2013) conclude that the role and development of the coupling patterns in the beach evolution remains a difficult problem as it depends on so many factors (wave transformation, wave breaking, wave driven currents and the morphology of sandbar and shore line). They therefore

state that quantitative observations regarding sandbar-shoreline coupling generation and the temporal variation in that are needed to advance the theoretical modelling. Furthermore, Van de Lageweg et al. (2013) and Quartel et al. (2008) found contradicting results in the behaviour of the beach in terms of beach width and volume changes under certain wave conditions (section 2.3.3). But process/reasons for these contradicting results are still not clear and, therefore, also more insight in intertidal beach behaviour should be acquired.

Moreover, the discussed morphological template concept (*2.4 Morphological coupling*) from Castelle et al. (2010a, 2010b) regarding the morphological coupling, has not yet been studied in the field. Their hypothesis, that the onshore morphological patterns are controlled by the altering of the wave field through subtidal bars, is still to be tested due to a lack of hydrodynamical data. In addition, Castelle et al. (2010b) state that the understanding of the morphological development of bars, and predicting rip channel dynamics, is important for shoreline evolution, localised beach and dune erosions and safety issues. So further detailed research in the dynamics of the intertidal beach is needed. Especially during low-energetic wave conditions. Also, a better understanding of alongshore variable swash processes is needed as well as the accompanying beach development.

Observations and measurements of the hydro- and morphodynamics are needed to provide better process understanding. This can improve the existing intertidal beach and shoreline morphological evolution models, which are important for predictions of beach evolution in the future.

In order to provide more information regarding some of the understudied processes/mechanisms described above, the aim of this MSc research is to unravel the alongshore variation in morphological development of the intertidal beach in relation to the incident wave conditions after crossing the subtidal bars during low-energetic wave conditions.

The main research question is: How does the intertidal beach behave spatially and temporally during a period of mild weather conditions?

This main research question can be subdivided into the following:

- What is the alongshore evolution of the intertidal beach morphology from days to weeks?
- To what extent is the incident wave energy at the low tide coastline alongshore variable and is there a coupling with the morphological evolution?

My hypothesis is that the morphodynamics of the intertidal beach will be governed by the incident wave conditions. And that, during consistent low energetic conditions and the presence of a crescentic subtidal bar, the development of the intertidal beach will be coupled to the morphology of the subtidal bar and, consequently, also to the wave conditions arriving at the intertidal beach. This morphological coupling would follow the morphological template concept proposed by Castelle et al. (2010a, 2010b) (section 2.4).

To accomplish the aims, this research also consists of a fieldwork campaign (*Chapter 4*). During this fieldwork, the bathymetry/topography, and changes herein, of the intertidal beach were observed under mild weather conditions for 3 weeks. The incident wave conditions were also measured at the seaward border of the intertidal beach, this was done to take the effects of subtidal bars into account. The changes in bathymetry along with the wave conditions have been analysed (*Chapter 4*) and the results are presented in chapter 5. Possible processes behind the development of the intertidal bar/beach under these conditions will be discussed, along with possible coupling mechanisms (*Chapter 6*).

4. Methods

4.1 Study site

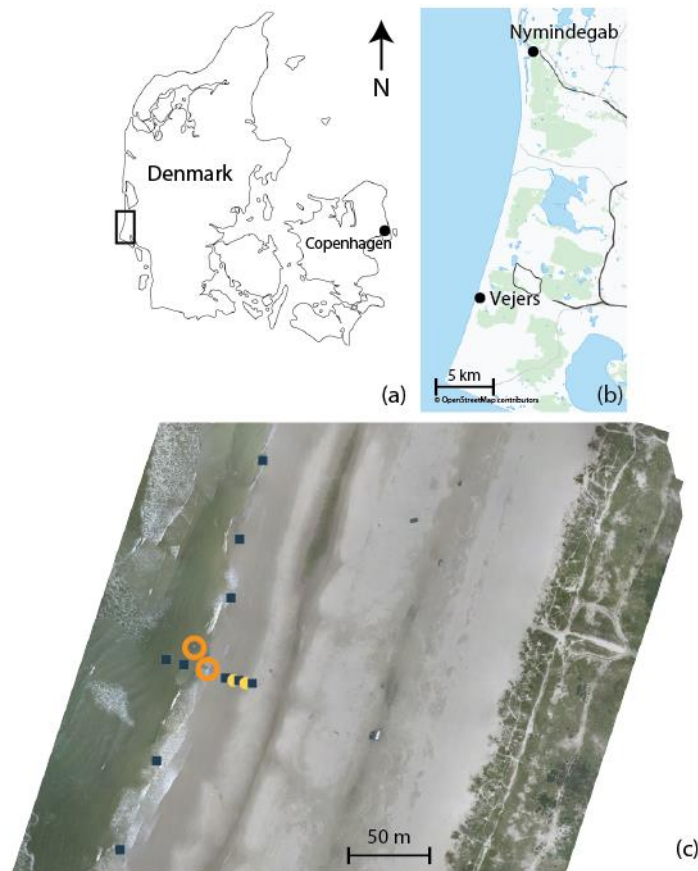


Figure 20: The locations of the study area in Denmark (a), the fieldsite at Vejers and waverider buoy Nymindesgab (b) and an orthophoto of the study area during low tide (c). The symbols in (c) indicate the locations of the instruments: the cross-shore and alongshore OSSIs (blue squares), the large-frames (orange circles) and the mini-frames (yellow circles).

The data for this research was collected during a field experiment, which took place at the beach near Vejers, on the exposed North Sea coast of Denmark (Figure 20), between September 18 and October 10, 2016 (a period of 23 days). The yearly average offshore significant wave height of this beach is 1.3 m and the mean wave period is 4.3 s (Aagaard, 2011). Tides are semidiurnal, ranging from approximately 0.6 m (neap) to 1.2 m (spring). The upper shoreface consists of sand with a mean grain size of about 180 μm (Aagaard et al., 2008). The mean slope of the upper shoreface is 0.006 and the nearshore usually consists of a three to four bar system. The bars show a net offshore migration, at a rate of 45-75 m/yr, and decay in approximately 6 m water depth, which is about 900 m from the shoreline. The beach accretes approximately 6-7 $\text{m}^3/\text{m}/\text{yr}$ due to a gradient in alongshore sand transport by wave-driven currents and the typical beach width is about 150 m (Aagaard, 2011; Aagaard et al., 2008). The shore-normal is oriented 288° with respect to the north (Figure 20). The area which was studied stretches about 300 m alongshore and from the dunes to approximately -1 m below mean sea level, cross-shore.

4.2 Data

4.2.1 Morphological data

To measure the alongshore variability in intertidal beach development (first sub-question) a RTK GPS system was used to gather morphological data of the intertidal beach. Elevation measurements were done every day during low tide. However, these measurements only started on day 3 of the

campaign. Point measurements were used to make cross-sections of the intertidal beach at each alongshore location of the OSSIs up until the 25th of September (day 8). These point measurements were continuously done throughout the campaign at the location OSSI 3, but not at the other OSSI locations. From the 26th of September (day 9), until the end of the campaign, the intertidal beach was surveyed with the RTK GPS system coupled to a one-wheel-stick. This enhanced the speed of elevation measurements, which made it possible to survey most of the intertidal beach. The settings of the RTK GPS system were changed to a continuous topographic measurement, to make one measurement point every second. This negatively influenced the precision of the measurements. Because, during point measurements the points were determined by averaging the location over a couple of seconds, while during the continuous topographic measurements this was not the case. Furthermore, it was more difficult to keep the RTK GPS system perfectly straight while using the one-wheel-stick. The surveyed area stretches alongshore from about 150 m north to 150 m south of the cross-shore array and from the dunes to approximately -1 m below mean sea level, cross-shore. During the storm (days 11-14) a large part of the intertidal beach could not be measured due to very high-water levels. With the use of a go-pro camera on top of the foredune a time-exposure image was created on some days of the campaign, by averaging 10 minutes of 2 Hz video images. This was done to estimate the locations of wave breaking, and thus the locations and alongshore variability of the subtidal bars.

Also, sand samples were taken and sieved to determine the grain size distribution.

The gathered GPS data points were rotated to a new coordinate system, where the alongshore stretch of the beach represents the x-axis, with positive values to the north, and the shore normal line represent the y-axis, with positive values seaward. The origin of this coordinate system was chosen at a position south-east of the study area. The points from the continuous topographic measurements were used to make an interpolated map of the area on a new grid of 330 x 190 m (100-430 m alongshore and 60-250 m cross-shore) with a spacing of 0.5 m in both alongshore (x) and cross-shore (y) direction, which also resulted in some loss of detail. As there was more variation in elevation in the cross-shore than in the longshore direction, the interpolated points were determined from measured points over a longer longshore than cross-shore stretch. This was done using the loess interpolation method, which applies length-scale dependent smoothing and is a fitting method for the interpolation of beach bathymetry (Plant et al., 2002). Smoothing scales used were; $L_x=80$ m and $L_y=10$ m. Furthermore, only the points every 2.5 m cross-shore and every 20 m alongshore of the grid were variable, in between those points the grid was filled with a linear interpolation between those points.

Digital elevation models of the intertidal beach, and the changes within, were made throughout the campaign. Furthermore, morphological changes during the campaign and alongshore variations thereof were quantified, by defining specific features of the intertidal beach described below (e.g. intertidal bar elevation, contour lines and beach slope; section 4.3). For day 1-8 the data analysis was focussed on the cross-sections made with the point measurements, as there was no other data available, while for the rest of the campaign the interpolated maps were used.

4.2.2 Wave data

During the fieldwork (besides the intertidal beach morphology), waves, currents, angle of wave incidence relative to the shore normal, sediment concentrations, turbulence and small-scale morphology were measured. A cross-shore array was deployed in the middle of the study area, consisting of five individual pressure sensors, Pressure sensor Ocean Sensor Systems OSSI-010-003C-1 (from now on referred to as 'OSSI'), one large-frame and two mini-frames (Figure 21). All OSSIs made continuous measurements, in burst of 30 minutes, at a 5 Hz measuring rate. The large-frame

was equipped with three vertically spaced acoustic current meters (ADV) to estimate the vertical variability in turbulent fluctuations at 10 Hz. Sand concentrations were measured with a vertical stack of five optical backscatter sensors (OBSs) for near-bed measurements (normally distributed at 0.04 – 0.17 m above the bed) and two individual OBSs were deployed higher in the water column (0.25 and 0.30 m above the bed). High-resolution circular elevation models were measured every 30 minutes using a 1.1 MHz 3D profiling Sonar 2001 to monitor bedforms. Furthermore, data loggers and batteries were included. The mini-frames were equipped with a pressure transducer, an electromagnetic flow meter (EMF) to measure horizontal velocities and three vertically spaced OBSs. The nominal height above the bed for the pressure transducers was 0.10 m, for the EMFs 0.15 m and for the OBSs 0.05, 0.10 and 0.15 m. To give an insight in the alongshore variation in wave conditions (second sub-question), an alongshore array of pressure sensors (OSSIs 1-6, with OSSI 3 also being part of the cross-shore array) was deployed along the low water line of day 2 of the campaign (September 19, 2016), both to the north and south of the cross-shore array (Figure 20). Finally, a barometric pressure sensor was installed at the field station. As mentioned, the alongshore OSSIs were deployed to measure alongshore differences in wave characteristics and collected the data which I mostly used. The cross-shore array was mainly deployed for the research of my fieldwork companions.

In summary, the instruments that I used were from the alongshore array consisting of 6 pressure sensors (OSSIs), ordered 1-6 from south to north (Figure 20), with OSSI 3 being part of the cross-shore array in the middle of the study area (Figure 21). The OSSIs were deployed on day 2 of the campaign. To be able to correct the measured pressure data with the heights of the OSSIs above the bed, the instrument heights above the bed were measured once a day during low tide and linearly interpolated in between these height measurements. If the instruments were too high above the bed or (likely to be) buried (during the next high tide), the heights were readjusted. Obviously, the bed level could change non-linearly during the high tides, altering the OSSI heights above the bed during the measurements. So, this causes possible deviations from the real bed elevations of the OSSIs and therefore the correction might be slightly off. Furthermore, offshore significant wave height data was measured by a wave buoy near Nymindegab (Figure 20) at a water depth of 16 m.

The pressure data was converted to different parameters: the total water depths, Low- and high frequency significant wave heights, peak periods and the wave spectra. To convert the data the following steps were taken. The correlation coefficient was determined in the lab for the calibration of the data. The data was corrected for the barometric pressure and the instrument height above the bed. With the use of the linear wave theory the sea surface elevation in the 0.0 to 1.0 Hz range was determined, of which the second order trend was removed. The low- and high frequency significant wave heights, peak periods and wave spectra were obtained from spectral analysis. Furthermore, the total water depth was determined as the averaged water level over one burst. This was done for every burst of 30 minutes, resulting in one outcome per parameter each 30 minutes.

These wave parameters were used to determine the hydrodynamics present at each alongshore OSSI during high water. Furthermore, the hydrodynamical conditions between the OSSI locations were compared and the alongshore differences quantified, focussed on the significant wave height and spectral energy. Unfortunately, the pressure data from OSSI 6 appeared to be unusable.



Figure 21: A side picture of the cross-shore array faced towards the north. Indicated are the instruments, with OSSI 3 located within the red oval. Instrument order from left to right: OSSI - OSSI - large-frame - OSSI 3 - mini-frame - OSSI - mini-frame - OSSI.

4.3 Data analysis

Based on the hydrodynamics the whole campaign was subdivided into three main periods (Figure 24): pre-storm (days 1-10), storm (days 11-14) and post-storm (days 15-23). Where the pre-storm period was separated into two parts based on the wave-energy spectra and angle of wave incidence: the first part (tides 1-7) and the second part (tides 8-17).

Unfortunately, the morphological measurements could not be done throughout the campaign. During the storm period the water levels became too high to fully survey the whole intertidal beach. Therefore, with the morphological analysis of the storm period, the before and after storm situations were used. Furthermore, post-storm water levels were extremely low (Figure 24b) and almost continuously below the instrument heights due to offshore directed winds, limiting the hydrodynamic data during that period (Figure 37). Hence, the hydrodynamic data of the post-storm period could not be analysed. Therefore, the focus of both the morphological and hydrodynamical analysis was on the first 14 days of the campaign (pre-storm and storm). Additionally, hydrodynamical measurements started on day 2 and morphological measurements on day 3 of the campaign.

4.3.1 Morphological data

Some parameters were determined to analyse the morphological data (Figure 22). This was done for each alongshore OSSI location as the morphological data was compared with the OSSI data.

Parameters concerning the intertidal bar: the peak intertidal bar elevation relative to the Danish Vertical Reference 1990 (DVR90) (z_b), the height of the bar based on the landward trough (h_b) and the cross-shore position of the bar (X_b). Additional parameters: the cross-shore location of the 0-meter elevation bed level relative to DVR90 ($z=0$), the seaward slope of the bar (β) which is calculated and analysed as the ratio of the slope: $1/xx$ (the slope is expressed as 1 meter elevation change over xx m cross-shore distance), and the volume of the intertidal beach (V). As the shoreline had a crescentic shape, the same relative cross-shore area for each OSSI had to be taken when

determining β and V . Therefore, the ranges were determined around the $z=0$ contour point for each alongshore OSSI location. The β was determined between the peak of the bar and 5 meters landward of $z=0$. This was done to determine the intertidal slope seaward of the bar while excluding the gentle sloping part of the lower intertidal beach for all the OSSIs, making the results more comparable. The landward end of the volume range ($z=0 - 30$ m) was determined as such that it would include the sediment volume under the bar crest for all the OSSIs. To use the maximum stretch the seaward end ($z=0 + 7.38$ m) was chosen furthest offshore while still data was present at all the OSSI locations (Figure 22).

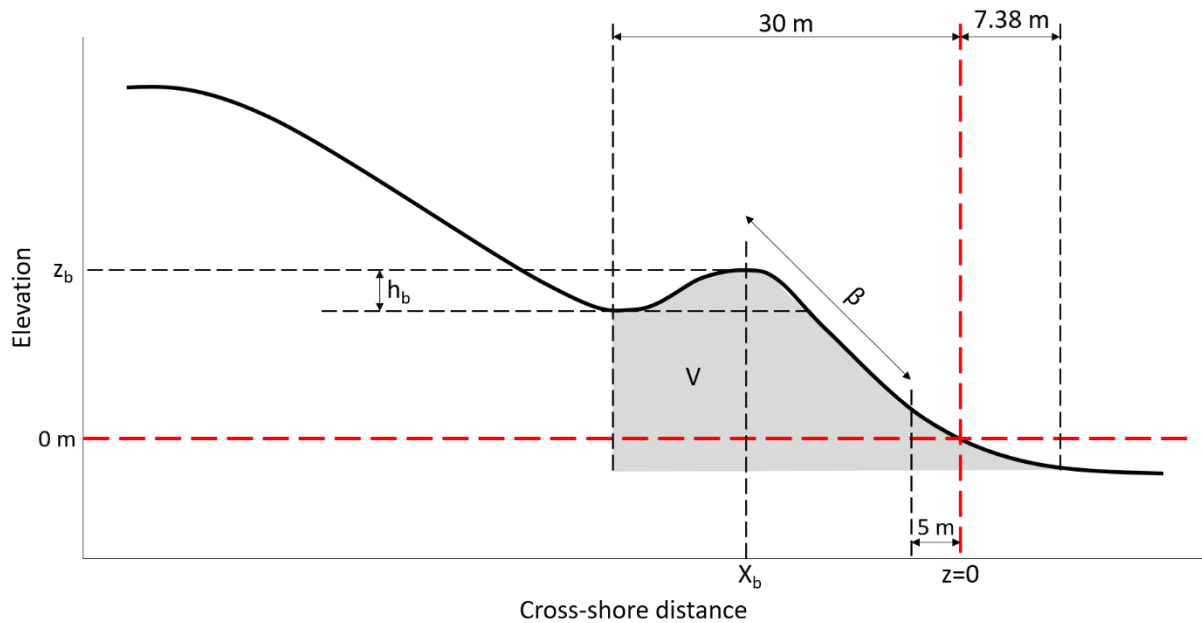


Figure 22: Schematic overview of the morphological parameters determined. Red dashed lines indicate the 0-meter elevation (horizontal) relative to the Danish Vertical Reference 1990 (DVR90) and the cross-shore location of the 0-meter elevation bed level ($z=0$) (vertical). Further indicated are; The peak bar elevation relative to DVR90 (Z_b), the height of the intertidal bar based on the landward trough (h_b), the cross-shore location of the peak bar (X_b), the seaward slope of the bar determined between X_b and 5 meter landward of $z=0$ (β) and the sediment volume (V) indicated as the grey area between 30 meter landward and 7.38 m seaward of $z=0$.

4.3.2 Alongshore comparison of hydrodynamic data

Further steps were taken to enable the alongshore comparison of hydrodynamic data, as the water depth (i.e. the bed elevation) is not equal at each OSSI (Figure 37). Consequently, the H_m0 (and the alongshore differences herein) in Figure 37 cannot be compared one on one. Ideally, to compare alongshore wave heights, the wave height at each alongshore location should be measured at the same water depth, to prevent a depth induced variability in wave height. Since, waves break due to their interaction with the bottom, leading to wave energy dissipation and the decrease in wave height. Consequently, when an OSSI is located at a position with a higher bed elevation, naturally the waves that arrive there have already travelled in lower water depths, and the probability of wave energy dissipation is therefore higher compared to an OSSI which is located at a lower bed elevation. This means that one cannot argue that the alongshore variation in local wave height, measured by the OSSIs, is caused by differences in the alongshore wave height (due to modifications of the wave height further offshore) or by differences in wave energy dissipation due to variations in the local positions of the OSSIs. To rule out the variation caused by the differences in OSSI positioning, I determined the differences in wave heights with the following method.

For each half hour, per tide, a significant wave height was calculated. For most tides the H_{m0} showed a linear trend (Figure 23). With the use of the linear trend I determined the wave height at the same water depth for each alongshore OSSI. For the pre-storm period, I used a water depth of 0.48 m, while during the storm I used a water depth of 1.0 m. Linear fits with a $R^2 < 0.7$ are not considered.

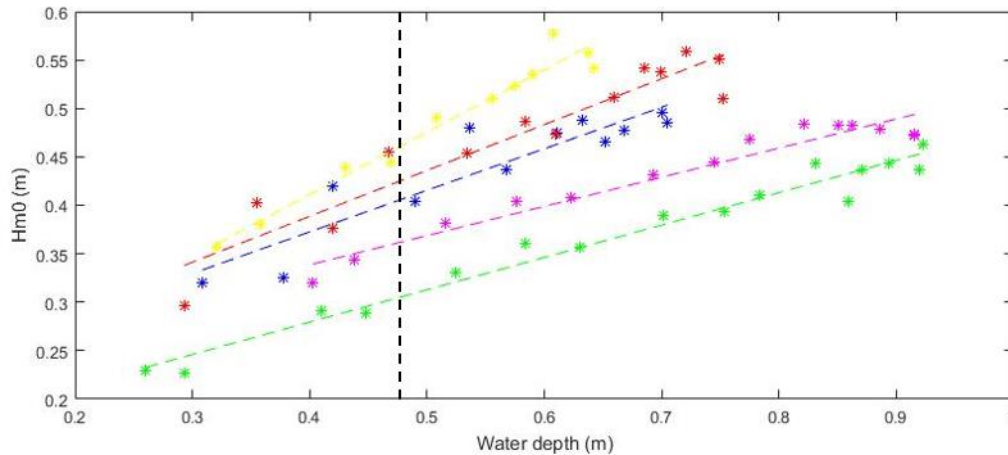


Figure 23: Linear fits of the wave heights during one tide at day 4 at the different alongshore locations of the OSSIs: 1 (blue), 2 (red), 3 (yellow), 4 (magenta) and 5 (green). Black dashed line indicates a 0.48 m water depth.

To compare the wave spectra, the water depth in which it was measured was taken approximately the same. I determined per OSSI (and per tide) which block of 30 minutes was closest to the appointed water depth and used those spectra for the alongshore comparison.

Furthermore, each spectrum was divided into a high and a low frequency part, to distinguish between infragravity waves and (short period) incident waves and to calculate the ratio between total energy in low-frequency waves and total energy in high-frequency waves (LF/HF). The boundary was determined at the commonly chosen 0.05 Hz. As, when waves break, energy is dissipated from the short period waves and partly transferred to infragravity waves (section 2.1.1), the LF/HF will be higher when waves break seaward of the measuring point. This means that the LF/HF may indicate differences in wave conditions due to wave breaking between certain points. The energy of the spectra is calculated as the area under the curve of the wave-energy spectra.

4.3.3 Morphological vs. hydrodynamical data

To find significant correlations between the alongshore differences in morphological development and the alongshore differences in hydrodynamic conditions the statistical t-test was used. Two variables (e.g. differences in bar migration and differences in significant wave height, between two alongshore points) were compared with one another and with the use of the t-test it was determined whether there was a significant correlation between the two and how strong, positive or negative, the correlation was.

To indicate if it really was an alongshore variation, the variables were taken as relative values between two alongshore locations. Where, for the hydrodynamical variables these are the differences in wave conditions between two locations, while for the morphological variables these are the differences in the development of the morphological features between two points. This was done for all morphological features described, resulting in; relative bar elevation change (ddz_b), relative bar height change (ddh_b), relative bar migration (ddx_b), relative $z=0$ position change ($ddz=0$), ($dd\beta$) and relative volume change (ddV).

5. Results

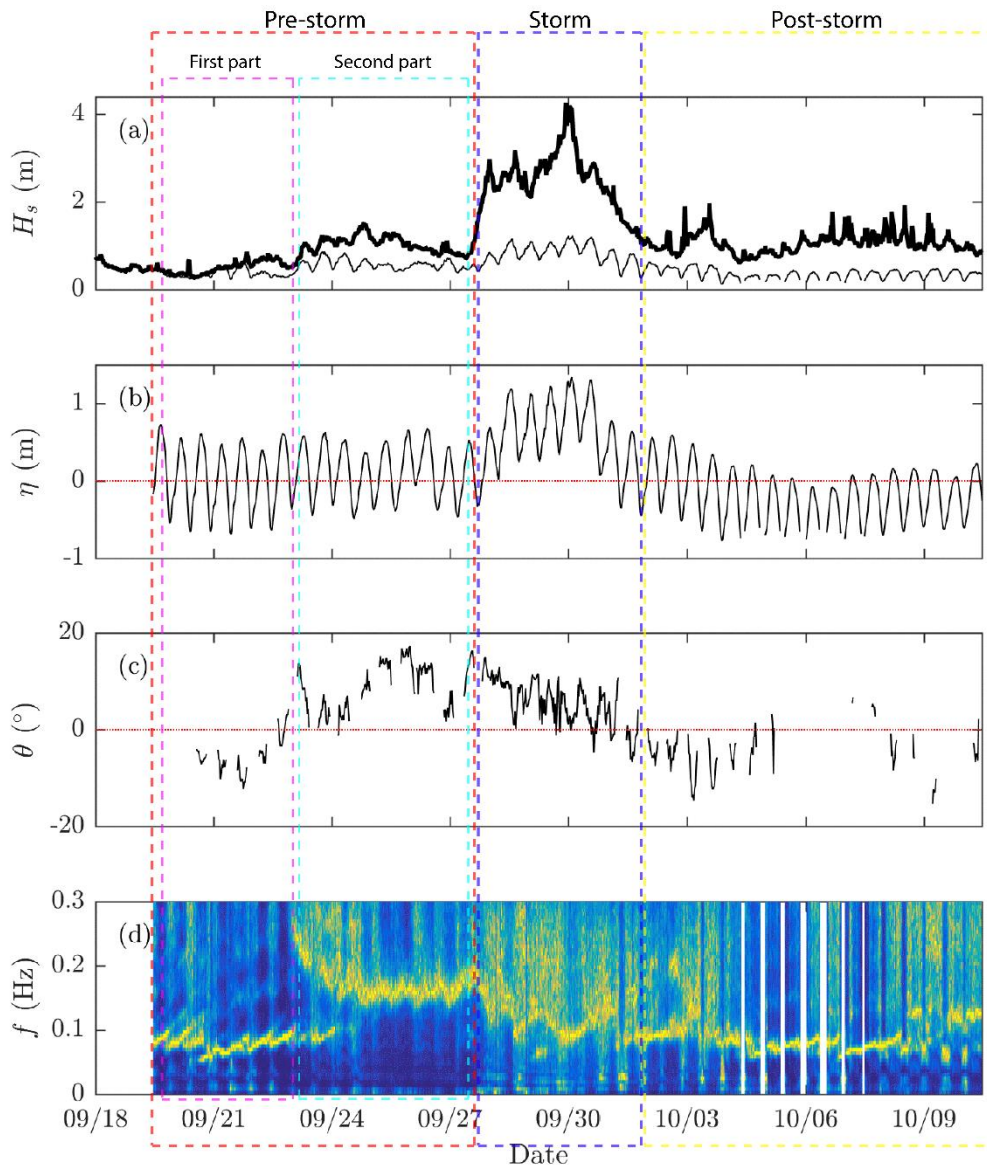


Figure 24: Wave conditions during the campaign. (a) the significant wave height H_s at the offshore wave buoy (bold) and at the most seaward pressure sensor (not part of the alongshore array), (b) the water level η in respect to ordnance datum (DVR90), (c) wave angle of incidence ϑ at the large-frame (positive angles arrived from the south) and (d) normalized wave-energy spectra at the most seaward pressure sensor. The dashed boxes indicate the distinct time periods.

5.1 Offshore conditions

Figure 24 shows the timeseries of the measured significant wave height H_s , water level, wave angle of incidence and normalised wave-energy spectra throughout the campaign. The whole campaign can be subdivided into three main periods based on the hydrodynamics: the pre-storm (days 1-10), storm (days 11-14) and post-storm period (days 15-23). Where the first period is separated into two parts: the first part (tides 1-7) and the second part (tides 8-17). The subdivision is based on the offshore significant wave height, which was generally low during the pre-storm period ($H_s < 1$ m), high (up to 4 m) during the storm and low again during the post-storm period ($H_s < 1$ m). The pre-storm period was separated based on the wave-energy spectra and angle of wave incidence. The timeseries of the spectrum shows that swell waves arrived during the first part, with an angle of wave incidence of 5° - 10° north of the shore normal, while during the second period sea waves arrived (shorter period) with an angle of wave incidence about 10° - 15° south of the shore normal

(Figure 24c). Additionally, during the first period the wave heights measured at the most offshore OSSI (of the cross-shore instrument array) did not differ much from the offshore wave heights. During the second part, however, the wave heights at that OSSI were lower than the offshore wave heights (Figure 24a), indicating that a part of the wave energy dissipated seaward of that OSSI.

5.2 Morphology

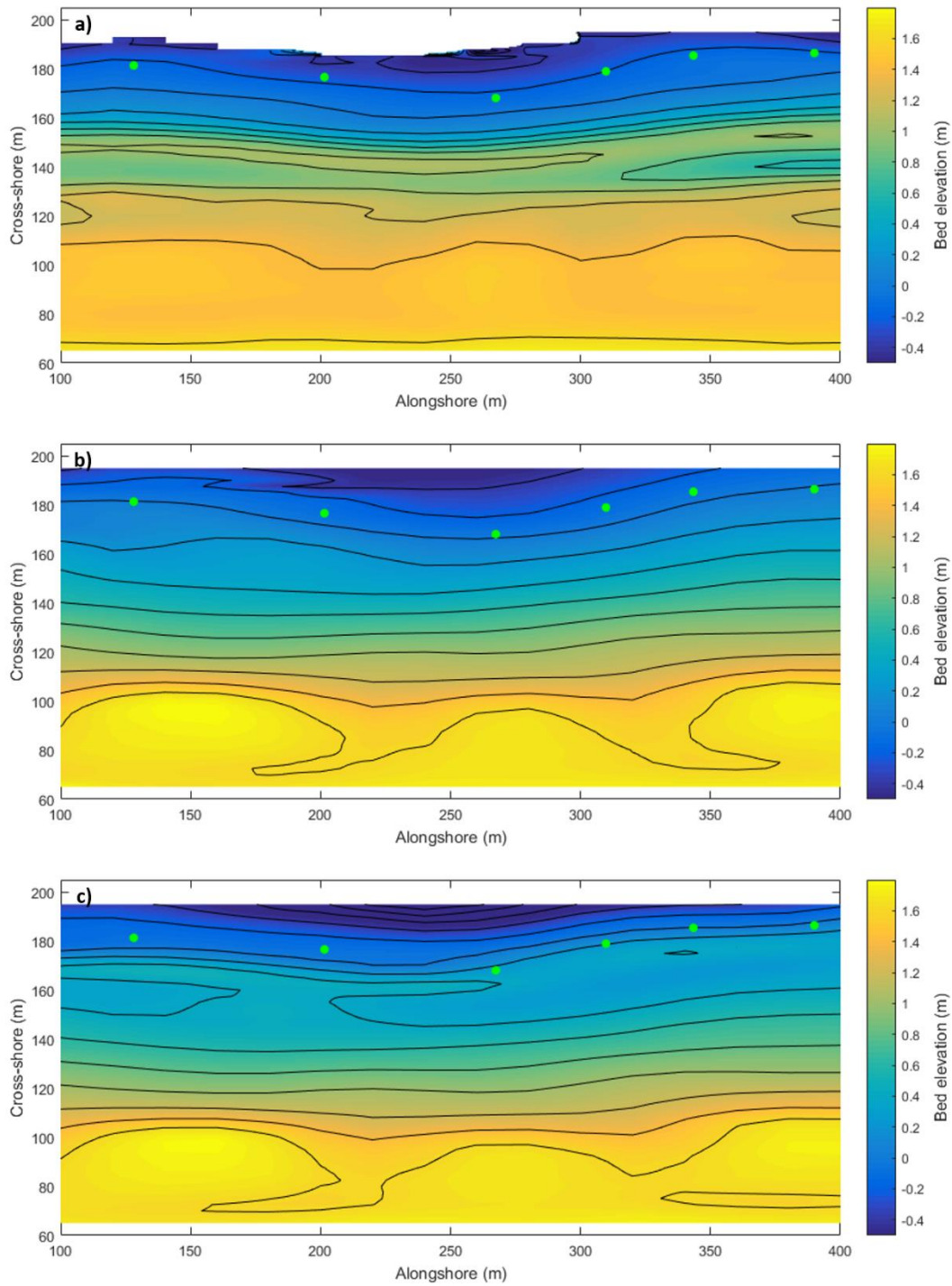


Figure 25: Bathymetric maps of the study area at day 10 (a), day 15 (b) and day 23 (c) with 0.20 m spaced contours. Alongshore OSSI locations are indicated (green dots).

5.2.1 Bathymetric/topographic maps

An overview of the study area at three moments during the campaign is provided in Figure 25. The crescentic shape of the coastline is clearly visible and reflected in the intertidal bar (around 140-160 m cross-shore) at day 10 (Figure 25a). A deeper trough/runnel at OSSIs 5 and 6 is also noticeable around 140 m cross-shore (Figure 25a). The morphology near the dunes on the supratidal beach (cross-shore < 110 m) might be a result from previous extremely high-water levels. On day 15, the intertidal bar was flattened by the storm, resulting in a uniform plain intertidal beach (cross-shore > 110 m, Figure 25b). Although, the contour lines (especially at the seaward side, around 180 m cross-shore) were still crescentic. The bed elevation change map between days 10 and 15 (Figure 26a), the storm, shows a large area with bed lowering in the middle of the map (the flattening of the upper intertidal beach, around 110-160 m cross-shore), where a dark blue band indicates the position of the erased intertidal bar. Just landward of this band (140 m cross-shore) less to no elevation change and even deposition in the northern part was found (140 m cross-shore and 350-400 m alongshore), as this was the position of the trough before the storm. More landward of this trough the beach also eroded. Although, close to the dunes (cross-shore < 110 m, Figure 26a) accumulation of sediment occurred, resulting in an increase in bed level elevation. The previously recognised morphological features, close to the dunes, seemed more pronounced (Figures 25b and 26a), showing some sort of outflow channel structure suggesting that two channels were formed during the extreme high water of the storm. Also on the far seaward side of the area deposition of sediment occurred (Figure 26a). Sand from the middle part of the area (the bar) was partly moved landwards to be deposited on the supratidal beach (between 80-100 m cross-shore), but more than half of it was transported and deposited at the seaward side of the beach (also outside of the measured area), where the bed elevation was about 20-30 cm lower before the storm. During the week after the storm a new intertidal bar formed (around 160-180 m cross-shore, Figure 25c). The new intertidal bar (Figure 25c) had almost the same crescentic shape as the first intertidal bar (Figure 25a), but shifted a little towards the south. The bed elevation change map between days 15 and 23 (Figure 26b) indicates the newly formed bar as a red elevation heightening band (around 160-180 m cross-shore). The red band is broader in the middle of the study area, indicating that more sediment accumulated in this part. The seaward part of the area underwent bed lowering, where the sand was supposedly transported landward and made the intertidal bar. Landward of the deposition band (cross-shore < 140 m) nothing happened as this part didn't inundate due to low water levels.

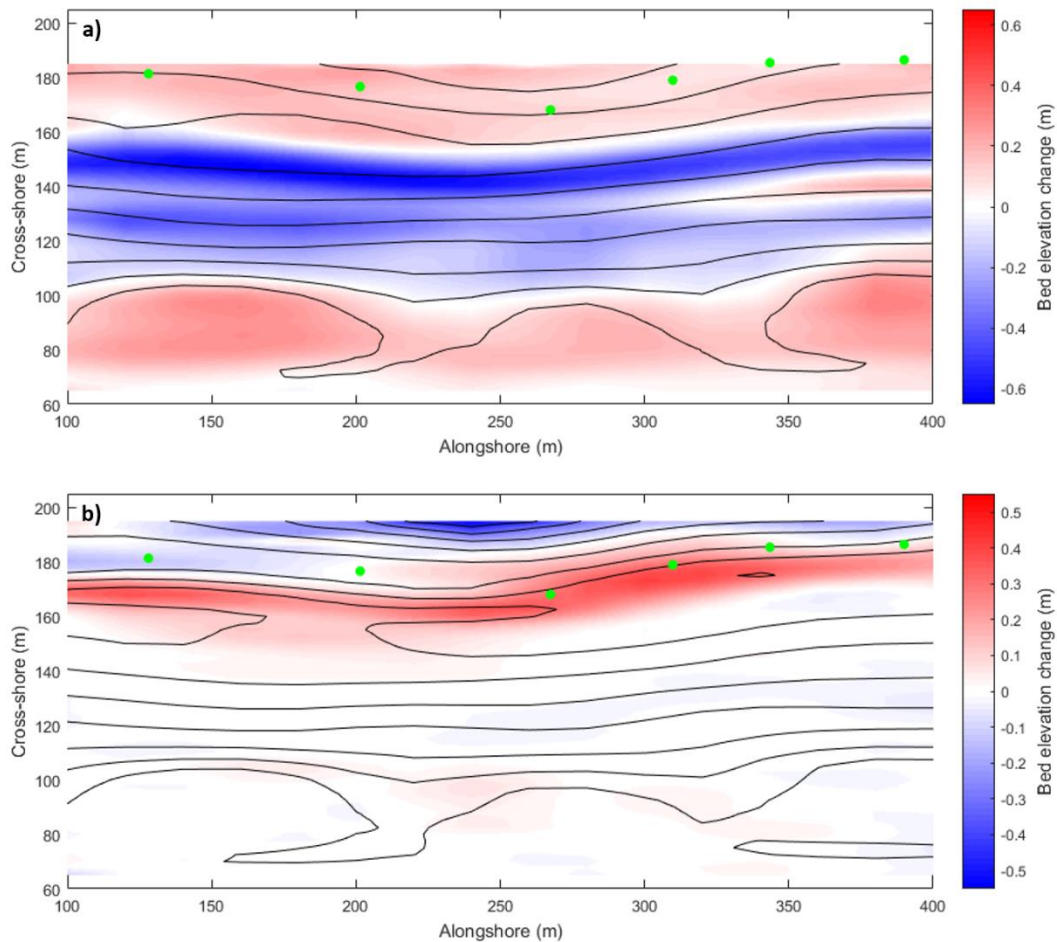


Figure 26: Maps of the study area, indicating the bed elevation change between: day 10 and day 15, the contours indicate the bed level at day 15 with 0.20 m spacing (a), and day 15 and day 23, the contours indicate the bed level at day 23 with 0.20 m spacing (b). Alongshore OSSI locations are indicated (green dots).

5.2.2 Cross-sections

To be able to compare the morphological development with the hydrodynamical data measured by the OSSIs, the cross-sections at the alongshore locations of the OSSIs will be used to analyse this development. In this section, the general evolution of the different cross-sections is shown.

Figure 27 indicates the general evolution of the cross-section of the intertidal beach at the location of OSSI 3. The cross-section of OSSI 3 is shown, as this profile was used as a reference profile for the comparison of morphological development. Mild to moderate wave conditions occurred during the pre-storm period. Where the cross-section indicates an intertidal (swash) bar (around 25 m cross-shore), which steepened and migrated landward during this period. A subtidal bar was also present. After this period the storm passed by, which wiped out the morphological features of the intertidal beach, flattening the profile. The cross-section of day 22 (Figure 17) indicates the re-occurrence of an intertidal (swash) bar at a more seaward location (around 40 m cross-shore), which developed after the storm during the post-storm period with mild wave conditions and extremely low high tide water levels.

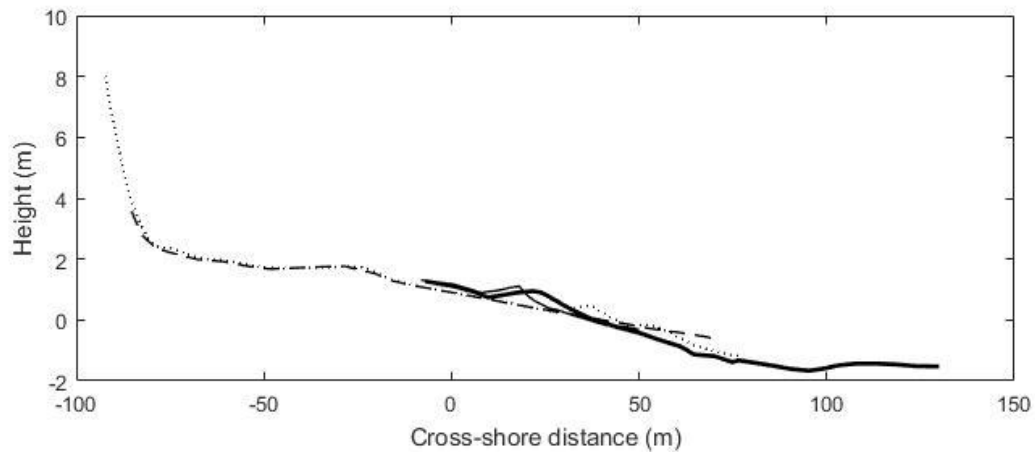


Figure 27: Four cross-sections at the location of OSSI 3 at days 4 (bold solid line), 9 (solid line), 15 (dashed line) and 22 (dotted line).

To make a better indication of the evolution of the cross-section, and of the whole intertidal beach within the study area, the cross-sections at every alongshore located OSSI are plotted through time alongside each other (Figure 28). The figure contains data from both the point GPS (up until day 8) and the continuous GPS (wheeled) (days 9-23) measurements. As the wheeled measurements are interpolated to make bathymetry maps, from which the cross-sections are taken, some detail is lost. This is reflected in the shape of the intertidal bar, which seems much more symmetric in these interpolated cross-sections, which was not the case in reality. Furthermore, the peak of the bar is located at the seaward side of the bar crest, whereas the interpolated cross-sections suggest that the peak of the bar is in the middle of the crest. This is clearly visible when comparing the cross-sections from day 8 (point measurements) and 9 (from the interpolated maps).

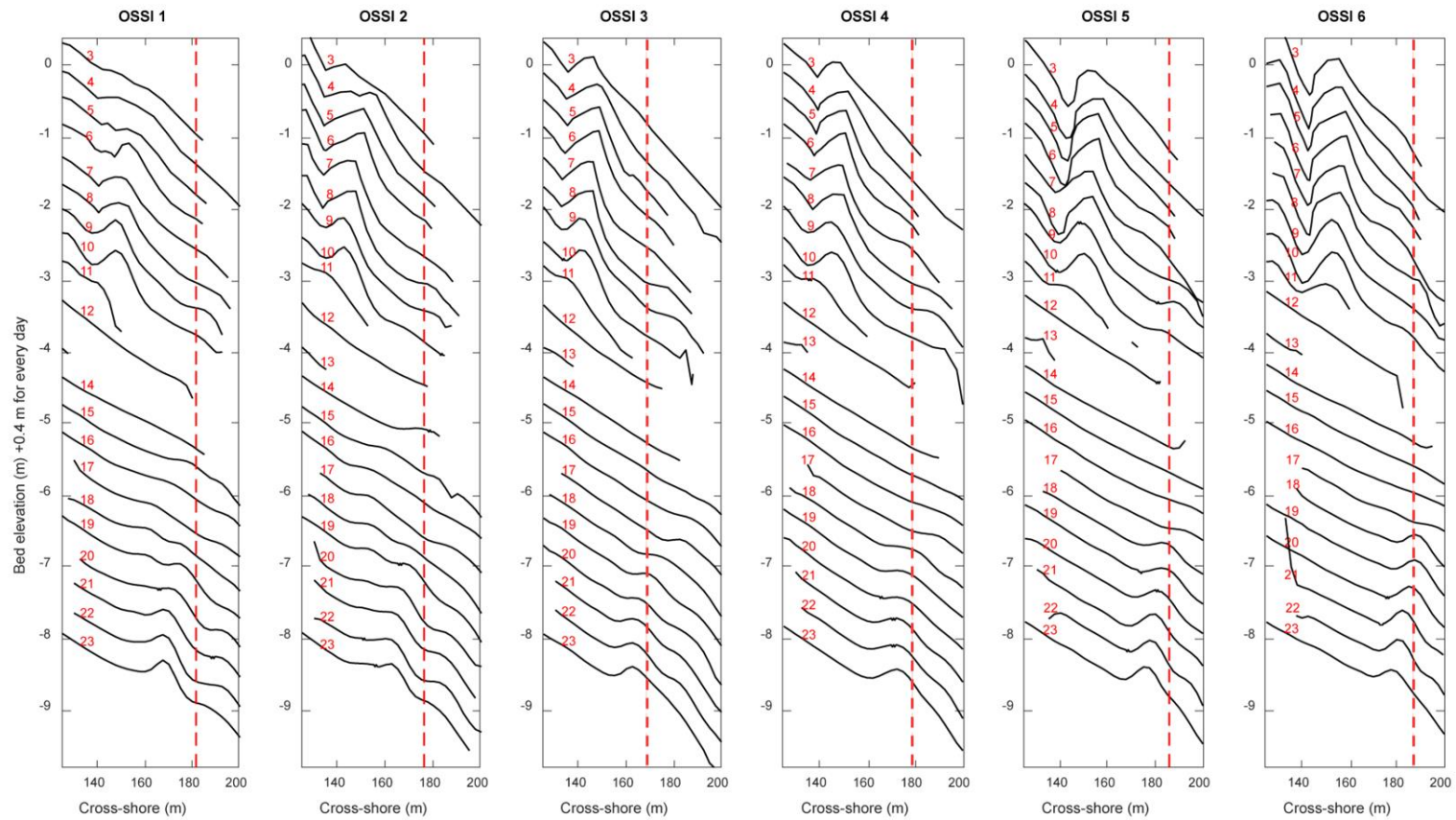


Figure 28: The cross-sections throughout the campaign at the locations of the alongshore OSSIs, sorted from south to north, with OSSI 1 being the most southern OSSI. The cross-shore locations of the OSSIs are indicated at each location (red dashed line). Note: up and including day 8 the RTK GPS data from the point measurements is used, while after that the data from wheeled RTK GPS measurements is used.

At the beginning of the campaign (day 3, Figure 28) an intertidal bar was already present at the locations of OSSIs 3, 4, 5 and 6 but not yet at OSSI 1. At OSSI 2 it is unclear whether that is the same bar as on day 4 (Figure 28). The bar was located most landward in the middle of the study area, at OSSI 3, and both in the north and south of the study area the bar was closer to the sea, resulting in a crescentic shape of the bar. At OSSIs 5 and 6 the bar was more pronounced, as the trough was much deeper. Also, the landward side of the bar shows a sort of slip-face at these locations. As mentioned before, the bar at the alongshore position of OSSI 1 came later to existence. At all locations, the bar seemed to migrate landward during the first ten days of the campaign, until the storm arrived. The impact of the storm was alongshore uniform: an almost complete wipe-out of morphological features on the intertidal beach, making it flat but preserving the crescentic shape of the beach. However, this was not the case for the supratidal beach (section 5.2.1). In just a couple of days after the storm, at all locations, a new intertidal bar developed more seaward than the previous bar due to very low water levels during this period. Again, the bar developed in a crescentic shape, being the most seaward at the location of OSSI 6, and most landward at OSSI 3. The timing in the development of the bar was alongshore slightly different. The shape of the bar was, once more, more pronounced at OSSIs 5 and 6, as the crest became relatively higher.

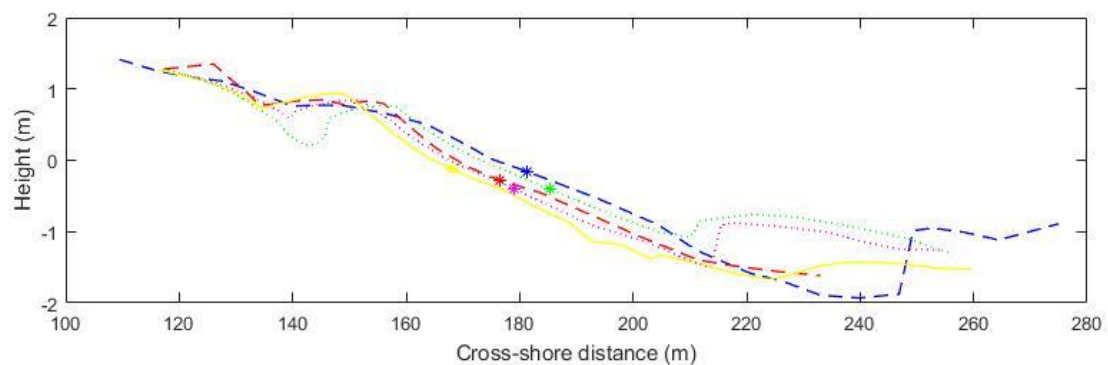


Figure 29: Cross-sections at the alongshore locations of OSSI: 1 (blue), 2 (red), 3 (yellow), 4 (magenta) and 5 (green) along with the positions of the OSSIs (stars) at day 4.

The cross-sections from day 4 indicate the alongshore variability in cross-shore location and height of the subtidal bar (between $x = 200 - 260$ m) at each OSSI (Figure 29). The lowest intertidal bar crest was at OSSI 3, and the distance between the subtidal bar and the shoreline, as well as the depth of the subtidal bar, decreased from OSSI 3 to the north and to the south. As such, the location of the intertidal bar was coupled to the subtidal bar depth and position.

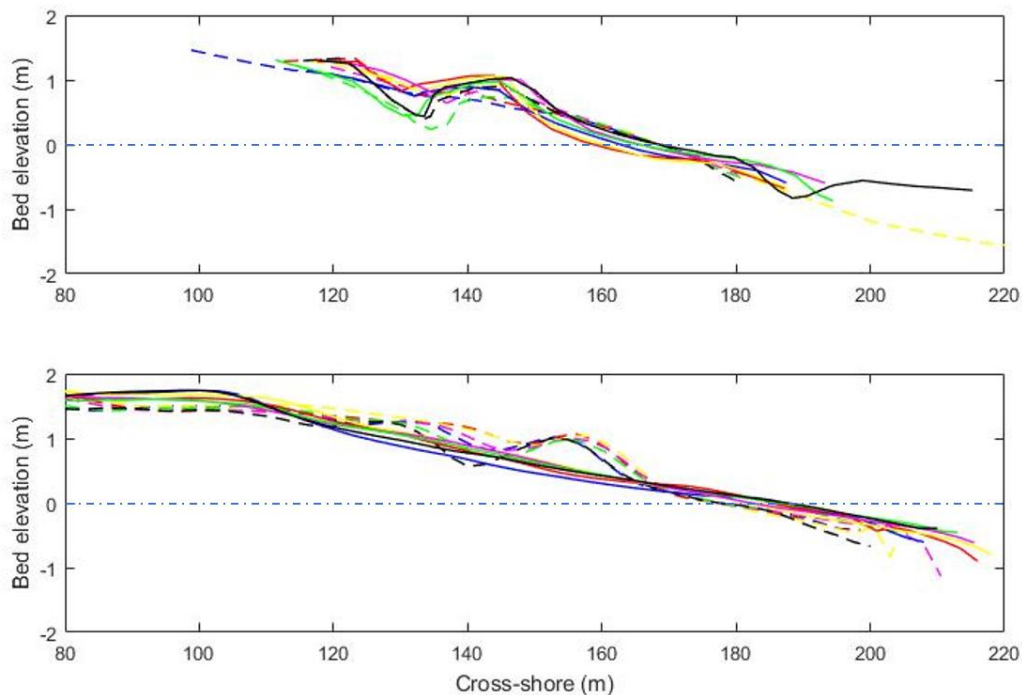


Figure 30: Cross-sections at the alongshore locations of the OSSIs: 1 (blue), 2 (red), 3 (yellow), 4 (magenta), 5 (green) and 6 (black). a) Dashed lines indicate the cross-sections at day 3 and the solid lines at day 8. The cross-sections are corrected for their cross-shore position of the $z=0$ point at day 3, so that $z=0$ for each cross-section at day 3 is on the same point. b) dashed lines indicate the cross-sections at day 10 and the solid lines at day 15. The cross-sections are corrected for their cross-shore position of the $z=0$ point at day 10, so that $z=0$ for each cross-section at day 10 is on the same point.

Both panels in Figure 30 indicate the evolution of the cross-sections between two days during the campaign for all the alongshore locations. The positions of the cross-sections are corrected in a way that the alongshore different cross-shore locations of the $z=0$ m are now plotted with respect to the same cross-shore position, for the first of the two days per panel (the second day has the same correction factor). This way the crescentic shape of the shoreline is removed enabling a comparison between the cross-sections and the relative differences in intertidal bar position.

Both on day 3 and day 8, the intertidal bar position was located alongshore at almost the same position relative to the $z=0$ m (Figure 30a). There was, however, a difference in the development of the intertidal beach at the seaward side of the bar. Here, the elevation of the beach became lower for OSSIs 2 and 3, less for 1, compared to OSSIs 4, 5 and 6. Figure 30b indicates that the intertidal bar was alongshore located at (almost) the same cross-shore position relative to the $z=0$ m elevation point. The landward trough was not alongshore uniform in shape, however, being more pronounced/deeper and elongated in the landward direction at OSSIs 5 and 6, while it was rather shallow at OSSIs 2 and 3. This figure also indicates that sand was deposited on the far landward end, as well as at the seaward end of the cross-sections during the storm.

5.2.3 Bar characteristics

To point out the alongshore differences in the cross-sections, several aspects of the cross-sections are quantified and compared (Figure 22), as introduced in section 4.3. In this section, the bar characteristics throughout the campaign and the alongshore differences herein are described. In the next section, other intertidal features; the slope, volume and shoreline position are treated.

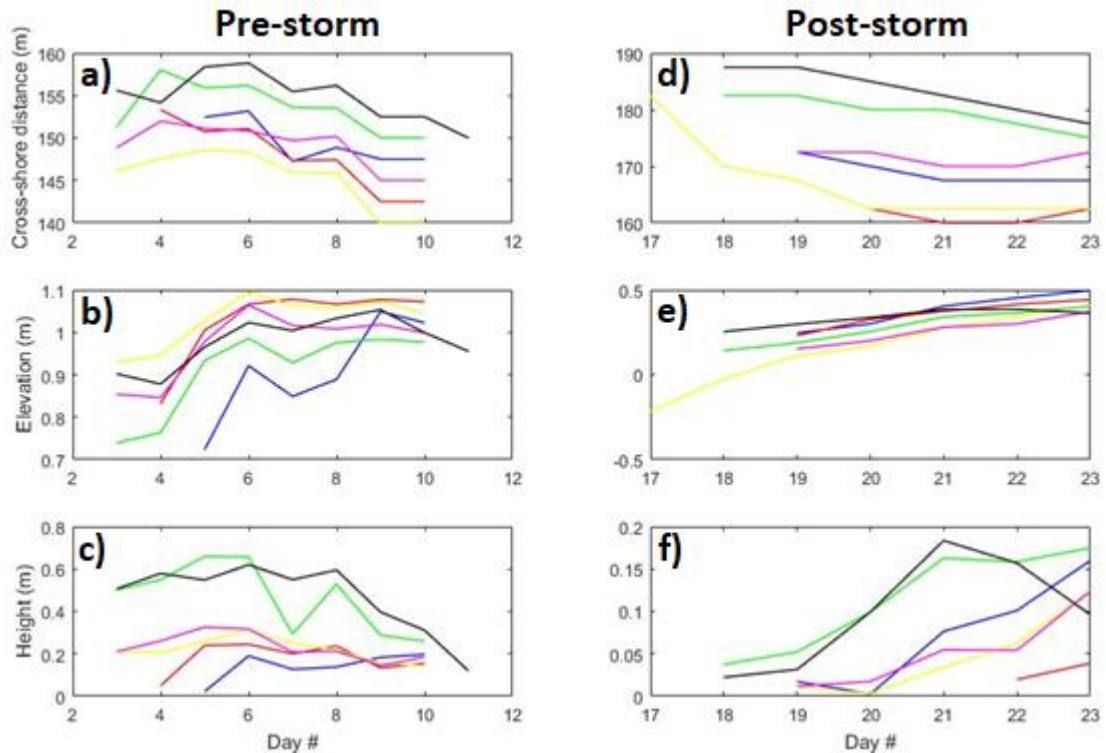


Figure 31: Bar features at the alongshore locations of the OSSIs, 1 (blue), 2 (red), 3 (yellow), 4 (magenta), 5 (green) and 6 (black), at each day of the campaign (a-c: pre-storm, d-f: post-storm). a) and d): The cross-shore location of the bar (X_b) (positive is seaward). b) and e): the peak bar elevation (z_b). c) and f): bar height based on landward trough (h_b). Note the different y-axis ranges between pre- and post-storm.

Figure 31 shows the bar characteristics of all alongshore cross-sections. During the pre-storm period, the bar was most landward located at OSSI 3, and both north and south of this position the bar was more seaward (up to 12.5 m), as (like mentioned before) the bar had a crescentic shape. During the post-storm period this was also the case, although the bar at the location of OSSI 2 was situated around the same position as at OSSI 3, suggesting that the crescentic shape of the bar had shifted slightly towards the south compared to pre-storm. Also, the cross-shore range of the bar location within the study area was a bit larger post-storm, up to 22.5 m. At most locations, the bar migrated a little seaward between the first and second measuring day (day 3 and 4), but during the rest of this period the bar migrated slightly landward at all alongshore OSSI locations. Post-storm, after the bar was eroded by the storm, the new bar developed far more seaward (± 20 m). Initially there was a landward migration of the bar at all OSSIs, but this migration continued only at OSSIs 5 and 6, whereas the onshore migration seized after a few days at the other OSSIs. Note: the bar positions (from day 9 onward) are derived from the interpolated cross-sections from the interpolation bathymetry maps, which means that only every 2.5 meters there is a cross-section point, defined in the grid for the interpolation bathymetry maps (section 4.2.1). This means that the seaward migration on the last day, suggested at OSSIs 2 and 4, was not necessarily a seaward migration (or at least not of 2.5 meters), but could also be due to minor differences which only just alter the position of the peak of the bar in the interpolation maps.

The peak bar elevation, z_b , throughout the campaign, is shown in Figure 31 (b + e). As the reformed bar, post-storm, was located further seawards than the initial intertidal bar, it was located on a lower part of the beach. This is also reflected in the elevation (Figure 31 b + e), as the elevation of the initial bar was more than 0.5 m higher than that of the new bar. The elevation of the bar is a factor of both the cross-shore position/migration and the net vertical growth of the bar. Since, if the bar migrates landward it goes up the slope of the beach. During both the pre- and post-storm period of the

campaign the bar showed an increase in elevation, along with, as earlier noted, the landward migration. However, during the pre-storm period the alongshore bar elevations remained about equal after a few days. The alongshore differences in bar elevation became gradually less throughout the pre-storm period, from a maximum difference of ± 0.3 m to ± 0.1 m, with the lowest elevation initially found at OSSI 1 but later at OSSI 5, and the highest bar elevation found at OSSIs 2 and 3. Post-storm, the evolution of the bar elevation showed the same trend alongshore, where the bar had the lowest elevation at OSSIs 3 and 4 and the highest at OSSI 1.

The bottom panels of Figure 31 illustrate the bar height based on the landward trough (h_b), throughout the campaign. Pre-storm, the bar seemed to remain around the same height at OSSIs 1, 2, 3 and 4 (± 0.2 m). The height was larger at OSSIs 5 and 6 (± 0.6 m) compared to the other locations due to a deep trough (runnel) in the northern part of the study area, although, the height decreased towards the end of this period at these locations (between day 8 and 11, Figure 31). This possibly happened due to filling of the trough with sediment, or due to the loss of the real shape of the trough in the interpolated cross-sections. On day 7, at OSSI 5, the bar height seemed to suddenly decrease, to be increased again the next day. When looking at the cross-sections at OSSI 5 (Figure 28), it seems that there has been a measuring mistake, reducing the depth of the trough. During post-storm period there was an alongshore steady heightening of the bar, except at the location of OSSI 6 which showed a decrease in height at the end of this period. The bar firstly appeared at OSSIs 5 and 6 (day 18, Figure 31f), where it remained more pronounced during the post-storm period, while at OSSI 2 the bar only appeared at the very end (day 22), as the bar was more of a terraced feature before that (Figure 28).

To compare the evolution of these bar characteristics and the alongshore variation herein, the developments in the characteristics per day were calculated at the location of each OSSI: the migration distance (dX_b), the change in peak bar elevation (dz_b) and the change in peak bar height based on the landward trough (dh_b).

Figure 32 indicates changes in bar characteristics at different alongshore locations per day pre-storm. The migration distance of the bar per day showed the same trend alongshore, with an alternation between landward migration and little to no migration per day. However, the magnitude of the migration distance did vary alongshore, up to 5 m. A notable point is that the location of maximum migration (or minimum migration) did not repetitively occur at the same position. The trends in elevation change and height change were also alongshore similar, with the only alongshore variation being the magnitudes of the changes, up to 0.15 m and 0.25 m, respectively. As mentioned before, most likely due to a measuring error, the bar height at OSSI 5 suddenly decreased at day 7, which resulted in a height decrease and increase between days 6 and 7 and days 7 and 8, respectively.

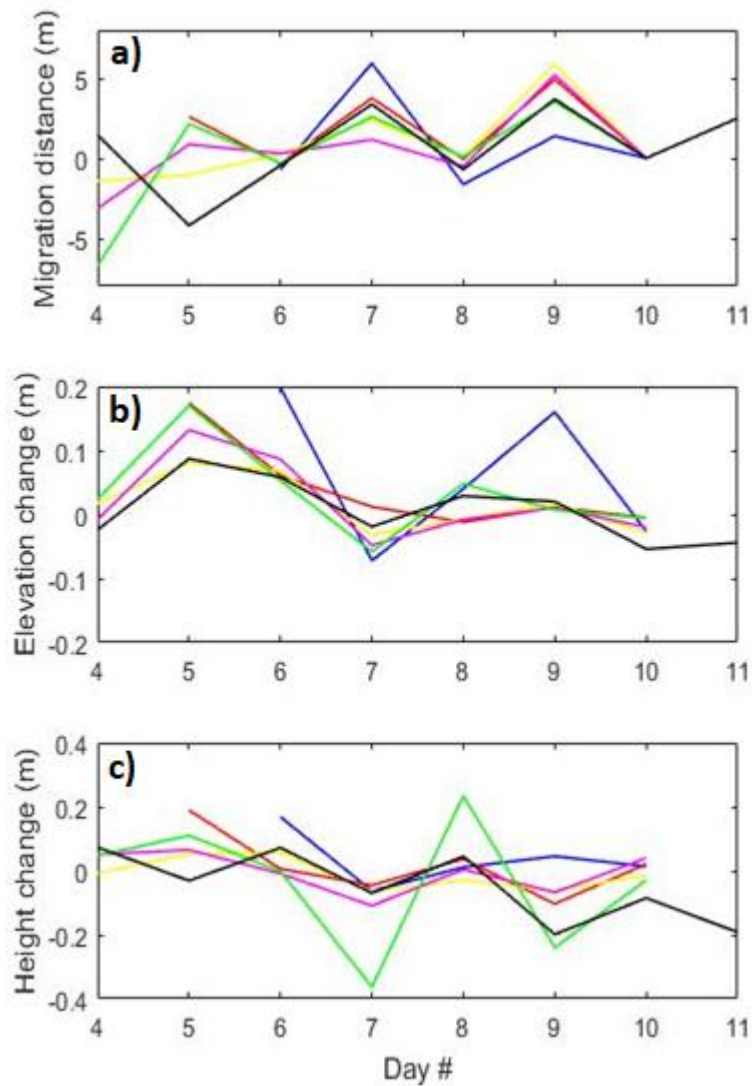


Figure 32: Changes in bar characteristics at the alongshore locations of the OSSIs, 1 (blue), 2 (red), 3 (yellow), 4 (magenta), 5 (green) and 6 (black), between each day before the storm (day number indicate the second day). a) The bar migration distance (dX_b) (positive is landward migration). b) The peak bar elevation change (dz_b). c) Bar height based on landward trough change (dh_b).

5.2.4 Slope, Volume and $z=0$ contour line position

The seaward slope of the intertidal bar was determined between the peak of the intertidal bar and a point 5 m landward of the $z=0$ contour line (section 4.3.1, Figure 22). If the bar was not yet present (e.g. at the beginning of the campaign at OSSI 1), the landward point was determined at the location where the future bar would come to existence. The volume was determined between 30 m landward and 7.38 m seaward of the $z=0$ contour point, as explained in section 4.3.1 (Figure 22).

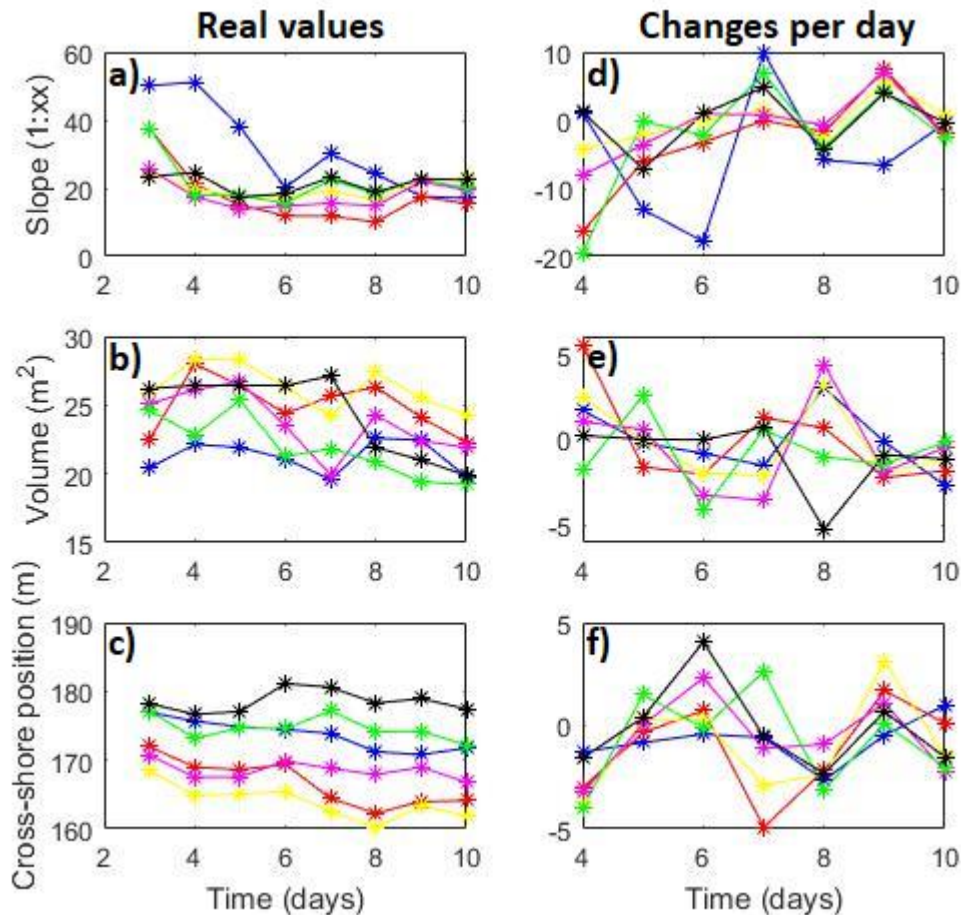


Figure 33: a-c) Morphological features at the alongshore locations of the OSSIs, 1 (blue), 2 (red), 3 (yellow), 4 (magenta), 5 (green) and 6 (black). d-f) The changes between each campaign day pre-storm (day number indicate the second day). a) and d) Slope change ($\delta\beta$). b) and e) Volume change (δV). c) and f) $z=0$ contour line position change ($\delta z=0$), where positive change is seaward.

Figure 33 indicates the slope, volume and cross-shore position of the $z=0$ m contour line, along with their changes per day for each alongshore OSSI location during the pre-storm period. The slope was initially very gentle at the location of OSSI 1 (about 1:50), as the intertidal bar was not yet present at that location, but later the intertidal beach steepened and became about the same slope as at the other locations (around 1:20). The initial slopes at OSSIs 2 and 5 were about equal (1:38) and at both locations the slope steepened between days 3 and 4. But at OSSI 2 it steepened even further (although less fast), while at OSSI 5 the slope remained relatively constant. At the end of the pre-storm period the slope was alongshore nearly equal. The trends in slope change, except at OSSI 1, were approximately the same (Figure 33d).

At OSSIs 4, 5 and 6 a significant volume change occurred between the beginning and end of the pre-storm period (up to 5 m^2), while at the other locations only gentle changes took place (Figure 33b). The amount of the cross-shore sand volume was alongshore variable during this period, up to 6 m^2 . With the largest volume at OSSI 3 ($25\text{--}28 \text{ m}^2$) throughout almost the whole pre-storm period. The volume changes per day were very different between the alongshore locations (Figure 33e).

The coastline had a crescentic shape, as mentioned before, and this is reflected in the cross-shore position of the $z=0$ (Figure 33c). With the $z=0$ the furthest onshore at OSSI 3 and more offshore north and south of that position. The changes in cross-shore position show roughly the same trend alongshore, but with a variation in the magnitudes (Figure 33f). Figure 34 indicates the changes in the

$z=0$ contour line between the beginning and end of the pre-storm period and during the storm, which roughly shows that the crescentic shape was enhanced during both periods. From ± 9 m to ± 15 m cross-shore difference in maximum and minimum $z=0$ position during the pre-storm period and from ± 15 m to ± 22 m during the storm. Furthermore, pre-storm the $z=0$ contour line migrated onshore, while during the storm the contour line migrated offshore (Figure 34).

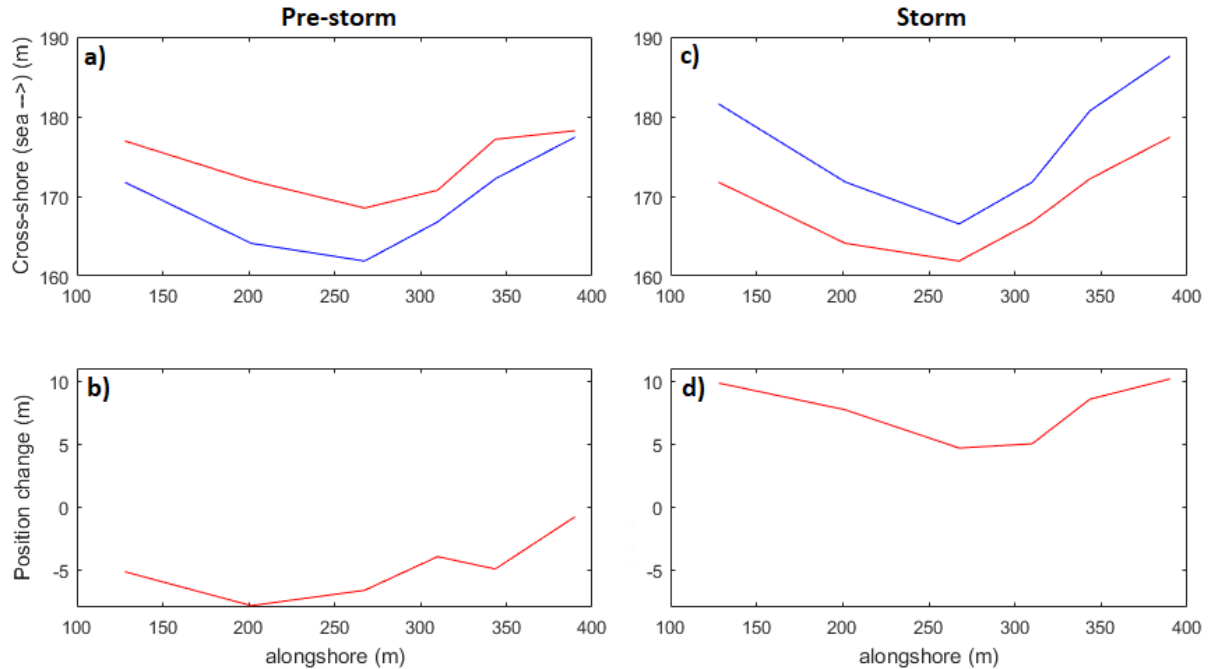


Figure 34: a-b) The $z=0$ contour lines at (a) the beginning (red) and the end (blue) of the pre-storm period and (b) the net change in contour line position between these days. c-d) The $z=0$ contour lines (c) before (red) and after (blue) the storm and (d) the net change in contour line position between these days.

The changes during the storm in volume and $z=0$ at each OSSl location are indicated in Figure 35. These changes in volume are based on the entire volume per intertidal cross-section. Most sediment volume loss occurred in the south and middle of the study area, while almost no volume change occurred at OSSl 6. This might be due to the pre-storm presence of the deep trough/runnel at OSSls 5 and 6, which filled in with sand during the storm (Figures 25a and 26a). The $z=0$ m point shifted in the seaward direction for all alongshore locations. The distance, however, indicates a crescentic trend of the shoreline, with the most change in both the northern and southern limits and the least change in the middle of the study area. This enhanced the crescentic shape of the contour line, as the horns shifted relatively more seaward than the embayment (Figures 34d and 35).

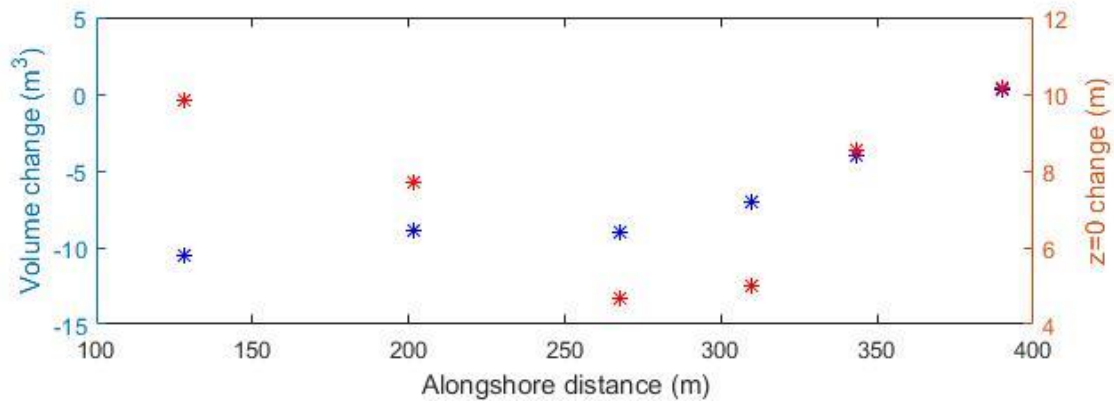


Figure 35: The volume change over the whole intertidal cross-section (blue) and $z=0$ contour position change (red) per alongshore OSSI location during the storm. Between day 10 and day 15. Note: positive change is seaward directed and alongshore distance increases towards the north. Remember: the OSSIs are ordered, from left to right, 1 - 2 - 3 - 4 - 5 - 6.

5.2.5 Location subtidal bars

The first (crescentic) subtidal bar was located close to the coast. During the campaign, several time-averaged pictures of the study area were made to illustrate areas of wave breaking (and thus the location of the subtidal bar). Furthermore, during extremely low water on day 19, a GPS survey was made across the crest of the subtidal bar (Figure 36b). As the water levels were still too deep to do the GPS survey at certain parts between the subtidal bar and beach (between 100-250 m alongshore and 210-240 m cross-shore, Figure 36b) no data is available there (white area). Here it is visible that the bar was smaller (less broad in cross-shore sense), with a lower crest, at the alongshore location between OSSIs 2 and 3. The horns of the subtidal bar coincided with the horns of the intertidal bar and the embayment of the subtidal bar coincided with the embayment of the intertidal bar, which is defined as an out-of-phase coupling (section 2.4.1). A little north, outside of the study area the subtidal bar gradually welded to the coast at the location of both the sub- and intertidal bar horns, throughout the post-storm period (around 450 m alongshore and 230 m cross-shore, Figure 36b). Although the location of the subtidal bar could not be measured during the pre-storm period of the campaign, visual observations suggest that the subtidal bar position and, more importantly, shape did not show major changes during the campaign. On the time-averaged image a rather straight second subtidal bar is visible (Figure 36a).

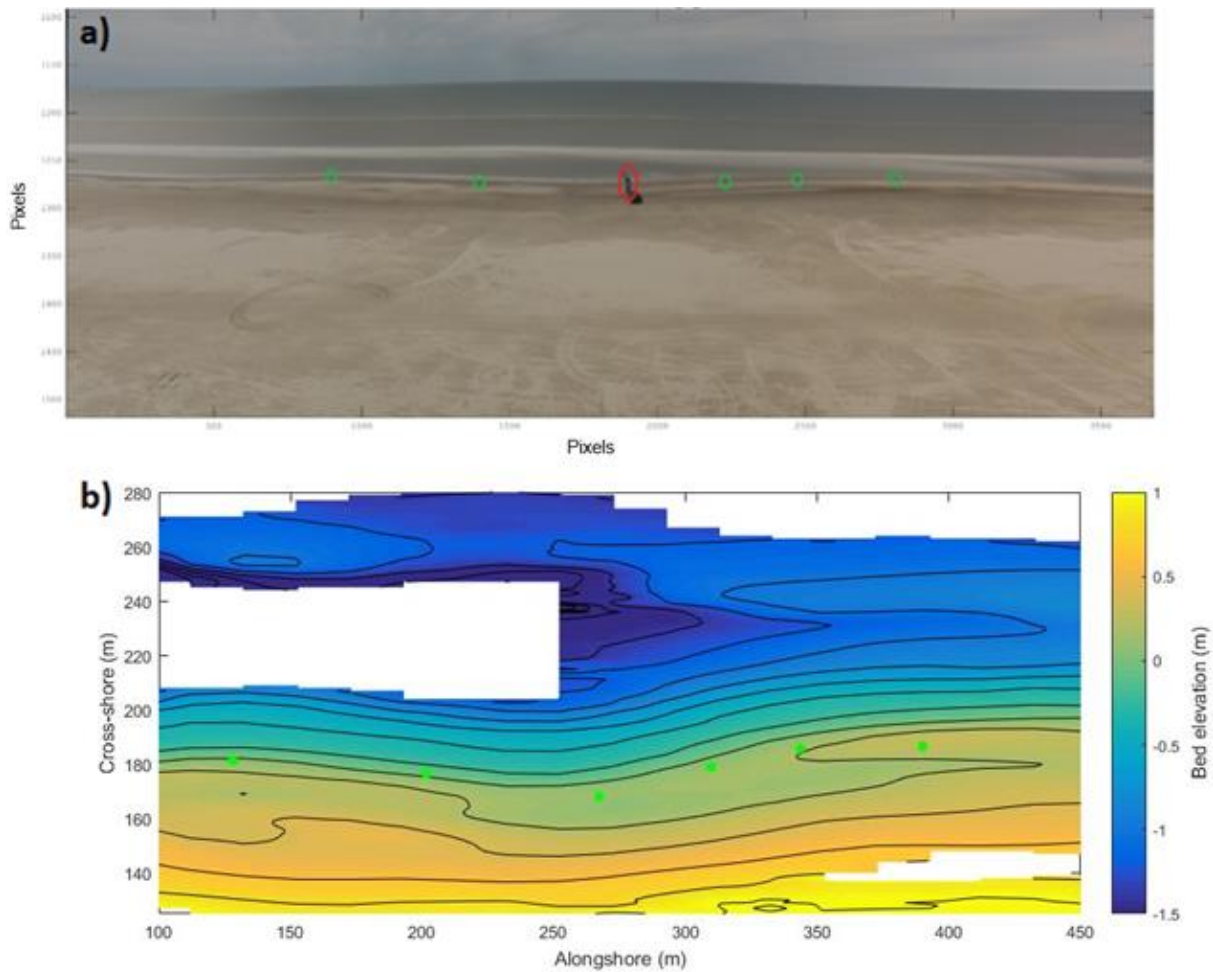


Figure 36: a) Time averaged picture of the study area at day 20. Indicated are the cross-shore array (red oval) and the alongshore OSSIs (green ovals). North is on the right-hand side. b) Bathymetric map of the study area at day 19 and a part of the subtidal bar with 0.20 m spaced contours. Alongshore OSSI locations are indicated (green dots).

5.3 Hydrodynamics

As discussed in sections 4.3 and 5.1, the study period was divided into three main periods based on the significant wave height and wave-energy spectra throughout the campaign (Figure 24): pre-storm, storm and post-storm, where the pre-storm period was further separated into two shorter periods (the first and the second part).

As mentioned before (section 4.3), during the post-storm period hydrodynamic data is limited as the water level was extremely low (Figure 37) due to offshore directed winds. Therefore, the hydrodynamic data during the last week was not included in the analysis. Unfortunately, the data from OSSI 6 appeared to be unusable.

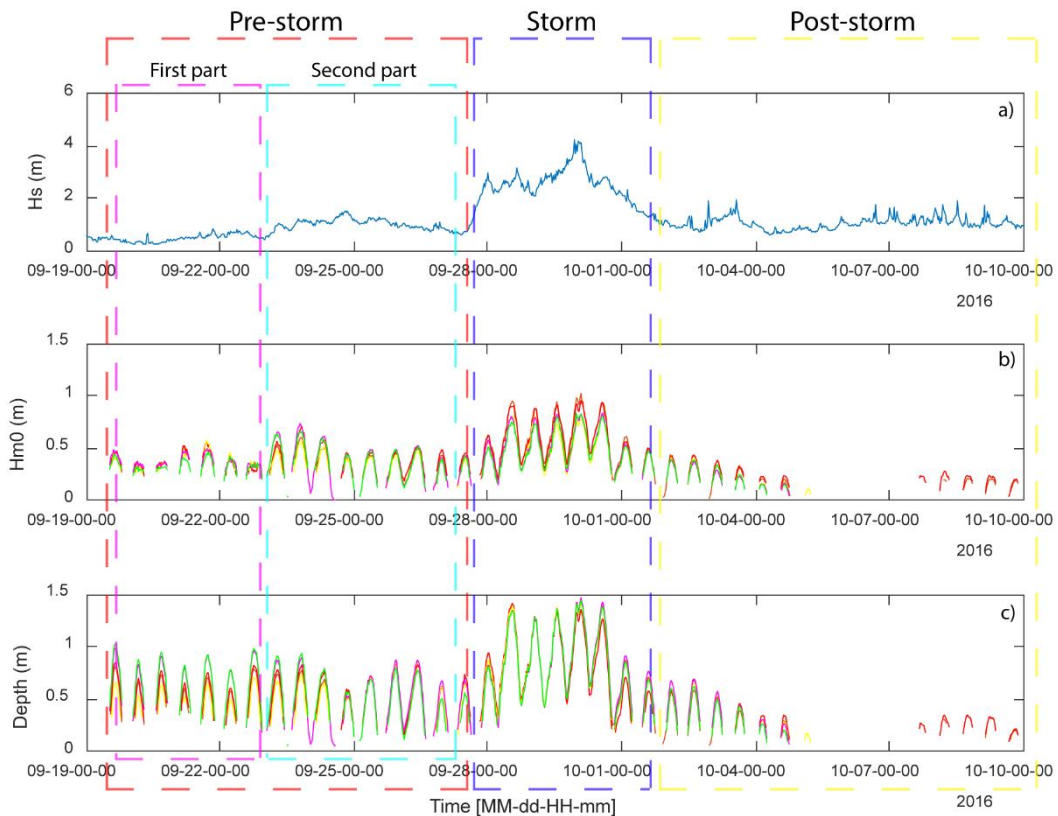


Figure 37: a) The offshore significant wave height. b) The significant wave height and c) the water depth at the alongshore OSSIs: 1 (blue), 2 (red), 3 (yellow), 4 (magenta), 5 (green).

5.3.1 Wave height

In this section, the significant wave heights at the different OSSI locations (H_{m0}) and the alongshore differences herein, during the pre-storm and storm period, are described. In the next section, the spectral energy will be treated.

Figure 38a indicates the H_{m0} at the same water depth (as described in section 4.3.2) at each alongshore location for each tide (17 tides) during the pre-storm period. The significant wave height varied alongshore up to 0.15 m during one tide throughout this period. Where, during the first six tides, the lowest H_{m0} was found at the alongshore location of OSSI 5, which corresponds to the increased wave breaking over the shallow subtidal horn, located seaward of this point. Although, this was not the case for the rest of the pre-storm period, with less variation in the middle of the period (tides 8-11), up to 0.05 m, and not one location with consistently the highest/lowest H_{m0} . During the last tides of this period (tides 12-17) the lowest significant wave height was found at OSSI 3 (and OSSI 4), in contrast to the measurements during the first six tides.

As the alongshore differences in significant wave height show an inconsistent trend during the pre-storm period, the averaged H_{m0} during this period was calculated to indicate alongshore differences in the wave height over a longer period (Figure 29b). The averaged H_{m0} was calculated over the first part, the second part and the whole pre-storm period. The results indicate that the alongshore differences in averaged wave height were very small (< 0.09 m). With almost all error bars (of one standard deviation) overlapping one another. The averaged H_{m0} suggest slightly higher waves at OSSI 3 during the first part, while slightly lower waves occurred at OSSI 5 (± 0.09 m difference between OSSI 3 and 5) compared to the other locations. During the second part, the averaged H_{m0} appeared to be lowest at OSSI 3. Furthermore, over the whole first period the averaged H_{m0} was alongshore nearly equal, indicating the same inconsistency in the significant wave height differences,

and therefore suggesting no correlation between significant wave heights and the subtidal morphology during (relatively) low energetic conditions.

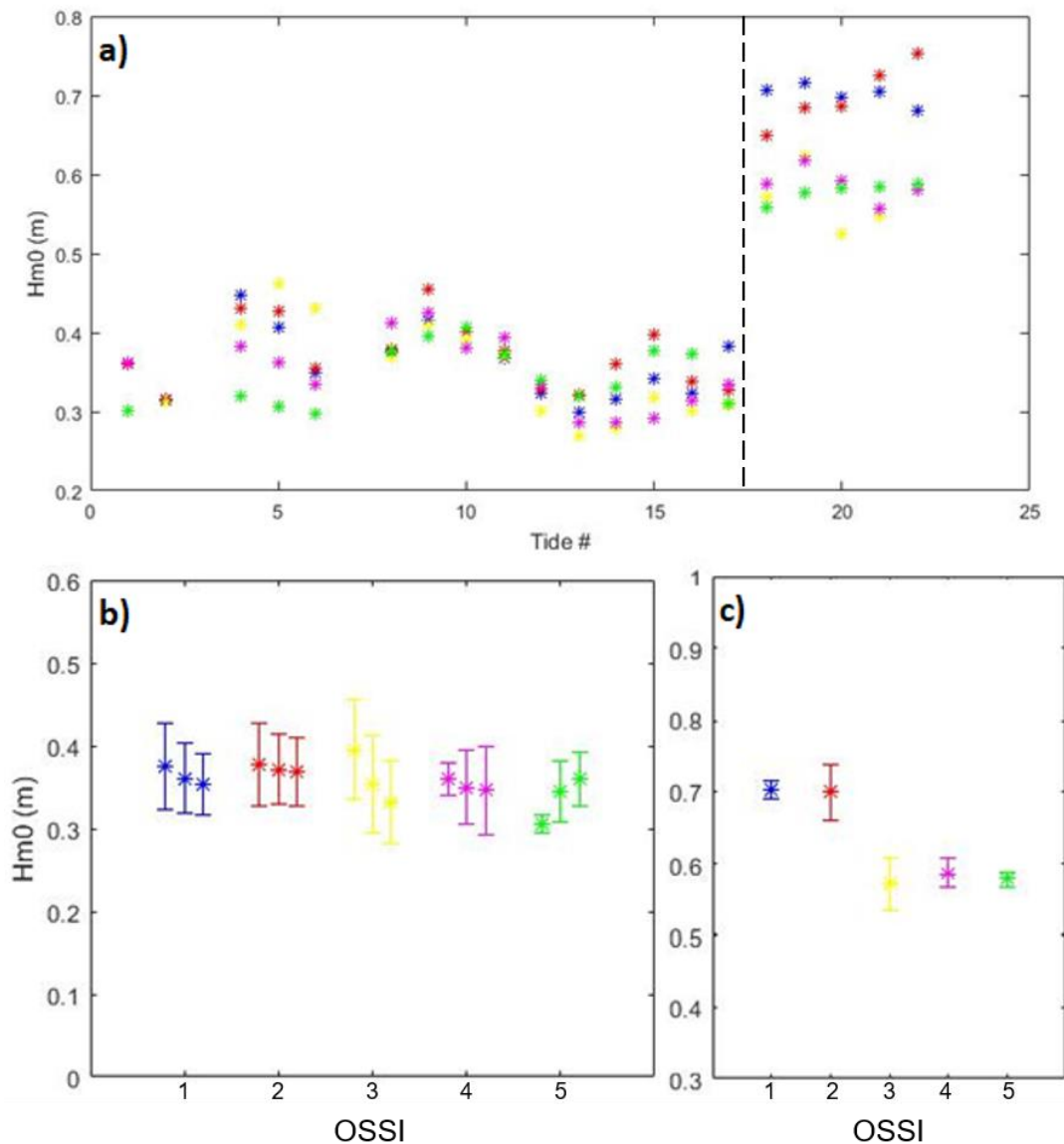


Figure 38: Hm0 at a water depth of 0.48 m (from the linear fits), for each tide before the storm (day 3-10, tides 1-17) and Hm0 at a water depth of 1.0 m (from the linear fits), for each tide of the storm (day 11-13, tides 18-22) at the different alongshore locations of the OSSIs: 1 (blue), 2 (red), 3 (yellow), 4 (magenta) and 5 (green). Black dashed line separates pre-storm – storm. b) Averaged Hm0 at a water depth of 0.48 m (from the linear fits) during, the first 7 tides (left point), all tides during the pre-storm period (middle point) and the last 10 tides during the pre-storm (right point), at the different alongshore locations of the OSSIs. c) Averaged Hm0 at a water depth of 1.0 m (from the linear fits) during the storm, at the different alongshore locations of the OSSIs. The error bars indicate the range of one standard deviation from the average.

Figure 38a (tides 18-22) indicates the wave heights for each tide during the storm in a water depth of 1.0 m at the alongshore locations. Naturally, the Hm0 was higher during the storm (Figure 24a). It seems that the significant wave height was higher at OSSIs 1 and 2 than at the other locations. Furthermore, this alongshore variation appeared to be consistent during the storm, meaning that the wave height was highest throughout the storm at the same locations. The averaged Hm0 (Figure 38c) suggests the same alongshore differences in wave height, with higher waves (± 0.10 - 0.15 m) in the southern part of the study area (OSSIs 1 and 2) during the storm.

5.3.2 Spectral energy

The (relative) amount of energy in the infragravity waves can influence the sediment transport direction (section 2.3.3) and swash characteristics (section 2.1.1), and thus the morphology (sections 2.3.1, about swash bars, and 2.3.3). Furthermore, the differences in wave energy and relative amount of energy in the infragravity frequencies are indications for differences in the amount of wave dissipation further offshore (section 2.1.1). Therefore, the wave spectra were investigated to further explore the alongshore differences in wave climate (see section 4.3.2). Similar to the analysis of alongshore variations in wave height, for each tide at each OSSI a spectrum, which was made over 30 minutes of measurements, was chosen based on the water depth during the measurements, such that the water depths of the chosen spectra were near equal (section 4.3.2). This was done to avoid variations within the spectra caused by measurements in different water depths.

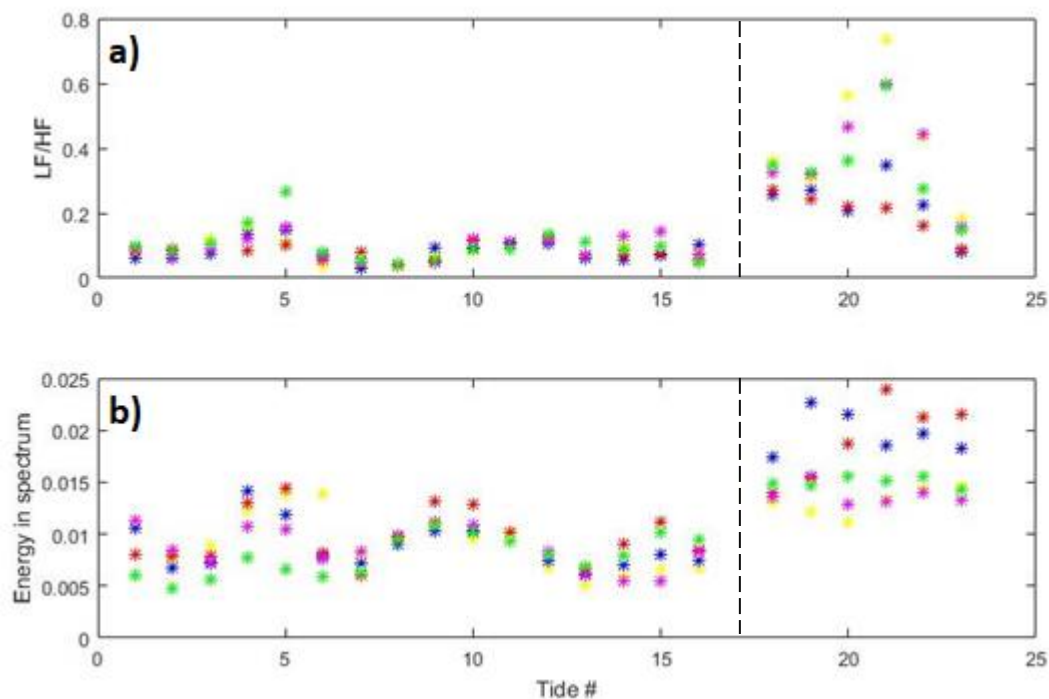


Figure 39: a) The low/high frequency ratio in spectral energy and b) the total spectral energy at the same water depth (0.48 m) per tide during the pre-storm period (tides 1-16) and at the same water depth (1.0 m) per tide during the storm (tides 18-23). For the different alongshore locations of the OSSIs: 1 (blue), 2 (red), 3 (yellow), 4 (magenta) and 5 (green). Black dashed lines separate pre-storm – storm

The LF/HF ratio per tide for each alongshore OSSI location is shown in Figure 39a for the pre-storm and storm period, where the ratio is generally higher during the storm. Figure 39b displays the total spectral energy per tide per OSSI.

During the first part of the pre-storm period (tides 1-7) it seems that the highest LF/HF ratio was found at the location of OSSI 5 (Figure 39), while also at this location the lowest total energy is found during those tides (up to ± 0.003 , area under the curve, lower). During the rest of the pre-storm period no consistent variations between the alongshore locations were found. The averaged total spectral energy (Figure 40a) indicates that the energy was indeed lower at OSSI 5 during the first part of the pre-storm period. The figure also indicates that during the second part of the pre-storm period (tides 8-17) the spectral energy was nearly equal at the alongshore locations. During the storm, the LF/HF ratio seemed lower at OSSIs 1 and 2 while the total spectral energy seemed higher at these OSSIs (Figure 39). This is confirmed in Figure 31 (b+c) as the averaged LF/HF ratio and averaged total spectral energy show the same results. In addition to the fact that these results suggest an

alongshore variation in wave conditions, the results also indicate an inverse correlation between total spectral energy and the LF/HF ratio, which is expected as a part of the energy from high frequency wave is transferred to the low frequency waves during wave energy dissipation by breaking (section 2.1.1). Furthermore, the total spectral energy shows the same results as the significant wave height during the storm; highest at OSSIs 1 and 2, which makes sense as the wave energy is proportional to the wave height. Additionally, the averaged total spectral energy indicates a slight variation between the other three OSSIs (3, 4 and 5), as the energy seemed to be lowest at OSSI 3 and showing a minor increase towards the north.

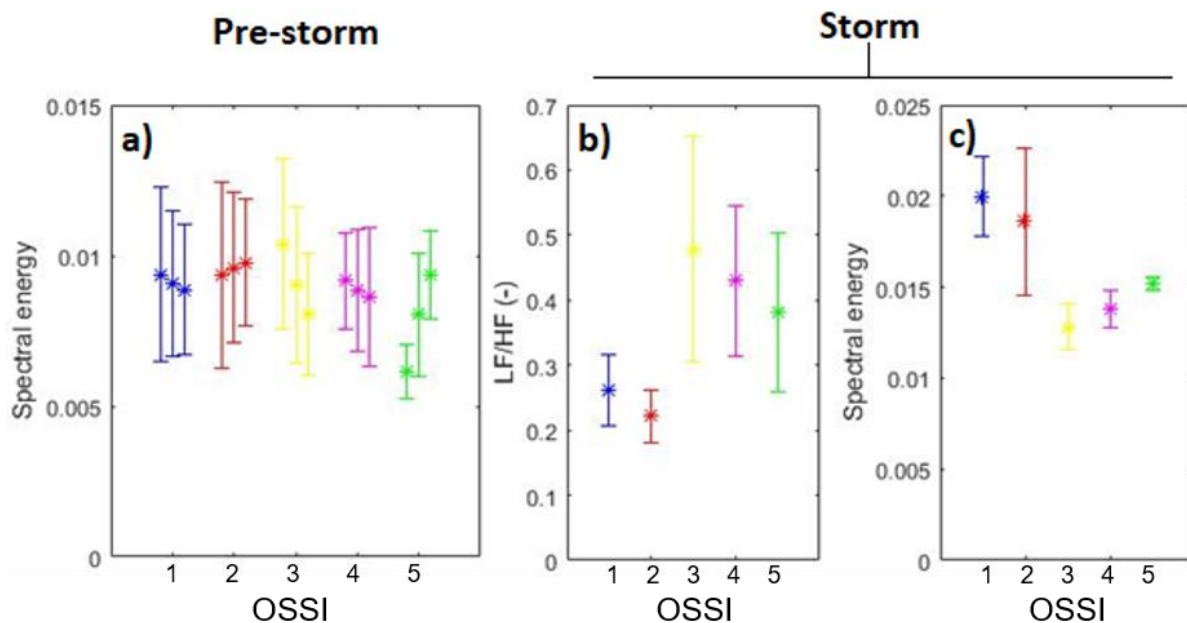


Figure 40: a) Averaged total spectral energy at the same water depth during, the first 7 tides (left point), all tides during the pre-storm period (middle point) and the last 10 tides of the pre-storm period (right point). b) Averaged low/high frequency ratio in spectral energy during the storm at the same water depth. c) Averaged total spectral energy during the storm at the same water depth. All for the different alongshore locations of the OSSIs: 1 (blue), 2 (red), 3 (yellow), 4 (magenta) and 5 (green). The error bars indicate the range of one standard deviation from the average.

5.4 Morphological changes vs. hydrodynamics

5.4.1 T-test results

The second aim of this research is to examine possible relations between alongshore variations in morphodynamics and alongshore variations in hydrodynamics. The previous results indicate that there are some alongshore variabilities in morphodynamics and hydrodynamics. Although, the variations are not consistent per tide, meaning that the differences are not always at the same alongshore location (e.g. the highest migration distance was not always found at the same OSSI location).

The statistical t-test was used to determine if two variables (a hydrodynamical and morphological variable) show a significant correlation and how strong, positive or negative, the correlation is. To indicate if it really was an alongshore variation, the variables are taken as relative values between two alongshore locations. For example, the difference in significant wave height between the location of OSSI 3 and 5, the relative H_{m0} . For the analysis of the morphological changes the alongshore variations were considered between two measurements over time (i.e. between two days). For example, the intertidal beach slope (β) is determined for day 3 and day 4 of the campaign at the location of OSSI 3 and 5, after which the development of the slope between the days is determined for both locations ($d\beta$) (so the slope difference between day 4 and 3). Subsequently, the

difference in the development between the two locations is determined, leading to a variable which describes the alongshore variation in slope development ($dd\beta$). This was done for all morphological features described in section 4.3.1, resulting in; ddz_b , ddh_b , ddX_b , $ddz=0$, $dd\beta$ and ddV .

Table 1 shows all the statistical t-test results which indicated a significant correlation between the two variables. As mentioned, only the pre-storm period is investigated (section 4.3). The variations used are not always between all alongshore locations or between each measuring day. As clarified in the table some are only; the relative variation between all the other OSSIs and OSSI 3, the conditions at OSSI 5 relative to OSSI 3 or the changes between the beginning and the end of the whole pre-storm period with the mean wave conditions.

Furthermore, the correlations between the wave conditions and volume/ $z=0$ contour position change during the storm were also determined. But the mentioned variables did not show a significant correlation and are therefore not listed in Table 1.

Table 1 presents the results of the correlations. The R-value in the table indicates how strong, positive or negative, the correlation between the variables is. With an R-value of 1.0 indicating a perfect 1 on 1 positive correlation, an R-value of -1.0 indicating a perfect negative (inverse) correlation and an R-value of 0.0 indicating no correlation at all. The t-value indicates if there is a significant correlation between the variables, being significant if the t-value is greater (positive or negative) than the corresponding t-critical value, which is based on the number of observations (degrees of freedom, which is also indicated in Table 1). The P-value also indicates if the correlation is significant, where there is a significant correlation if the P-value is lower than the level of significance ($\alpha=0.05$). Some t-test results are highlighted and visualised in the next section by figures with a linear trendline to indicate the relation between the data.

	R-value	t-value	P-value	Deg. Of freedom
All OSSIs relative to the conditions at OSSI 3				
Relative LF/HF energy ratio (not at same h) vs. ddh _b	-0.44	-2.79	0.009	32
Relative Hm0 vs. ddz _b	-0.67	-4.65	8.436E-05	26
Relative Hm0 vs. ddh _b	-0.48	-2.82	0.009	27
Relative Hm0 vs. ddX _b	-0.72	-5.55	5.551E-06	29
Relative LF/HF energy ratio vs. ddz _b	0.39	2.31	0.028	30
Relative LF/HF energy ratio vs. ddX _b	0.39	2.41	0.021	33
Relative total spectral energy vs. ddz _b	-0.51	-3.25	0.003	30
Relative total spectral energy vs. ddh _b	-0.38	-2.32	0.027	32
Relative total spectral energy vs. ddX _b	-0.57	-3.96	3.758E-04	33
Relative total spectral energy vs. ddβ	-0.54	-3.49	0.001	30
All OSSIs relative to the conditions at the other OSSIs				
Relative Hm0 vs. ddz _b	-0.25	-2.12	0.038	67
Relative Hm0 vs. ddX _b	-0.28	-2.42	0.018	70
OSSI 5 relative to the conditions at OSSI 3				
Relative Hm0 vs. ddz _b	-0.91	-4.39	0.012	4
Relative Hm0 vs. ddh _b	-0.82	-3.22	0.023	5
Relative Hm0 vs. ddX _b	-0.94	-7.00	2.125E-04	7
Relative Hm0 vs. ddβ	-0.94	-5.34	0.006	4
The changes between begin-end pre-storm period with the mean wave conditions				
Hm0 vs. dV	0.88	3.24	0.048	3
Total spectral energy vs. dz _b	-0.99	-15.61	0.041	1
Total spectral energy vs. dh _b (between day 4 and 10)	0.99	18.37	0.003	2
Total spectral energy vs. dV	0.95	5.32	0.013	3
Migration and elevation change between begin-end first period (except day 3: 09-20)				
ddX _b vs. ddz _b , at all OSSIs relative to OSSI 3	0.96	18.92	6.114E-19	32

Table 1: The t-test results which indicated a significant correlation between the two variables, during the pre-storm period (days 1-10). Remember: morphological measurements started at day 3. Note: for top correlation, the relative LF/HF energy ratio was not taken at the same water depth, for all the other correlations the wave conditions were taken at the same water depth.

5.4.2 Significant correlations

This section highlights some of the more important and noticeable correlations, all other figures presenting the significant correlations can be found in the Appendix. First, correlations in alongshore variation between OSSI 5 and OSSI 3 were determined, as the subtidal bar morphology differed the most between these points. After that, correlations between more points were determined.

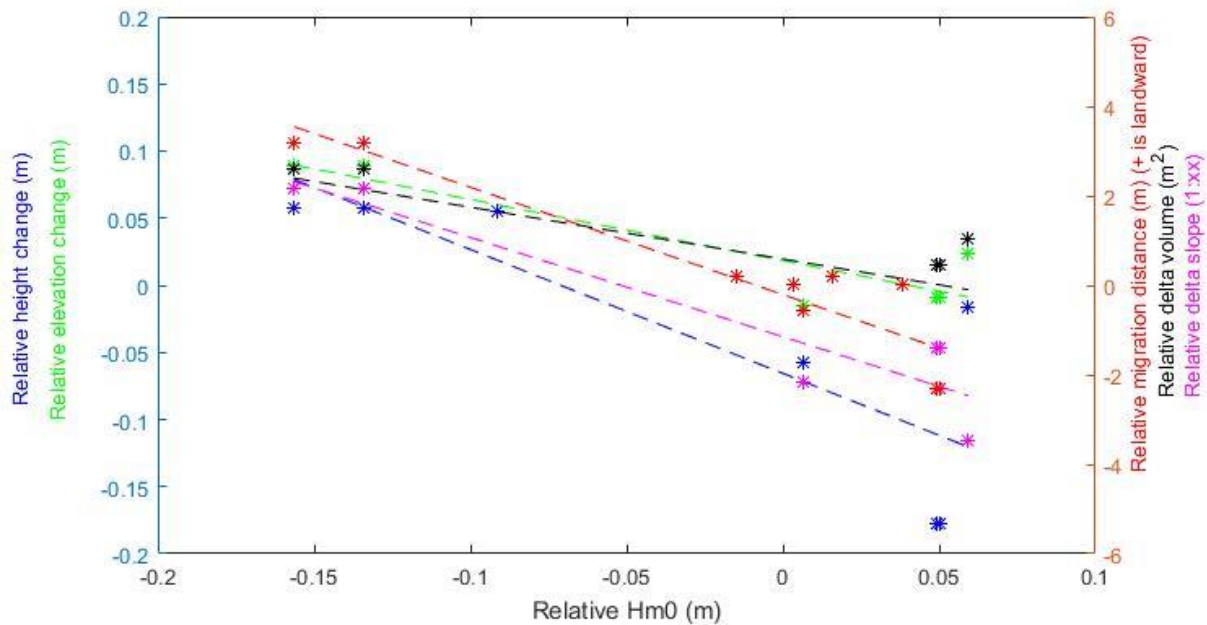


Figure 41: Morphological changes vs relative Hm_0 at the same water depth, during the pre-storm period between each day, at OSSI 5 relative to OSSI 3. The colours in the figure correspond to the colours at the y-axis. Note: positive migration is landward.

Figure 32 indicates the correlations between the relative morphological changes and relative Hm_0 between OSSI 3 and 5 (see Table 1), so between the middle and the north of the study area. Note that the relative volume change did not have a significant correlation with the relative Hm_0 . These results are of substantial importance as they show that there are possible correlations between alongshore variations in morphodynamics and hydrodynamics. The relation between the relative wave height and all these relative morphological changes is a negative one. And as the variations are expressed as relative variations the differences in morphological response can either be more in one direction or less in the opposite direction. In Figure 41 for example, if the Hm_0 is higher, the bar height and elevation became less high/lower, the bar migrated less landward/more seaward and the slope became less gentle/steeper. So, from these results one cannot directly indicate the direction in which the development went, only the relative differences between the alongshore locations.

Some significant correlations at all other OSSIs relative to OSSI 3, between the relative variation in alongshore development and variation in alongshore wave conditions are shown in Figure 42. Figures visualising the other significant correlations (Table 1) are found in the Appendix. This figure indicates a negative relation between relative significant wave height and relative bar height change/relative bar migration, indicating that when the Hm_0 was higher at one location relative to the other location, the bar got lower or grew less/the bar migrated less landward or more seaward at that location. Furthermore, there is a negative relation between the relative total spectral wave energy and relative slope change, indicating that if the total energy at one alongshore location is higher than at another location, the slope became relatively steeper at that location (so steeper or less gentle).

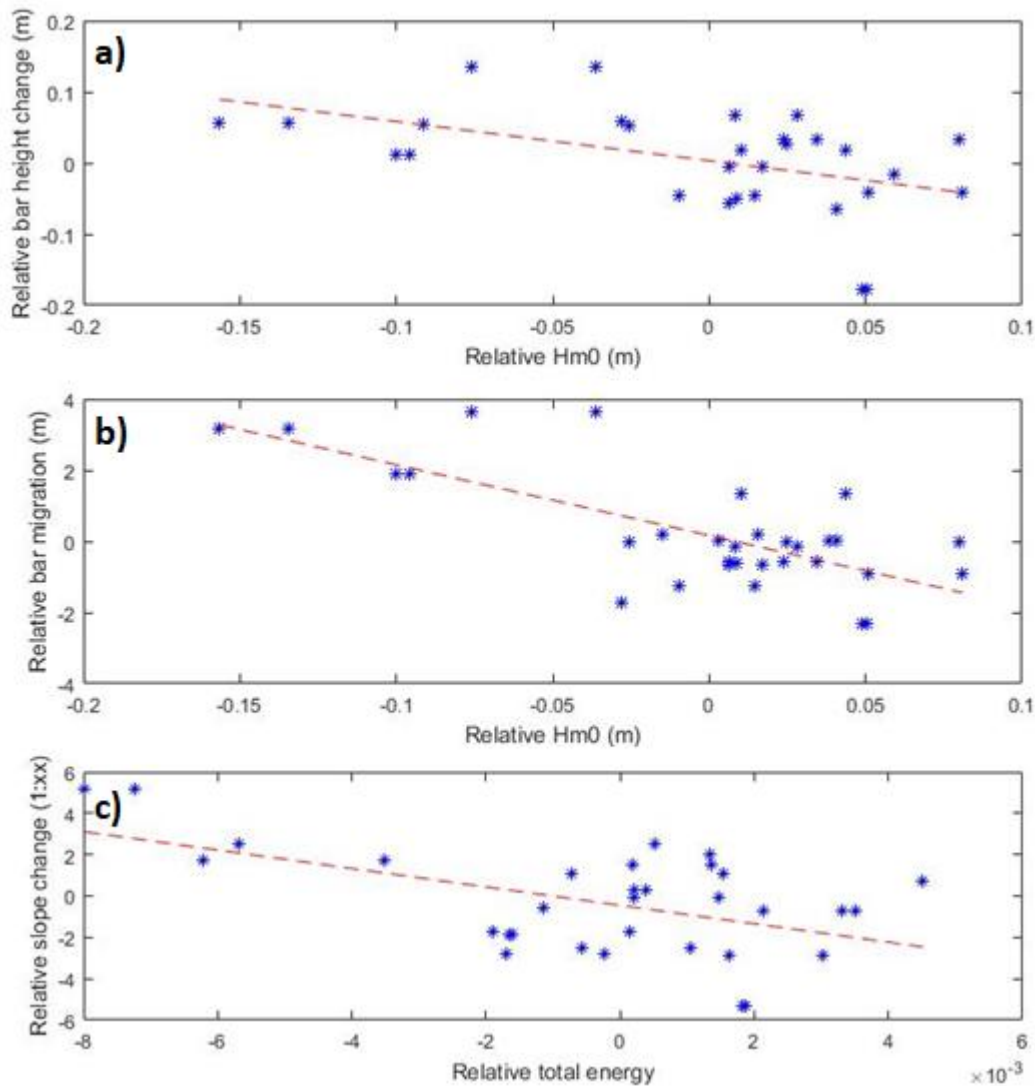


Figure 42: a) Relative bar height change vs relative Hm0 at the same water depth. b) Relative bar migration vs relative Hm0 at the same water depth. c) Relative slope change vs relative total wave energy at the same water depth. All during the pre-storm period between each day, at all other OSSIs relative to OSSI 3. Note: positive migration is landward.

Figure 43 indicates the correlation between various morphological developments between begin and end of the pre-storm period and the mean wave conditions throughout that period at the different alongshore locations. As the correlations are significant (even though there are only a few data points) it seems that the wave conditions influenced the morphological development, and that this could be alongshore variable. Figure 43 shows that the higher the mean total wave energy: the less the bar elevation increased, the higher (or less low) the bar became and the least the volume got reduced. Furthermore, the volume shows the same correlation with the significant wave height.

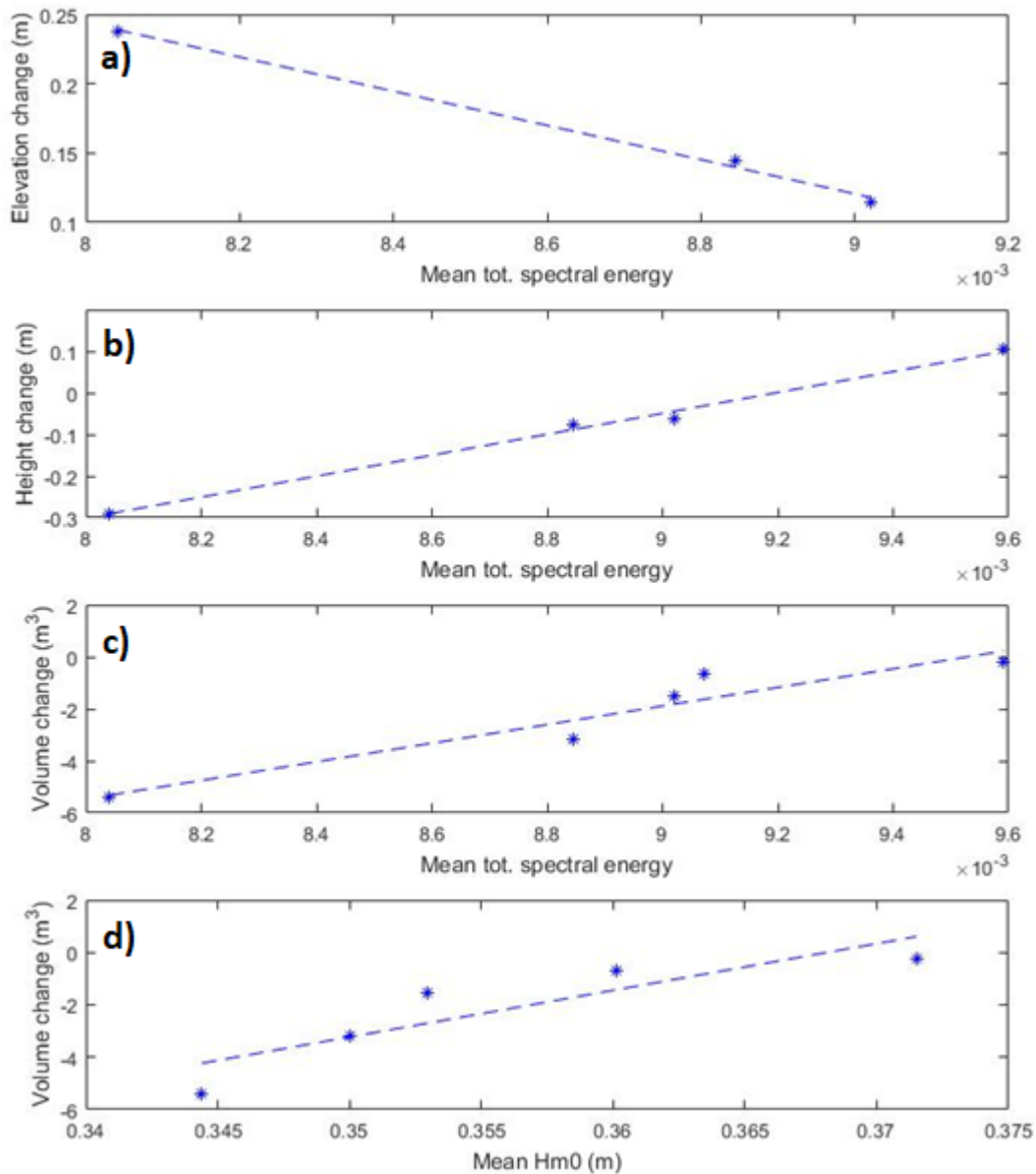


Figure 43: Elevation change vs mean total spectral energy at the same water depth (a), bar height change vs mean total spectral energy at the same water depth (b), intertidal beach volume change vs mean total spectral energy at the same water depth (c), intertidal beach volume change vs mean Hm0 at the same water depth (d), between the beginning and end of the pre-storm period. Obtained from the different alongshore OSSI locations. Note: at some locations the bar was not present, or was not fully formed, at the first day of the campaign.

Generally, the bar migration and bar elevation change indicated similar correlations with the wave conditions. Figure 44 indicates the (almost 1:1) significant positive correlation between the relative bar migration and the relative bar elevation change. This correlation is rational, because when the bar migrates further landward it moves up the beach slope, which leads to a likely increase in bar elevation, and vice versa.

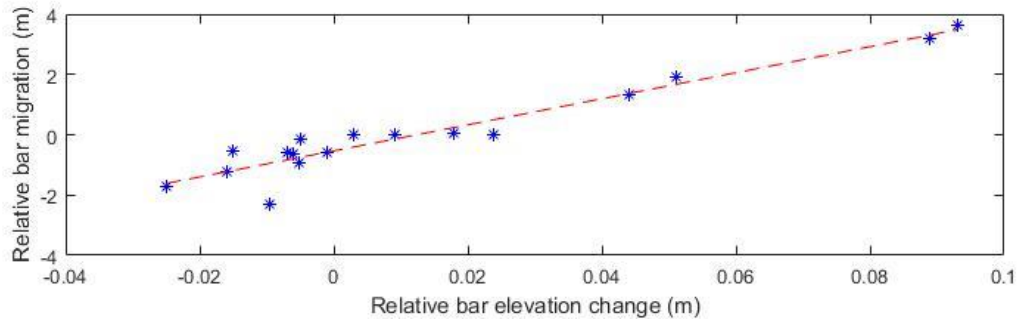


Figure 44: Relative bar migration vs relative bar elevation change, during the pre-storm period between each day, all other OSSIs relative to OSSI 3. Note: positive migration is landward.

6. Discussion

6.1 Large scale variation

Before the start of the campaign there was already variation in shoreline location (i.e. a crescentic shoreline). This crescentic shape of the intertidal beach appears to have a 180° out-of-phase coupling with the crescentic shape of the subtidal bar (Figure 36). Where, the deeper part of the subtidal bar (embayment) coexisted with the embayment of the beach. This corresponds to the out-of-phase coupling found by the modelling work of *Castelle et al. (2010a, 2010b)*. Who found that if wave breaking dominates over wave refraction over the subtidal bar, the wave energy shoreward of the subtidal bar embayment will be higher, leading to an alongshore variation in wave set-up and thus driving an offshore flow landward of the subtidal bar horns. Consequently, this can result in more seaward deposition of sand on the beach at the location of the subtidal bar horns, forming a crescentic shoreline. If this mechanism would be driving the crescentic shoreline shape, one would expect that there were alongshore differences in wave energy between the locations behind the subtidal bar embayment and horns. The averaged total wave energy during the pre-storm period (Figure 40) shows slightly larger values at OSSI 3, located landward of the subtidal bar embayment, than at OSSI 5, located landward of the subtidal bar horn. Although this supports the mechanism presented by *Castelle et al. (2010a, 2010b)*, the error bars (of one standard deviation) suggest that the higher energy at OSSI 3 (0.0025 difference in area under the spectra) did not deviate significantly. Because the wave energy was generally low during the pre-storm period, the absolute alongshore differences were very small. Therefore, it might be that the out-of-phase coupling was generated by an extended period of slight differences in wave energy. Another explanation would be that slightly higher energetic wave conditions in the period before the campaign, resulted in more pronounced variation in alongshore wave energy.

The changes of the $z=0$ m contour line during the pre-storm period (Figure 34) indicate that the crescentic shape was still enhanced during the pre-storm period, even though the mean wave energy was not significantly variable alongshore during this period (Figure 40). This might imply that even minor variations in the wave field can result in alongshore variations in the development of the shoreline, given sufficient time. In this case, the precedent morphology of the beach may determine the development due to self-organisation mechanisms (*Coco & Murray, 2007*).

During the storm, the crescentic shape of the shoreline enhanced even more due to a larger seaward migration of the contour line at the sides of the study area (the horns) compared to the middle part (the embayment). This might have been a result of more sediment deposition on the lower area of the intertidal beach at the locations of the subtidal bar horns. This could have been enabled by the possible occurrence of circulation patterns driven by the subtidal bar morphology (described in section 2.4.1), which has not been measured. The sediment deposition on the lower part of the

intertidal beach (Figure 26) pushed the $z=0$ contour line towards the sea as the lower part became higher. As mentioned, this seaward migration of the contour line was larger at both sides of the study area compared to the middle, which enhanced the crescentic shape (Figure 34). Because the waves were higher during the storm, the crescentic subtidal bar had more potential to generate an alongshore variation in the wave energy arriving at the intertidal beach as higher waves were more likely to dissipate energy over the subtidal bar. However, when looking at the hydrodynamic results (Figures 38 & 40), the spectral energy and significant wave heights during the storm do not support this theory. The spectral wave energy appeared to be lowest at the location of OSSI 3, which is in contradiction with the morphological template theory (Castelle et al., 2010a, 2010b) as OSSI 3 was located at the position of the subtidal bar embayment. This indicates, according to the study from Castelle et al. (2010a, 2010b), that wave refraction would be the dominant process over the subtidal bar, resulting in energy focusing shoreward of the subtidal bar horns (which corresponds with these results). However, the morphological response contrasts the expectations based on the alongshore variation in wave energy, as the shoreline developed more towards the out-of-phase coupling instead of in-phase. If waves arrive with an angle relative to the shore normal, the morphological template of the subtidal bar shifts alongshore, which might be an explanation for the contradicting results. However, the incident waves arrived with an angle between 0° and 10° south of the shore normal during the storm (Figure 24c), which would not have resulted in the sufficient shift explaining the contrast. As such, the theory proposed by Castelle et al. (2010a, 2010b) does not comply with the results during the storm of this field campaign.

6.2 The (intertidal) swash bar

6.2.1 General development of the bar

Looking at the cross-sections throughout the campaign (Figure 28), there appears to have been an intertidal sandbar. Real time observations indicate that this intertidal bar was mostly subject to swash processes, as it was located just above the high tide water level, and is therefore classified as a swash bar (Figures 14 and 45). During high tide the waves were breaking on the seaward slope of the bar and many up-swashes were able to overtop the crest of the swash bar, making the swash processes effective in causing an onshore bar migration (Masselink et al., 2006), further discussed below. The relative position of this swash bar was just above the high tide water level, which is comparable to the relative position of bar 1 indicated in Figure 7, indicating solely onshore sediment transport over the bar.

In general, a swash bar can be formed by the accretion of sediment due to swash motions as discussed in section 2.3.1. The accretion of sediment and an onshore migration of a swash bar can be caused by onshore mass transport by the swashes of gravity and infragravity waves along with a water circulation system on the intertidal beach. Such a circulation system includes an alongshore runnel (landward of the bar) which transports the water alongshore to an offshore discharge channel through the swash bar (Houser & Greenwood, 2007). This system was also present during the field campaign, with an alongshore runnel behind the bar and some drainage channels cutting through the swash bar (Figure 46). Unfortunately, the drainage channels are not visible on the interpolated bathymetry maps (section 5.2.1) as the channel widths (< 1 m) and elevation differences (± 0.1 m) were too small.

When such a water circulation system over the intertidal beach is present, the sediment which is transported landward over the bar crest by the up-swash cannot be transported back as the water is channelled alongshore in the runnel, leading to sediment deposition on the landward side of the bar and thus an onshore migration/accretion of the bar (Masselink et al., 2006). This is likely what happened at the study area, as an onshore migration of the swash bar was witnessed during both the

pre- and the post-storm periods (Figures 31 & 32). This onshore migration reflects the evolution from a swash bar to a berm under prolonged calm wave conditions (section 2.3.1), which was completed during the post-storm period (at day 21).



Figure 45: Photographs of the swash bar. On day 6, just after the maximum high tide water level (a) and on day 9, during high tide (b).

6.2.2 Alongshore variations in bar behaviour

The occurrence of an outflow drainage channel at the location of OSSI 1, which migrated southward, caused a later occurrence of the swash bar at this position (Figure 28). At the location of OSSI 2 the bar was also not yet present during the first measurements of the cross-sections (day 3, Figure 28). This might be explained by the southward migration of the drainage channel, as the channel might have been present at the location of OSSI 2 a few days before the measurements started.

The development of the bar during the pre-storm period, subdivided into distinct aspects (bar migration, peak bar elevation and peak bar height based on the landward trough), showed some alongshore variation (Figure 32). However, the alongshore variation was not consistent during the pre-storm period, as the location with the most development was different every day. This could possibly be explained due to the low wave energy conditions, which might cause inconsistent variation in the wave conditions. This inconsistency in alongshore wave energy variation is also indicated in the results (Figures 38 and 39). As the location of maximum/minimum H_{m0} , LF/HF or total spectral energy changed throughout the pre-storm period, especially during the second part (tides 8-17).

Differences in swash bar behaviour could be caused by alongshore variations in up-swash. According to the study from Guedes et al. (2011), differences in up-swash are mainly controlled by the amount of energy dissipation in the surf zone (section 2.1.1). The more energy was dissipated in the surf zone, the smaller the up-swash. Thus, alongshore differences in the amount of energy dissipation over the subtidal bar could have a significant role in the alongshore variations in up-swash and, therefore, (swash) bar development. According to the results, as mentioned above, the wave energy arriving at the intertidal beach was alongshore variable in an inconsistent manner, suggesting that the subtidal bar shape had minor to no influence on the wave field. Although, the alongshore variation in amount of wave breaking over the subtidal bar could have varied over time, resulting in variations over time in alongshore variations in wave height and energy landward of the subtidal bar throughout the pre-storm period (i.e. inconsistent variations) (Figures 38 and 39). Furthermore, this does not exclude that the significant wave height and wave energy had influence on the variations in bar development.

The correlation between the relative bar development (between two points over time) and relative wave conditions (both relative between two alongshore positions) was determined with the use of the statistical t-test (section 5.4). This was done to determine if the alongshore differences in wave conditions have had influences on the alongshore variations in bar development. Some tested variables were statistically significantly correlated, indicating a connection between the two variables. To test the correlations, different time periods of morphological change were used (i.e. between every day and between the beginning and end of the pre-storm period) and not all the alongshore points were always considered relative to each other (i.e. only relative between OSSI 3 and 5, only relative between all locations and OSSI 3 and all locations relative to each other). From this, the largest number of significant correlations were found between the relative differences from all the alongshore locations relative to OSSI 3. A significant negative correlation was found between the relative significant wave height and the relative bar elevation change, relative bar height change and relative bar migration, indicating that at a position with a higher significant wave height, compared to another alongshore position, less sediment accretion/more sediment erosion occurred. With sediment accretion standing for landward bar migration and bar growth. The relative total spectral energy shows a similar correlation with the bar developments, suggesting that lower energetic waves resulted in more sediment accretion at the swash bar.

These results indicate that there was a correlation between alongshore variations in bar development and alongshore variations in wave conditions. However, it is uncertain how the alongshore variations in wave conditions originated and if possible other alongshore variations (in the longshore current for example) play a role. Further research is necessary to investigate this, as will be discussed in section 6.4. Furthermore, these results indicate that if, somehow (e.g. by a consistent variation in wave energy dissipation over the subtidal bar(s)) during low energetic wave conditions, the wave conditions are always more/less energetic at one location compared to other

locations over an extended period (weeks to months), then there will be more deposition/erosion at that location, which might result in possible stronger and weaker spots due to the accumulation of sand on one location, while not at other locations, during beach recovery periods. Because the location with more sand accumulation builds a buffer, protecting the rest of the beach and dunes from eroding during high energetic storm wave conditions (Keijsers et al., 2014), while other locations, without this buffer, are more likely to be subjected to beach and dune erosion. To be able to predict the locations where these weaker spots can develop, more research is needed to fully understand the driving of alongshore variations in the wave field during low energetic wave conditions, and the corresponding development of the intertidal beach.



Figure 46: Photographs of outflow drainage channels cutting through the bar crest, along with current ripples in the runnel, on day 1 (a) and on day 21 (b).

6.3 Volume, slope and contour line

Alongshore differences in the changes in the intertidal beach slope, volume and the cross-shore position of the $z=0$ elevation contour line were determined and compared to the alongshore differences in wave conditions during the low-energetic wave conditions. Like with the bar developments, it was determined whether these alongshore variations had a significant correlation with the alongshore variations in wave conditions (section 5.4).

During the pre-storm period, a significant negative correlation was found between the relative slope change and the relative total spectral energy, as well as with the relative significant wave height. Furthermore, a significant positive correlation was indicated between the averaged significant wave height/total spectral energy and the volume change between days 3 and 10 (begin and end pre-storm period). These results indicate that at a position with higher energetic waves, the slope became steeper and the sediment volume increased (or decreased less) compared to another alongshore position. The steepening of the intertidal beach might have occurred due to the rise in peak bar elevation instead of erosion of the seaward face of the bar. Furthermore, the correlation with the volume change is based on only a few data points, which makes the correlation less convincing. Quartel et al. (2008) found that, under calm wave conditions, an intertidal beach steepening and increase in volume occurred. This happened due to a lack of wave breaking resulting in more influence by shoaling waves relative to the undertow. It might be that, during the pre-storm period, the waves were so extremely low, that the position with higher energetic waves was subjected to more energetic shoaling waves and not to a higher breaking intensity. This might indicate that too low energetic wave conditions can result in a lack of morphological change, as there is just too little energy.

In line with the previous section (6.2.2), potentially major alongshore differences in the intertidal zone can develop if the wave conditions show a consistent alongshore variation during low energetic wave conditions. Creating locations with sediment buffers against erosion due to the increase in sediment volume, while other locations might lack in beach recovery, becoming potential weak spots under storm wave conditions.

Table 1 indicates that most correlations between alongshore differences in morphological development and alongshore differences in wave conditions were expressed in bar dynamics (elevation, height and migration) and slope (which was determined as the seaward slope of the bar) instead of the other morphological parameters (volume and $z=0$). In other words, the intertidal bar evolution was most prone to behave alongshore variable under alongshore differences in wave conditions.

Furthermore, the correlations between the wave conditions and volume/ $z=0$ contour position change during the storm were also determined. As mentioned in section 5.4.1, these did not show a significant correlation, indicating that alongshore variations in changes in volume and $z=0$ position were not caused by alongshore differences in wave conditions.

6.4 Uncertainties and possible improvements

In this section, first the possible errors caused by uncertainties are discussed, followed by possible improvements concerning this research and suggestions for further research. The morphological data was measured by walking along the intertidal beach with the RTK GPS system. This includes some possible measurement errors as the GPS system had to be held horizontal at all time during the measurements, which was presumably not the case. Furthermore, the GPS data was interpolated to make an overview of the intertidal beach and to make the cross-sections, losing some detail. The point measurements taken during the 8 days of the campaign (section 4.2.1) were linearly

interpolated to create the cross-sections. And the continuous topographic measurements were interpolated along a new grid to make an overview of the whole study area. As the grid points were determined by the measurements around that point, the interpolated maps lack some detail (section 4.2.1). This also means that the cross-sections, taken from these maps, are smoothed, losing some detail. Accordingly, the calculated variation in the alongshore morphology might include some errors.

The OSSI data had to be corrected for the instrument height above the bed during the measurements. As the instrument heights were only measured during low tide, the heights during high tide are not known for certain. This might include some error in the water depth measurements as the correction factor might be off. As the alongshore variations in H_{m0} were quite small (with a maximum of 0.15 m), this might have influenced the results. Because, if the water depth measurements were slightly off, the method to find the H_{m0} at the same water depth alongshore (section 4.3.2) would give slightly different results, possibly affecting the relative alongshore differences in H_{m0} , as the alongshore variations were small.

To be able to determine the alongshore differences in wave conditions, the conditions were compared as if they occurred in the same water depth. This method, described in section 4.3.2, includes some errors as the linear fitted lines did not consistently fit the data. As described above, the possible errors in the measured water depth might have influenced the results of this method.

To improve this fieldwork campaign, I suggest that more alongshore hydrodynamic data should be gathered. To ensure a better comparison between alongshore wave conditions, 4 or more pressure sensors should be deployed at each alongshore location as a cross-shore array. As the hydrodynamics should, ideally, be measured during the same time and at the same relative cross-shore position. If a cross-shore array of pressure sensors is deployed it is more likely that the data is better comparable, as measurements will be easier (with less chance of errors) interpolated to find wave heights in the same water depths. Also, due to the measurements of wave heights at different cross-shore positions, more information about possible differences in the cross-shore development of the waves is provided. Furthermore, to give an insight in possible circulation cells and variations in longshore currents, current meters should be placed on the different alongshore positions. With this more enhanced instrument setting, a clearer overview of the alongshore variations in hydrodynamics on the intertidal beach can be created. Improving the knowledge about alongshore variations during low energetic wave conditions. Finally, offshore bathymetry should be measured or determined through remote sensing, including the subtidal bar(s) position(s) and shape. This could give insights in the possible variation in alongshore variation in wave breaking over the subtidal bar through time.

Further research, in the origin of alongshore variations in hydrodynamics and how this might vary through time, as well as the processes behind the development of alongshore differences in intertidal beach characteristics during mild weather conditions, is needed to fully understand possible alongshore variabilities in intertidal hydrodynamics and beach recovery, under low energetic wave conditions. A better understanding could improve future beach protection measures. As the natural processes leading to the accumulation of sand could be controlled to stimulate beach recovery/growth at weaker spots in the coastal defence system (against the future sea level rise), and beach growth can stimulate the growth of adjacent dunes.

7. Conclusion

The alongshore variability in intertidal beach morphodynamics and hydrodynamics, along with the correlations between them, were studied, using a 3-week data set of bathymetric measurements and wave data. From the data, changes in morphology and variations in wave properties were determined at 5 alongshore locations. In the middle of the fieldwork campaign a storm passed by (days 11-14), dividing the campaign in three periods: pre-storm, storm and post-storm. The data analysis was focused on the pre-storm and storm periods. The alongshore differences in morphological development of the intertidal beach were characterised as the relative changes of certain characteristics over time (between 2 days) between alongshore locations: relative bar height change, bar elevation change, bar migration, slope change, volume change and $z=0$ position change. The results of this study show that the behaviour of the intertidal beach was alongshore variable during mild weather conditions, with alongshore differences in bar migration, bar elevation change and bar height change (between two days), up to 5, 0.15 and 0.25 meter, respectively, during the pre-storm period. And the maximum alongshore difference in the cross-shore position of $z=0$ increased from ± 9 m to ± 15 m between the beginning and end of the pre-storm period. Furthermore, alongshore variation in the developments of these characteristics was inconsistent. Various differences in morphological developments appeared to be significantly correlated to the inconsistent alongshore variations in wave conditions measured at the low tide coastline. The main conclusion of this research is that there were significant correlations between alongshore variations in bar developments and alongshore variations in wave conditions, during a period of low-energetic wave conditions. However, it is uncertain how the alongshore variations in wave conditions originate, how they changed over time and which processes were responsible for the alongshore variations in bar development.

Further research, in the origin of alongshore variations in hydrodynamics and how this might vary through time, as well as the processes behind the development of alongshore differences in intertidal beach characteristics during mild weather conditions, is needed to fully understand possible alongshore variabilities in intertidal hydrodynamics and beach recovery, under low energetic wave conditions. To investigate this during future fieldwork campaigns, more hydrodynamic data, with the use of a cross-shore array of pressure sensors and current meters, should be gathered at multiple alongshore locations. Finally, offshore bathymetry should be measured/determined, including the subtidal bar(s) position(s) and shape (s).

Acknowledgements

I would like to thank Timothy for supervising me throughout this thesis, making time to have interesting discussions and providing useful feedback on my progress. Furthermore, I want to thank all my fieldwork companions for a wonderful (and educational) time in Denmark. A special shout out goes to Johnny, Vera and Joost for the invention of the chocolate-tea break and the discussions with Vera and Johnny during our lunch breaks in Utrecht.

References

- Aagaard, T. (2011). Sediment transfer from beach to shoreface: The sediment budget of an accreting beach on the Danish North Sea Coast. *Geomorphology*, 135(1–2), 143–157.
- Aagaard, T., Greenwood, B., & Hughes, M. (2013). Sediment transport on dissipative, intermediate and reflective beaches. *Earth-Science Reviews*, 124, 32–50.
- Aagaard, T., Hughes, M., Møller-Sørensen, R., & Andersen, S. (2006). Hydrodynamics and Sediment Fluxes across an Onshore Migrating Intertidal Bar. *Journal of Coastal Research West Palm Beach*, 22, 247–259.
- Aagaard, T., & Jensen, S. G. (2013). Sediment concentration and vertical mixing under breaking waves.
- Aagaard, T., Kroon, A., Andersen, S., Møller Sørensen, R., Quartel, S., & Vinther, N. (2005). Intertidal beach change during storm conditions; Egmond, The Netherlands. *Marine Geology*, 218(1–4), 65–80.
- Aagaard, T., Kroon, A., Hughes, M. G., & Greenwood, B. (2008). Field observations of nearshore bar formation. *Earth Surface Processes and Landforms*, 33(7), 1021–1032.
- Aagaard, T., Nielsen, J., & Greenwood, B. (1998). Suspended sediment transport and nearshore bar formation on a shallow intermediate-state beach. *Marine Geology*, 148, 203–225.
- Abdelrahman, S. M., & Thornton, E. B. (1987). Changes in the Short Wave Amplitude and Wavenumber Due to the Presence of Infragravity Waves, 458–478.
- Battjes, J. A. (1974). Surf similarity.
- Carson, M., Köhl, A., Stammer, D., Slangen, A., Katsman, C., van de Wal, R., ... White, N. (2016). Coastal sea level changes, observed and projected during the 20th and 21st century. *Climatic Change*, 134(1–2), 269–281.
- Castelle, B., Marieu, V., Bujan, S., Splinter, K. D., Robinet, A., Sénéchal, N., & Ferreira, S. (2015). Impact of the winter 2013-2014 series of severe Western Europe storms on a double-barred sandy coast: Beach and dune erosion and megacusp embayments. *Geomorphology*, 238, 135–148.
- Castelle, B., Ruessink, B. G., Bonneton, P., Marieu, V., Bruneau, N., & Price, T. D. (2010a). Coupling mechanisms in double sandbar systems. Part 1: Patterns and physical explanation. *Earth Surface Processes and Landforms*, 35(4), 476–486.
- Castelle, B., Ruessink, B. G., Bonneton, P., Marieu, V., Bruneau, N., & Price, T. D. (2010b). Coupling mechanisms in double sandbar systems. Part 2: Impact on alongshore variability of inner-bar rip channels. *Earth Surface Processes and Landforms*, 35(7), 771–781.
- Coco, G., & Murray, A. B. (2007). Patterns in the sand: From forcing templates to self-organization. *Geomorphology*, 91(3–4), 271–290.
- Galvin, C. J. (1968). Breaker type classification on three laboratory beaches. *Journal of Geophysical Research*, 73(12), 3651–3659.
- Guedes, R., Bryan, K. R., & Coco, G. (2012). Observations of alongshore variability of swash motions on an intermediate beach. *Continental Shelf Research*, 48, 61–74.
- Guedes, R. M. C., Bryan, K. R., Coco, G., & Holman, R. A. (2011). The effects of tides on swash

- statistics on an intermediate beach. *Journal of Geophysical Research: Oceans*, 116(4), 1–13.
- Houser, C., & Greenwood, B. (2007). Onshore Migration of a Swash Bar During a Storm. *Journal of Coastal Research Florida Journal of Coastal Research West Palm Beach*, 23(231), 1–14.
- IPCC. (2014). Synthesis Report, 1–169.
- Keijsers, J. G. S., Poortinga, A., Riksen, M. J. P. M., & Maroulis, J. (2014). Spatio-Temporal Variability in Accretion and Erosion of Coastal Foredunes in the Netherlands: Regional Climate and Local Topography. *PLOS ONE*, 9(3).
- Kroon, A., & Masselink, G. (2002). Morphodynamics of intertidal bar morphology on a macrotidal beach under low-energy wave conditions, North Lincolnshire, England. *Marine Geology*, 190(3), 591–608.
- Masselink. (1993). Simulating the Effects of Tides on Beach Morphodynamics.
- Masselink, G., Hughes, M. G., & Knight, J. (2014). *Introduction to coastal processes & geomorphology* (Second edition).
- Masselink, G., Kroon, A., & Davidson-Arnott, R. G. D. (2006). Morphodynamics of intertidal bars in wave-dominated coastal settings - A review. *Geomorphology*, 73(1–2), 33–49.
- Osborne, P. D., & Greenwood, B. (1992). Frequency dependent cross-shore suspended sediment transport. 1. A non-barred shoreface. *Marine Geology*, 106(1–2), 1–24.
- Plant, N. G., Holland, K. T., & Puleo, J. A. (2002). Analysis of the scale of errors in nearshore bathymetric data. *Marine Geology*, 191(1–2), 71–86.
- Price, T. D., & Ruessink, B. G. (2008). Morphodynamic zone variability on a microtidal barred beach. *Marine Geology*, 251(1–2), 98–109.
- Price, T. D., & Ruessink, B. G. (2011). State dynamics of a double sandbar system. *Continental Shelf Research*, 31, 659–674.
- Price, T. D., & Ruessink, B. G. (2013). Observations and conceptual modelling of morphological coupling in a double sandbar system. *Earth Surface Processes and Landforms*, 38(5), 477–489.
- Quartel, S., Kroon, A., & Ruessink, B. G. (2008). Seasonal accretion and erosion patterns of a microtidal sandy beach. *Marine Geology*, 250(1), 19–33.
- Quartel, S., Ruessink, B. G., & Kroon, A. (2007). Daily to seasonal cross-shore behaviour of quasi-persistent intertidal beach morphology. *Earth Surface Processes and Landforms*, 32(9), 1293–1307.
- Ruessink, B. G., van den Berg, T. J. J., & van Rijn, L. C. (2009). Modeling sediment transport beneath skewed asymmetric waves above a plane bed. *Journal of Geophysical Research*, 114(C11).
- Senechal, N. (2017). Alongshore variability in observed runup under dissipative conditions. *Coastal Dynamics*, (208).
- Short, A. D. (2006). Australian Beach Systems—Nature and Distribution. *Journal of Coastal Research*, 22(221), 11–27.
- Sonu, C. J. (1973). Three-dimensional beach changes.
- Southgate, H. N. (1995). The effects of wave chronology on medium and long term coastal morphology. *Coastal Engineering*, 26, 251–270.
- Sunamura, T., & Takeda, I. (1984). Landward migration of inner bars. *Marine Geology*, 60(1–4), 63–

78.

Van de Lageweg, W. I., Bryan, K. R., Coco, G., & Ruessink, B. G. (2013). Observations of shoreline-sandbar coupling on an embayed beach. *Marine Geology*, *344*, 101–114.

Wright, L. ., & Short, A. . (1984). Morphodynamic variability of surf zones and beaches : A synthesis. *Marine Geology*, *56*(1–4), 93–118.

Yates, M. L., Guza, R. T., & O'Reilly, W. C. (2009). Equilibrium shoreline response: Observations and modeling. *Journal of Geophysical Research*, *114*(C9).

Appendix

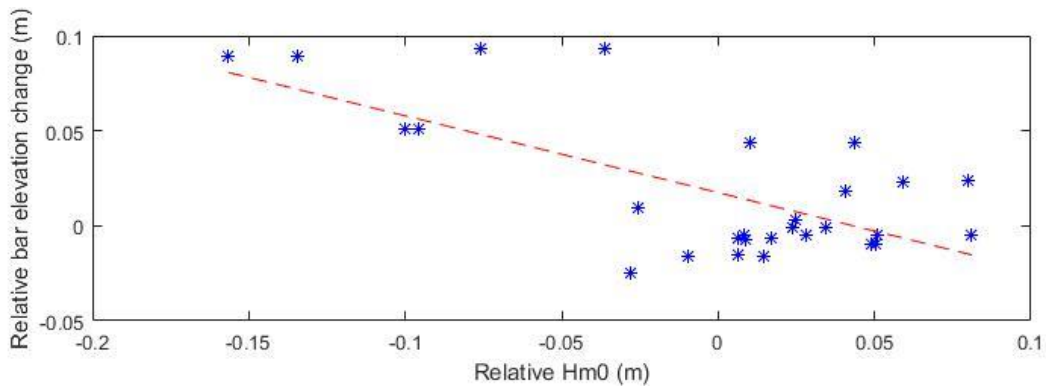


Figure 47: Relative bar elevation change vs relative Hm0 at the same water depth, during the pre-storm period between each day, all other OSSIs relative to OSSI 3.

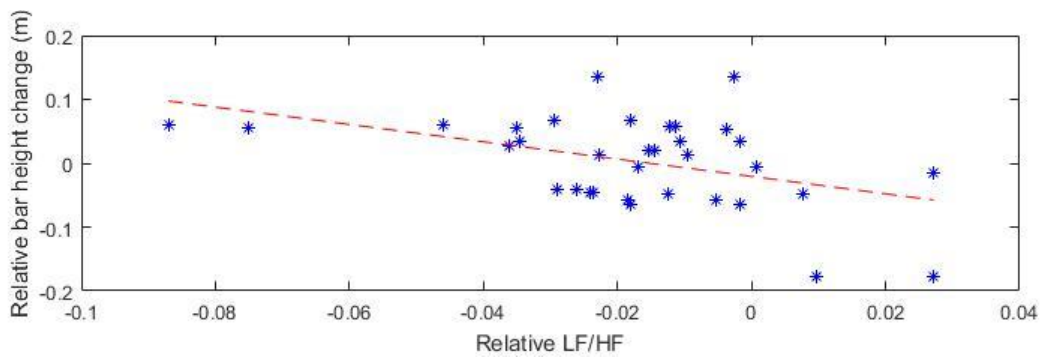


Figure 48: Relative bar height change vs relative LF/HF ratio not at same water depth, during the pre-storm period between each day, all other OSSIs relative to OSSI 3.

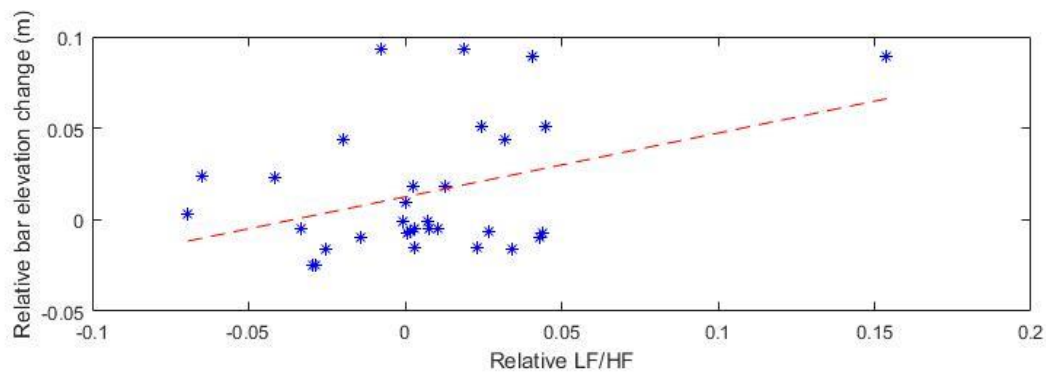


Figure 49: Relative bar elevation change vs relative LF/HF ratio at the same water depth, during the pre-storm period between each day, all other OSSIs relative to OSSI 3.

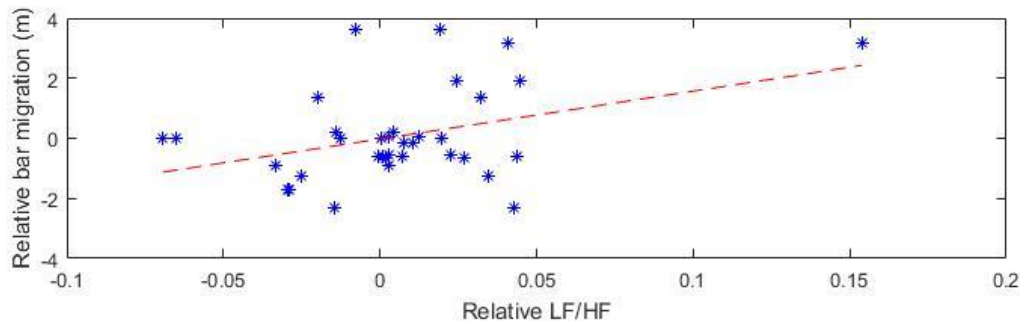


Figure 50: Relative bar migration vs relative LF/HF ratio at the same water depth, during the pre-storm period between each day, all other OSSIs relative to OSSI 3. Note: positive migration is landward

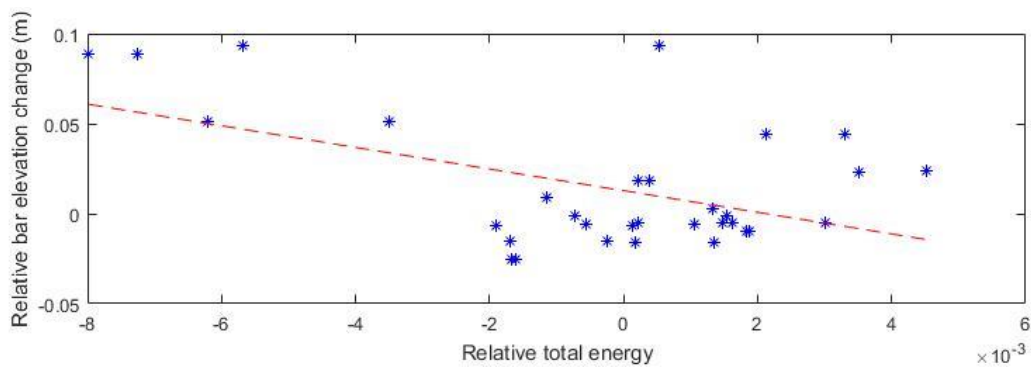


Figure 51: Relative bar elevation change vs relative total wave energy at the same water depth, during the pre-storm period between each day, all other OSSIs relative to OSSI 3.

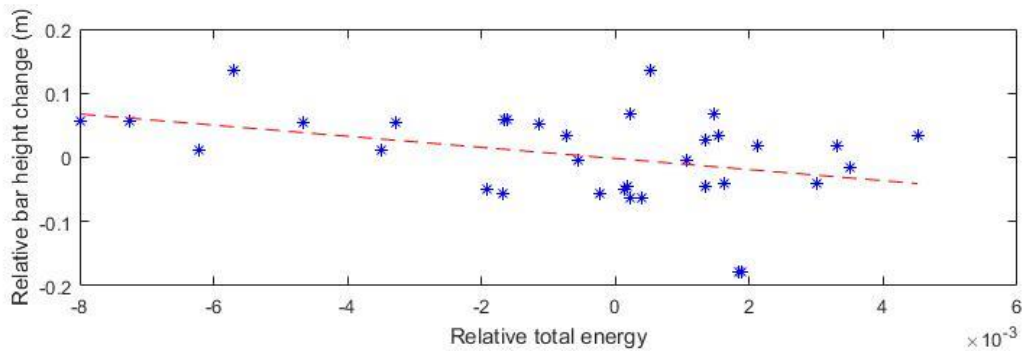


Figure 52: Relative bar height change vs relative total wave energy at the same water depth, during the pre-storm period between each day, all other OSSIs relative to OSSI 3.

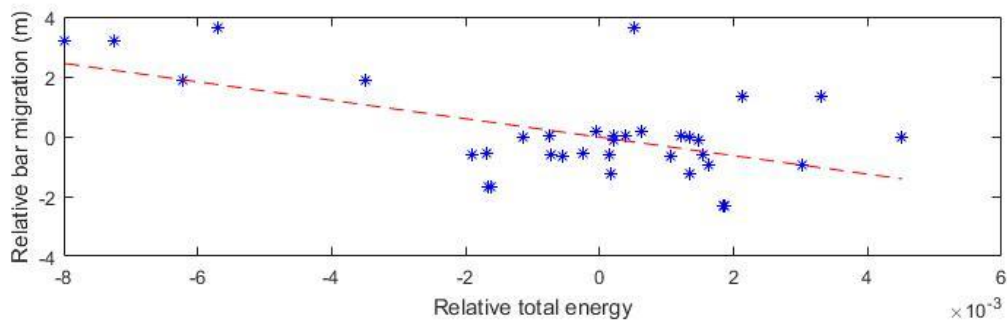


Figure 53: Relative bar migration vs relative total wave energy at same water depth, during the pre-storm period between each day, all other OSSIs relative to OSSI 3. Note: positive migration is landward.

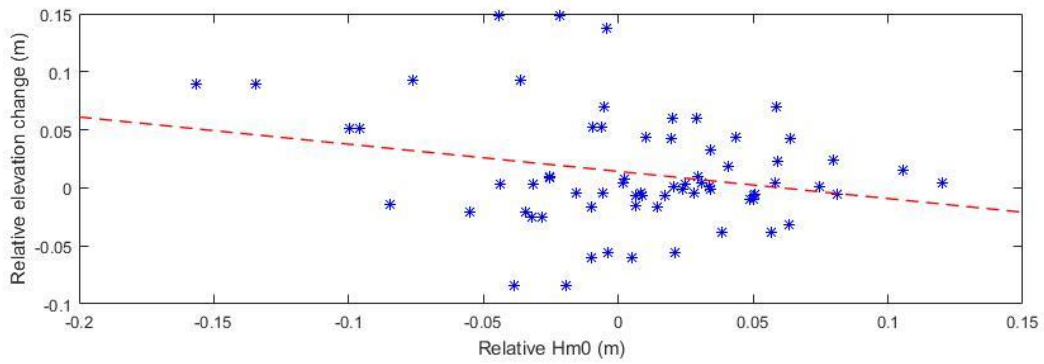


Figure 54: Relative bar elevation change vs relative Hm0 at the same water depth, during the pre-storm period between each day, all OSSIs relative to each other.

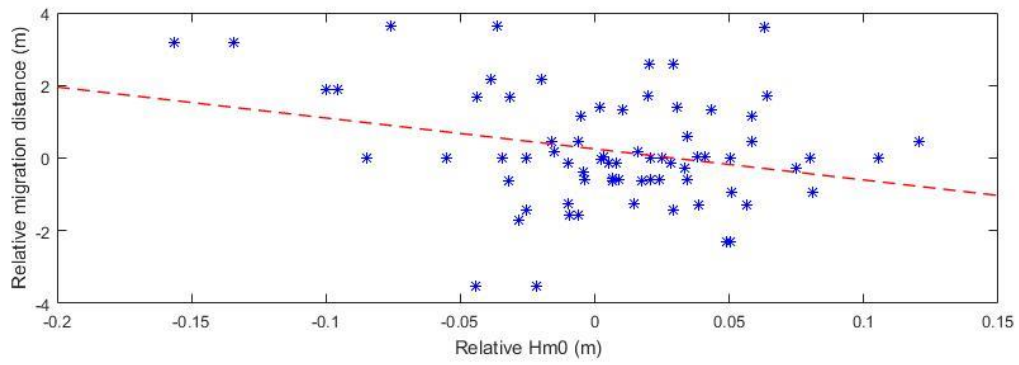


Figure 55: Relative bar migration vs relative Hm0 at the same water depth, during the pre-storm period between each day, all OSSIs relative to each other. Note: positive migration is landward